INVESTIGATION OF ANTARCTIC CRUST AND UPPER MANTLE USING MAGSAT AND OTHER GEOPHYSICAL DATA

by

C.R. Bentley and M.H. Ritzwoller

Contract #NAS5-25977

TECHNICAL REPORT STANDARD TITLE PAGE

1. Report No.	2. Government Accession No.	3. Recipient's Catalog No.

4. Title and Subtitle	5. Report Date
Investigation of Antarctic Crust and Upper Mantle using MAGSAT and other Geophysical Data	September 1, 1983
	6. Performing Organization Code
7. Author(s)	8. Performing Organization Report No.
Charles R. Bentley & Michael H. Ritzwoller	
9. Performing Organization Name and Address	10. Work Unit No.
Geophysical & Polar Research Center University of Wisconsin-Madison 1215 W. Dayton Street Madison, WI 53706	11. Contract or Grant No. NAS5-25977
12. Sponsoring Agency Name and Address	13. Type of Report and Period Covered
NASA, Code 269 Goddard Space Flight Center Greenbelt, MD 20771	Final Report September 1979- August 1983
	14. Sponsoring Agency Code

15. Supplementary Notes

Prepared as Master's degree thesis by M.H. Ritzwoller, University of Wisconsin-Madison, 1982

16. Abstract

Data selection and reduction procedures are described by which scalar and vector magnetic anomaly maps are constructed. The scalar and vertical magnetic anomalies are believed to be generated mainly in the earth's crust. The horizontal anomalies are believed to be mainly due to short-period field-aligned currents. The correlation of scalar magnetic anomalies with known oceanic structure is remarkable -- magnetic highs are associated with oceanic ridges and magnetic lows with abyssal plains. The correlation between anomalies and continental geology is not as clear. In East Antarctica, magnetic lows associated with the Ross Embayment and the Amery Ice Shelf are consistent with the hypothesis (Hayes and Davey, 1975) that these regions are failed continental rifts. The magnetic low over the Gamburtsev Mountains, as distinct from the highs over Wilkes Land and Enderby Land, may imply a tectonic history of the Gamburtsev Mountains that is different than that of the latter two surrounding regions (Drewry, 1975). The Wilkes Land magnetic high is consistent with the hypothesis (Veevers, 1982) that this region is the site of cool convergence in the mantle. In West Antarctica, Dalziel and Elliot (1982) have postulated the existence of five microplates. Separate anomaly features are associated with each of their microplates, supporting their hypothesis. Finally, the apparent mirroring of anomaly features on the other Gondwanaland continents implies that the sources of the anomalies have been stable since before the rifting occurred.

17. Key Words (Selected by Author(s))	18. Distribution Statement

19. Security Classif. (of this report)	20. Security Classif. (of this page)	21. No. of Pages	22. Price*
		141	

*For sale by the Clearinghouse for Federal Scientific and Technical Information, Springfield, Virginia 22151.

Figure 2. Technical Report Standard Title Page

INVESTIGATION OF ANTARCTIC CRUST AND UPPER MANTLE USING MAGSAT AND OTHER GEOPHYSICAL DATA

Dr. Charles R. Bentley and Mr. Michael H. Ritzwoller*
Geophysical and Polar Research Center
University of Wisconsin-Madison
1215 W. Dayton Street
Madison, WI 53706

September 1, 1983

Final Report for Period September 1979-August 1983

Prepared for:

National Aeronautics and Space Administration
Goddard Space Flight Center
Greenbelt, Maryland 20771

*Now at: Scripps Institute of Oceanography,
Mail Code A-008, LaJolla, CA 92093

TABLE OF CONTENTS

PREFACE

Data selection and reduction procedures are described by which scalar and vector magnetic anomaly maps are constructed. The scalar and vertical magnetic anomalies are believed to be generated mainly in the earth's crust. The horizontal anomalies are believed to be mainly due to short-period field-aligned currents. The correlation of scalar magnetic anomalies with known oceanic structure is remarkable -- magnetic highs are associated with oceanic ridges and magnetic lows with abyssal plains. The correlation between anomalies and continental geology is not as clear. In East Antarctica, magnetic lows associated with the Ross Embayment and the Amery Ice Shelf are consistent with the hypothesis (Hayes and Davey, 1975) that these regions are failed continental rifts. The magnetic low over the Gamburtsev Mountains, as distinct from the highs over Wilkes Land and Enderby Land, may imply a tectonic history of the Gamburtsev Mountains that is different than that of the latter two surrounding regions (Drewry, 1975). The Wilkes Land magnetic high is consistent with the hypothesis (Veevers, 1982) that this region is the site of cool convergence in the mantle. In West Antarctica, Dalziel and Elliot (1982) have postulated the existence of five microplates.

Separate anomaly features are associated with each of their microplates, supporting their hypothesis. Finally, the apparent mirroring of anomaly features on the other Gondwanaland continents implies that the sources of the anomalies have been stable since before the rifting occurred.

LIST OF FIGURES

LIST OF TABLES

1. INTRODUCTION

It is surprising and fortunate that magnetic fields generated by crustal sources can be isolated in satellite magnetic field data from those generated in the core and those external to the earth. It is surprising because crustal fields (0-25 nT) are so much smaller than the core field (30,000-60,000 nT) and external fields (0-2000 nT), and fortunate because geologic and tectonic features in the deep crust can result in long-wavelength magnetic anomalies (Pakiser and Zietz, 1965; Zietz et al, 1966: Hall. 1974; Krutikhovskaya and Pashkevich, 1977). Long-wavelength magnetic anomalies (> 200 km) were first mapped globally from data acquired by the POGO (Polar Orbiting Geophysical Observatories) satellites (Regan et al, 1975) and have compared favorably with upward-continued regional aeromagnetic surveys (Langel et al, 1980). The chief advantage of the MAGSAT data over the POGO data lies in the ability to study vector fields with MAGSAT and in the greater resolution MAGSAT's generally lower orbit affords (perigee 352 km, apogee 561 km). A disadvantage for Antarctic studies, outweighed by these advantages, is that MAGSAT's orbit is inclined at 7° off the earth's axis of rotation resulting in a data gap around the Pole in MAGSAT derived maps.

Attempts have been made to isolate anomalies both in the scalar field (Langel et al, 1982a; Coles et al, 1982; Ritzwoller and Bentley, 1982 (Appendix I)) and in the vector field (Langel

et al, 1982b; Coles et al, 1982). Sailor et al (1982) confirm the general reliability of such attempts and conclude that resolution is possible down to a 250 km spatial-wavelength in mid-latitudes; this being larger in higher latitude regions due to a smaller signal-to-noise ratio. The reduction in this ratio is due to the amplification of external magnetic fields in auroral regions. (Appendix IV describes the structure of current systems external to the earth and their implications to MAGSAT studies.) Magnetospheric ring-currents in low latitudes generate a temporally rather stable long-spatial wavelength signature (Langel and Sweeney, 1971) that is easily filtered. However, currents following magnetic field lines in auroral regions have temporal and spatial spectra covering quite a broad band of frequencies, thus making standard frequency-based filtering difficult. Therefore, only passes occurring during low field-aligned current periods can be used as data in high latitudes seriously reducing the size of the data set over Antarctica and in the Arctic (Coles et al, 1982). The map of Ritzwoller and Bentley (1982) over Antarctica demonstrated the signal detection problem by displaying serious non-physical radial striping.

Progress in modeling and interpreting satellite magnetic anomalies is short and generally qualitative. On a global scale, anomalies appear to be associated with such large structures as continental shields and platforms, subduction zones (positive),

oceanic ridges (positive), basins (negative), and abyssal plains (negative) (signs are for reduced-to-pole maps) and appear to be bounded by such "linear" features as sutures, rifts, folded mountains, and age province boundaries (Frey, 1982a). More detailed preliminary regional studies have been performed by Frey (1982b) for Asia, by Hastings (1982) for Africa, by Hinze et al (1982) for South America, and by Ritzwoller and Bentley (1982) for Antarctica.

A geologic interpretation of the maps must only be conducted in light of the probable mineralogy of the lower crust and upper mantle. Wasilewski et al (1979) argue that the mantle is probably non-magnetic so that if the Curie isotherm is below the crust the lower magnetic boundary is the Moho. Moreover, Wasilewski and Mayhew (1982) conclude that for some tectonic settings, at least, the lower crust may be the most magnetic crustal layer and that magnetization values for lower crustal xenoliths (specifically metabasic rocks of the granulite facies) have values consistent with those inferred from models of long-wavelength anomalies. Wasilewski and Fountain (1982) corroborate these findings with a study of the Ivrea Zone in Northern Italy, wh mafic granulite facies rocks are the only magnetic lithology present, are thick and laterally continuous, and thus provide a good candidate for a deep-crustal source of long-wavelength magnetic anomalies.

Along with regional mineralization variations, it is suspected that variations in the depth to the Curie isotherm (if above the Moho) will contribute to long-wavelength anomalies (Mayhew, 1982). Thus, the main sources of long-wavelength magnetic anomalies in continental regions are expected to reside above the Moho and the Curie isotherm but principally in the lower crustal layer. Consequently, since the causes of variations in heat flow and regional mineralization are many, ambiguity is injected into the interpretation of satellite magnetic anomaly maps. However, everything else being equal, heat flow and regional magnetic anomalies are inversely related, whereas the thickness of the magnetized crust and the regional magnetic anomalies are directly related. Therefore, continental highs indicate either a thin crust with a deep Curie isotherm (low heat flow), or exceptionally high magnetic susceptibility in the lower crust, or both. On the other hand, continental lows imply some combination of a thin crust, a shallow Curie isotherm (high heat flow), and low susceptibilities in the lower crust. An additional degree of ambiguity in the determination of the nature of the source of an anomaly is also added by the large areal extent of the potential source region. It remains uncertain to what degree continental remanent magnetization may affect long-wavelength magnetic anomalies. Wasilewski and Padovani (1980) argue that the effect should be minimal, but Galliher and Mayhew (1982) were not able to demon-

strate that fact from an equivalent-dipole analysis of data over the United States.

In the oceanic crust, the highest susceptibility region is in Layers 2 and 3, much nearer to the surface than in the continental crust, and generally well above the Curie isotherm, except right at spreading centers. Thus, oceanic magnetic anomalies should reflect regional crustal thicknesses and susceptibility differences, but generally will not reflect heat flow except in extreme circumstances. Therefore, oceanic basins with a thin magnetized crust are expected to display a negative anomaly relative to continental regions where the crust is generally thicker; but oceanic ridges can yield magnetic highs due to remanent magnetization even at satellite elevations, as has been shown by LaBreque (personal communication, 1983). Topographic variations near ridges, assuming induced magnetization alone, cannot account for the satellite magnetic highs associated with them.

II. DATA REDUCTION

Ritzwoller and Bentley (1982) described a method by which a preliminary map of the crustal scalar magnetic field was produced. The method was designed to filter non-crustal magnetic fields using scalar magnetic field data alone. However, since a great deal of information concerning the strength and direction of field-aligned currents is available in the vector magnetic-field data, the optimal data-reduction procedure must consider the vector data. With this in mind we have followed the data selection and reduction procedure described below in constructing the magnetic anomaly maps found in Figures 5-8.

After the NASA Investigator-B data tape had been translated into Harris-computer compatible code by the program IBMTR (all computer programs referred to in the text can be found in Appendix V) and reformatted by REFMT, the data were in a shape to be reduced and selected. If a pass over Antarctica took place during a relatively magnetically-quiet time period (planetary magnetic activity index, Kp, less than or equal to 1^- for 6 hours), the degree and order 13 spherical harmonic core-field model MGST(4/81) created by Langel et al (1980) and briefly described in Appendix III was subtracted from the scalar magnetic data calculated from the observed vector magnetic data. (The scalar magnetometer onboard the satellite malfunctioned, making it necessary to calculate the scalar field from the vector data.) Of the approximately 2400 passes over Antarctica between Novem-

ber 1, 1979 and April 1, 1980, 212 met this selection criterion; the remainder of the passes were discarded. To these passes a quadratic polynomial was least-squares fitted to the resulting spatial-series in an attempt to filter the effects of magnetospheric ring-currents, core field model bias, and other errors in measurement. (For more details see Langel et al, 1982a).

The vector and scalar magnetic anomalies were, thus, calculated in the following way. Let X_i, Y_i, and Z_i be spatial sequences of observed vector magnetic anomaly data in the right-handed rectilinear coordinate system (x,y,z) in which the positive x-direction is North, y is East, and the z-direction is positive down along a radial vector connecting the satellite with the center of the earth. Then the vector anomalies in each direction are the sequences ΔX_i, ΔY_i, and ΔZ_i calculated as follows:

$$\Delta X_i = X_i - XMOD_i - f_i \tag{1a}$$

$$\Delta Y_i = Y_i - YMOD_i - f_i' \tag{1b}$$

$$\Delta Z_i = Z_i - ZMOD_i - f_i'' \tag{1c}$$

The sequences $XMOD_i$, $YMOD_i$, and $ZMOD_i$ represent the vector core-field model values in the x,y, and z directions, respectively, and the sequences f_i, f_i', and f_i'' are quadratic polynomial sequences each least-squares fitted (Bevington, 1969) to the first two terms of the right-hand-side of (1a), (1b), and (1c), respectively. The quadratic polynomials were fit to the se-

quences in the hope of removing the long-wavelength magnetospheric ring-current effect described by Langel and Sweeney (1971). Magnetospheric fields tend to impart a random "level" offset and bias to each profile that renders the data set inconsistent. It has been shown (Regan et al, 1975) that subtracting a best fit linear, quadratic, or first zonal harmonic fit over a limited latitude range makes the data set internally much more consistent.

The scalar magnetic anomaly sequence, ΔB_i, was calculated as follows:

$$\Delta B_i = \sqrt{X_i^2 + Y_i^2 + Z_i^2} - \sqrt{XMOD_i^2 + YMOD_i^2 + ZMOD_i^2} - g_i \quad (2)$$

where g_i is the quadratic fit to the first two terms on the right-hand-side of (2). Figures 1a-d are graphs of the anomalies created by this process. This procedure was carried out by the program ANTAP. The data were then gridded by the program MRGRD.

At this stage in the processing the majority of the passes still showed field-aligned current effects in the vector data. Figure 1 demonstrates what these effects "look" like in the vector data. Since field-aligned currents, the assumed cause of these high amplitude disturbances, are nearly normal (within 20°) to the satellite's path within the region of high field-aligned current effects, we see from Maxwell's first law:

Figure 1: Example of data from a pass (Pass 51) believed to be relatively unaffected by field-aligned currents. Graphs from top to bottom: scalar anomalies, ΔB; vertical anomalies, ΔZ; radial anomalies, ΔX; and tangential anomalies, ΔY. The ΔB graph explicitly shows the polynomial fit to the data sequence corrrecting the "level offset". For simplicity the vector graphs leave this out.

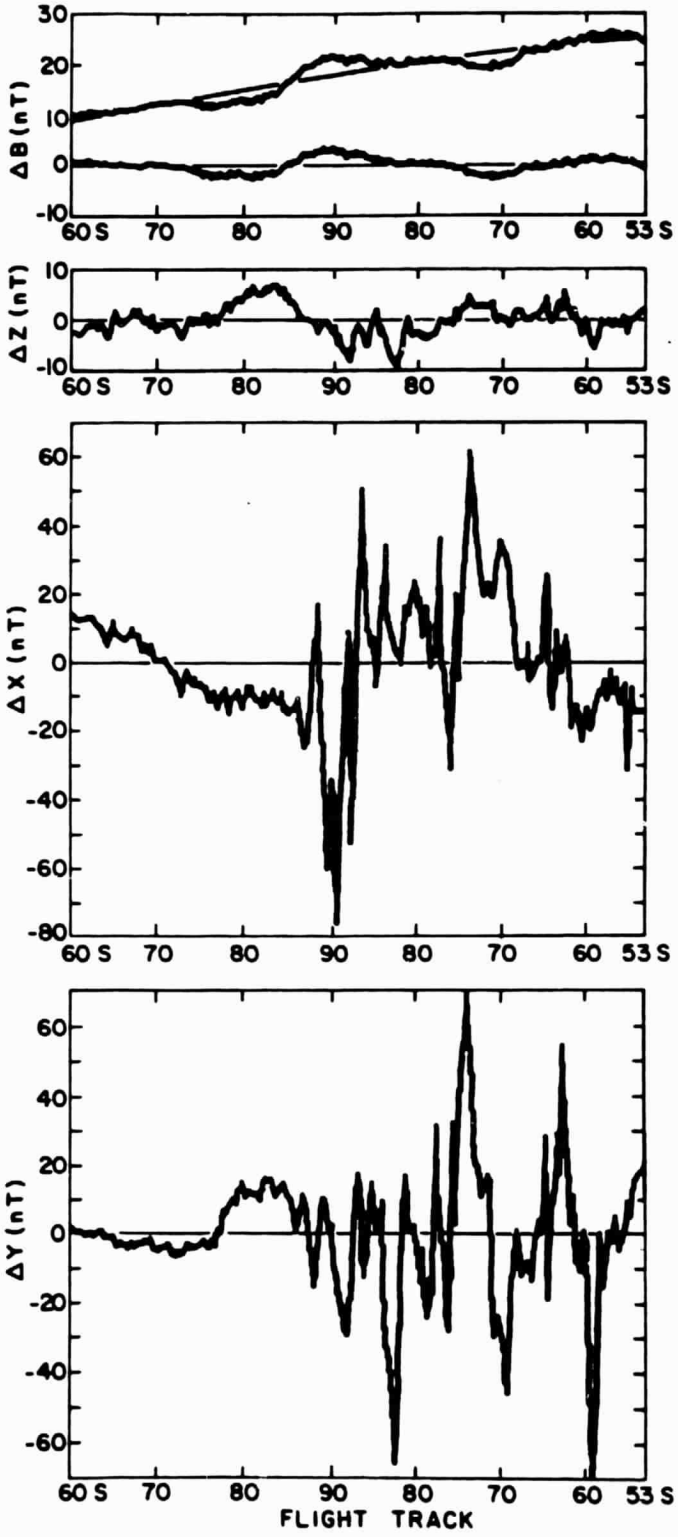

$$\bar{\nabla} \times \overline{\Delta B'} = \bar{J} \tag{3}$$

where $\bar{J}$ represents the time-varying field-aligned current and $\Delta B'$ the magnitude of the magnetic field induced by this current, that:

$$\bar{\nabla} \times \overline{\nabla B'} = J_z \hat{z} \tag{4}$$

where Jz is the component of $\bar{J}$ in the z-direction and $\hat{z}$ is the unit vector in the z-direction, so that if $\overline{\Delta B'}$ = (ΔB'x, ΔB'y, ΔB'z) then:

$$\frac{2}{2x} \Delta B'y - \frac{2}{2y} \Delta B'x = \mu J_z \tag{5}$$

That is, the majority of the magnetic field arising from field-aligned currents is to be found in the horizontal magnetic field. This is observed in Figure 1.

A couple of characteristics of the vector anomalies are worth noting. First, the location of the peaks in ΔX, ΔY, and ΔZ (here and afterwards subscripts will be suppressed) are highly correlated; notably, high-amplitude disturbances in ΔZ (> 25 nT) are always at points at which ΔX and ΔY are also disturbed but with the latter fields having higher amplitudes (50-300 nT). With respect to the horizontal field, a peak in ΔX often corres-

ponds to a peak and a trough pair in ΔY. This effect can be understood if we view the source of the disturbance as a line current nearly normal to the flight path. Then $\Delta B'$, resulting from Jz, will reside in the horizontal plane as shown in Figure 2 in which the satellite is at point A. As the satellite passes through quadrant III of the current's coordinate system, ΔX and ΔY will show effects due to $\Delta B'$. Specifically, ΔX and ΔY will both show negative anomalies due to $\Delta B'$. However, in quadrant IV, ΔX will show a negative anomaly but ΔY will show a positive anomaly due to $\Delta B'$. Table I summarizes the behavior of ΔX and ΔY resulting from crossing a given quadrant of the current's coordinate system. Thus, the disturbances in ΔX and ΔY can be understood as arising from multiple line-current sources, consistent with the belief that field-aligned currents are generating the horizontal disturbances.

Second, it is worth noting the relationship between the scalar anomalies and the vector anomalies from which they are calculated. Since positive ΔZ anomalies are directed toward the earth's surface, the expected positive correlation between the scalar anomaly and the vertical component of the vector anomaly would be expressed in Figures 1, 3, and 4 as negative correlations between ΔB and ΔZ. (In Figure 8, signs have been reversed to bring out the relationship with ΔB.) Thus, due to the nature of the coordinate system (x,y,z) a highly magnetized region of

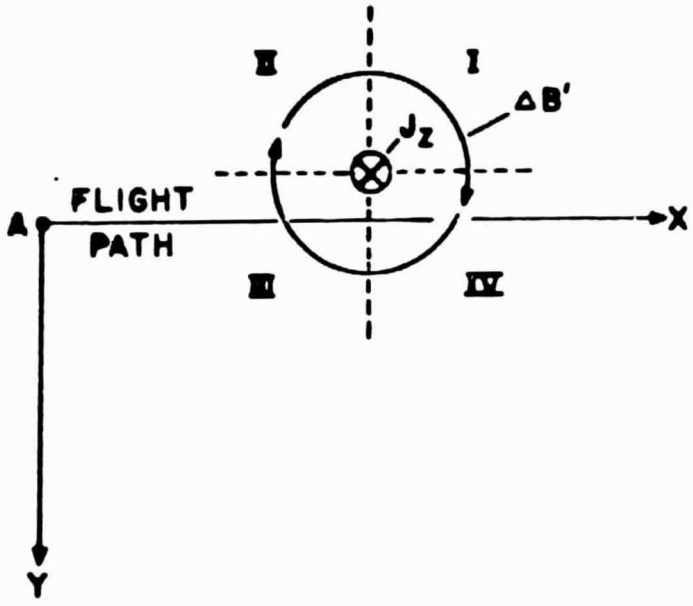

Figure 2: Schematic representation of the magnetic field, $\Delta B'$, generated by a field-aligned current, Jz. The satellite, A, follows the x-axis and crosses quadrants III and IV in the current-centered coordinate system. The effect that $\Delta B'$ has on ΔX and ΔY is summarized in Table I.

TABLE 1

Effect of a Field-Aligned Current on the Horizontal Anomalies in the Current's Four Quadrants

Quadrant	I	II	III	IV
ΔX	Positive	Positive	Negative	Negative
ΔY	Positive	Negative	Negative	Positive

Figure 3: Example of data from a pass (Pass 327) showing signs of a long-wavelength field-aligned current perturbation apparent on the scalar as well as the vector data. Short-wavelength variations apparent in the vector data do not appear on ΔB. This pass was discarded from the data set.

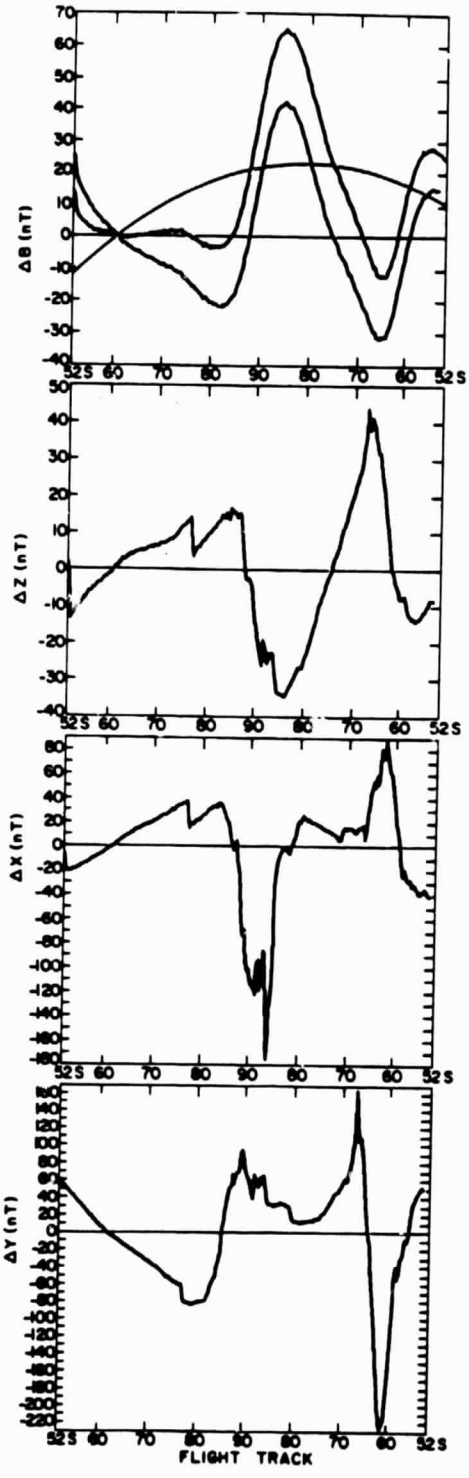

Figure 4: Example of data from a pass (Pass 1887) showing high amplitude short-period field-aligned current perturbations in the vector anomalies which do not appear on ΔB. However, long-wavelength perturbations due to field-aligned currents are believed to exist in ΔB since this pass is poorly correlated with nearby passes. This pass was also discarded from the data set and illustrates the necessity of the use of vector anomaly data to identify the effects of auroral currents.

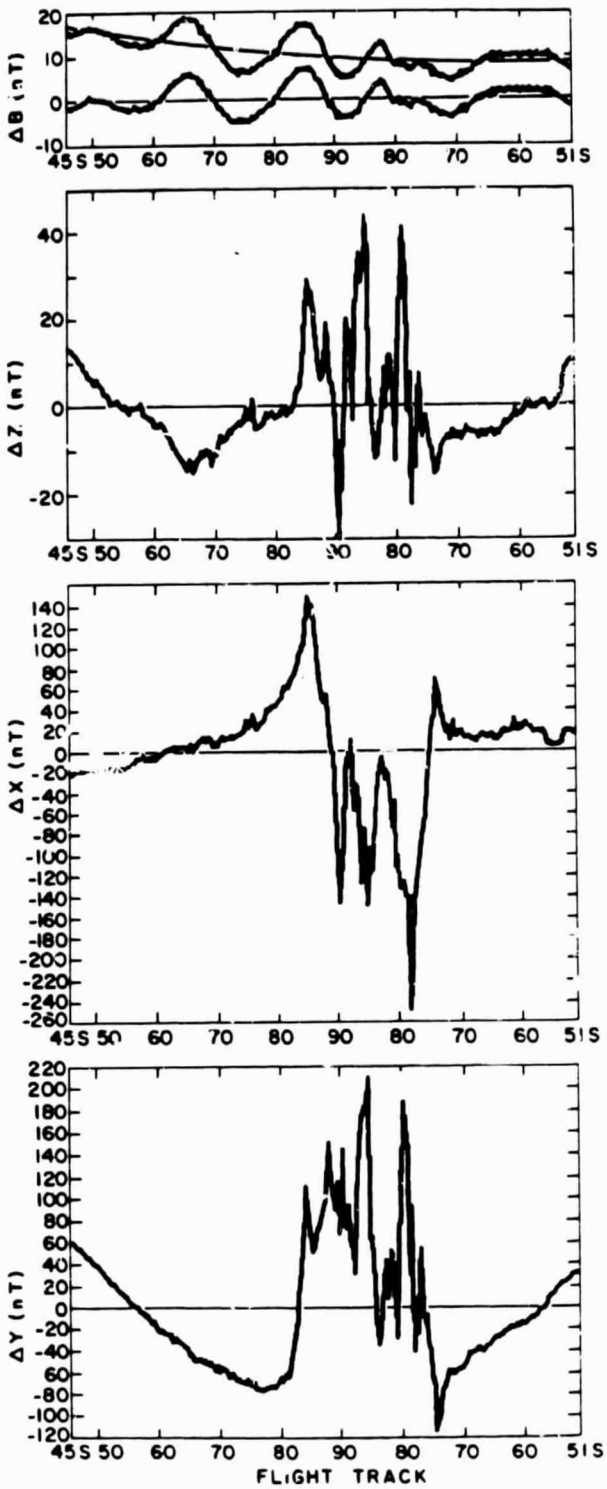

the crust would tend to increase ΔB and decrease ΔZ. Peculiarly, though in Figure 1 ΔZ is roughly anti-correlated with ΔB, it also shows larger high-frequency components and is generally higher in amplitude. Furthermore, the scalar anomalies in every pass do not show the high frequency variations which are observed in the vector anomalies. Data processing has been carefully checked and no unwanted averaging or low pass filtering has been performed. Furthermore, the effect is not observed at lower latitudes so that magnetometer error is unlikely. Thus the effect appears to have a physical source, presumably the field-aligned sheets (see Appendix IV). To a first approximation these may be viewed as carrying the same current density, and as being of large horizontal extent. Since the current is upward in one sheet and downward in the other, and since the magnetic field caused by a current sheet at a distance small with respect to the horizontal extent of the sheet depends only upon the current density and not upon that distance, the net effect observed in passing through the paired sheets would be a rotation of the ambient magnetic field without a change in its magnitude.

Interestingly, longer-period variations in ΔZ are observed in ΔB but the short-period variations superimposed on these are not observed (Figures 3a-d). Apparently either the fields produced by the two current sheets are not the same at longer

periods, or the longer-period effects result from currents elsewhere in the ionosphere or magnetosphere.

These examples show that studies performed with a scalar magnetometer alone will not be able to determine if moderate field-aligned currents are affecting a pass. Thus, the scalar anomaly map of Ritzwoller and Bentley (1982) is probably affected by field-aligned currents whose signatures were indistinguishable from crustal signatures in this scalar study. However, if by use of a vector magnetometer one can determine that high-amplitude rapid variations exist in ΔZ, then field-aligned currents are affecting the data and the pass can be deleted even though the scalar profile looks quite calm (Figures 4a-d). The pass represented in Figures 4a-d would provide undesirable scalar data. If the anti-correlation between ΔB and long-period variations in ΔZ is quite high, then the effect of field-aligned-currents can be taken as minimal.

With this in mind we have further required each pass to satisfy the following selection criteria to be accepted as an "unaffected" pass:

a. the maximum amplitude of the vertical vector anomaly, ΔZ, is less than 25 nT
b. the maximum amplitude of the scalar anomaly, ΔB, is less than 20 nT
c. ΔB and $-\Delta Z$ are highly correlated.

The data selected in this manner appear to strike the balance between the procession of desirable data density (approximately one pass per 2° on the average) and the minimization of field-aligned current effects. The scalar and vector magnetic anomaly data from the 88 passes satisfying these criteria were separately averaged in square bins measuring 330 km on a side and standard deviations were calculated. This was performed by the programs BIN and RDBIN. The data density for the 24 x 24 array centered on the geographical South Pole is found in Table I, Appendix VI. Tracks of these 88 passes can be seen in Figure 10 and pass numbers, dates, times, magnetic activity indices, and average elevations for each pass are listed in Table II, Appendix VI. Since NASA's pass numbering system begins each pass in the middle of Antarctica, each flight over Antarctica contains

Figure 5: MAGSAT total-field magnetic anomaly map over Antarctica. Units in nT. Average elevation 470 km. Capital letters indicate the approximate location of: A - Bellingshausen Abyssal Plain; B - Weddell Abyssal Plain; C - Enderby Abyssal Plain; D - Wilkes Abyssal Plain; E - Maud Rise; F - Kerguelen Plateau; G - juncture of the Mid-Indian Ocean Ridge and the East Pacific Ridge; H - South Sandwich Islands; I - Antarctic Peninsula; J - Ellsworth Mountains; K - Queen Maud Land; L - Enderby Land; M - Amery Ice Shelf/Lambert Glacier; N - Wilkes Land; O - Transantarctic Mountains; P - Ross Sea embayment; Q - Marie Byrd Land; R - Thurston Island; S - Gamburtsev Mountains; T - Weddell Sea embayment.

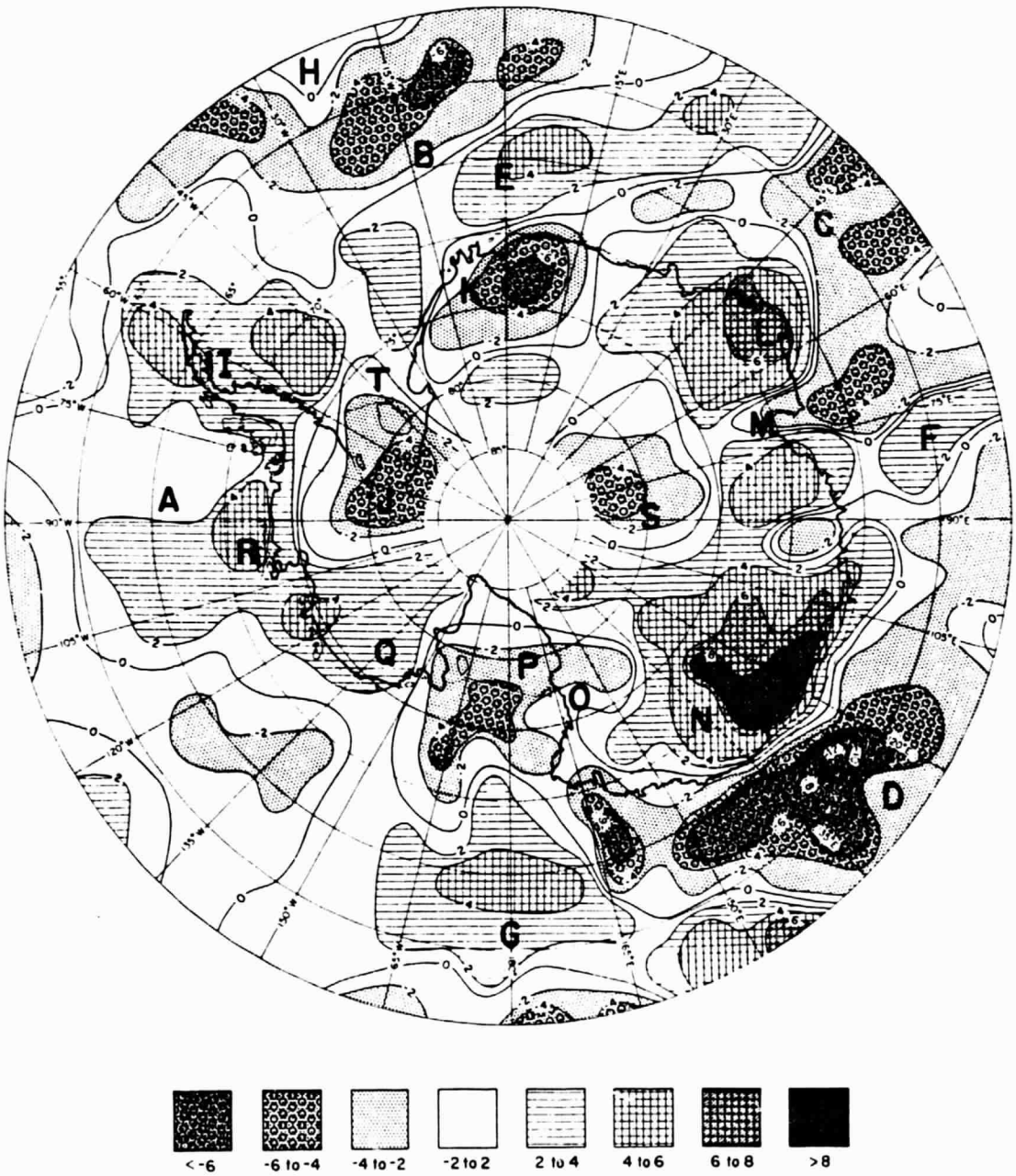

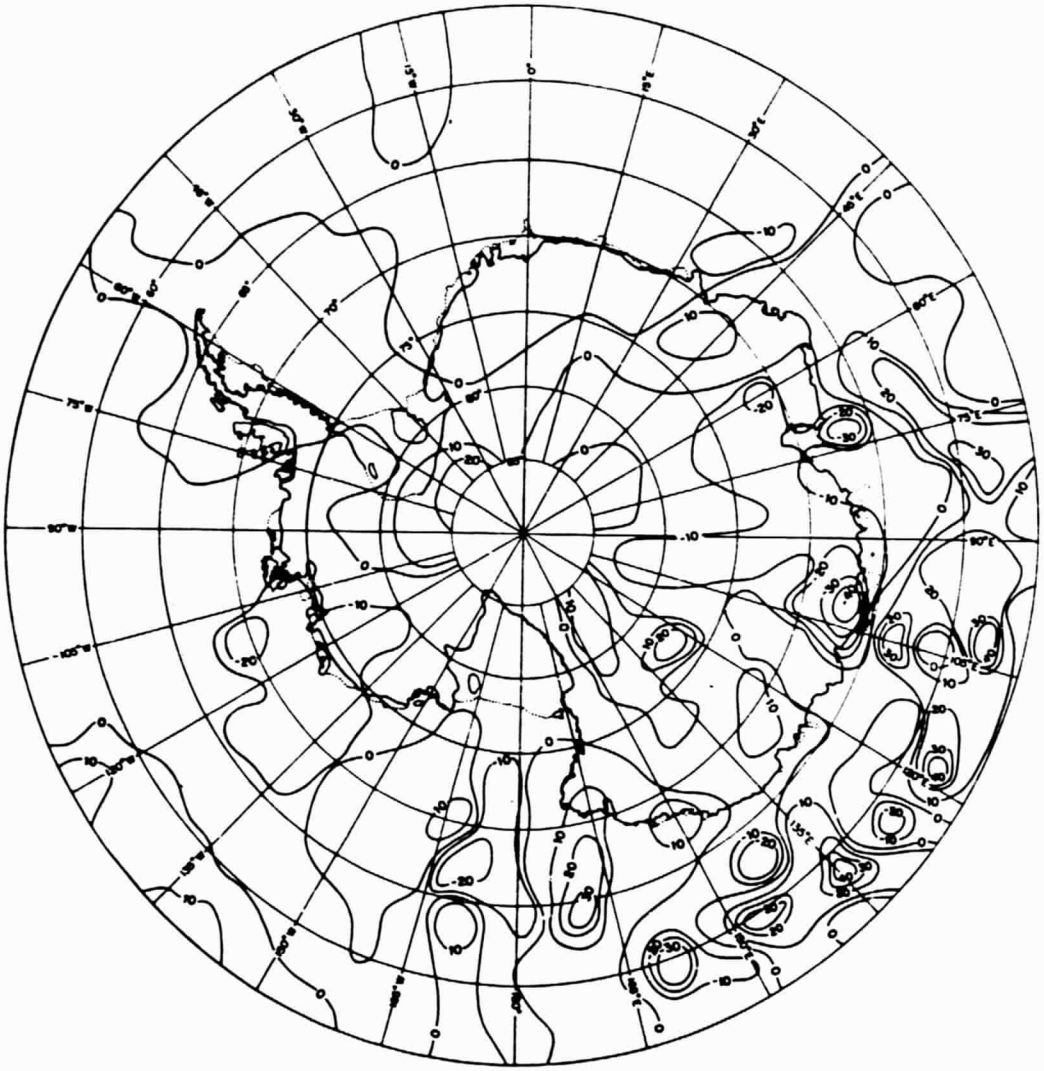

Figure 6: Radial, ΔX, anomaly map. Positive field directed radially away from the South Pole at each point. Average elevation: 470 km. Average standard deviation: 4.3 nT. Contour interval: 10 nT.

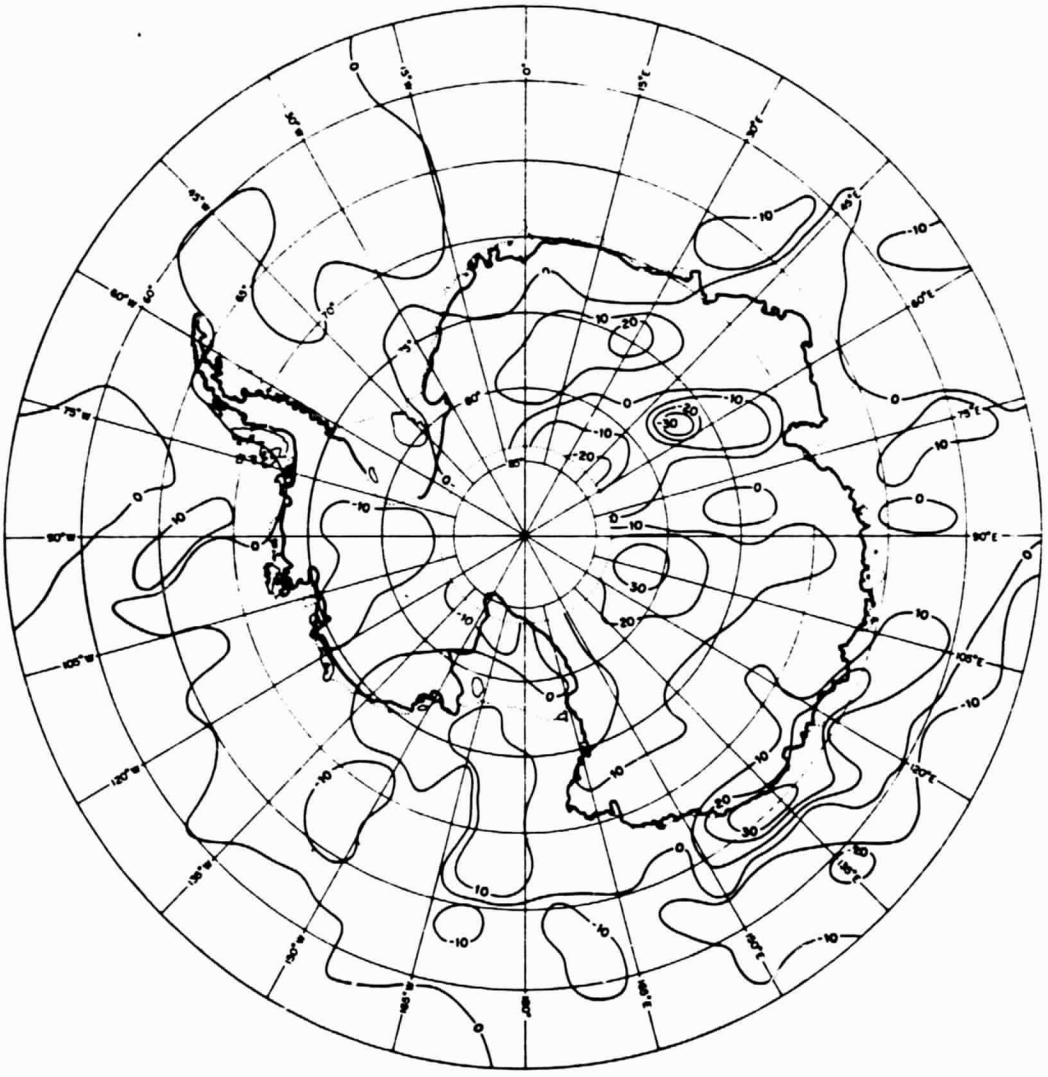

Figure 7: Tangential, ΔY, anomaly map. Field directed tangentially to latitude circle at each point. Positive is clockwise. Average elevation: 470 km. Average standard deviation: 4.3 nT. Contour interval: 10 nT.

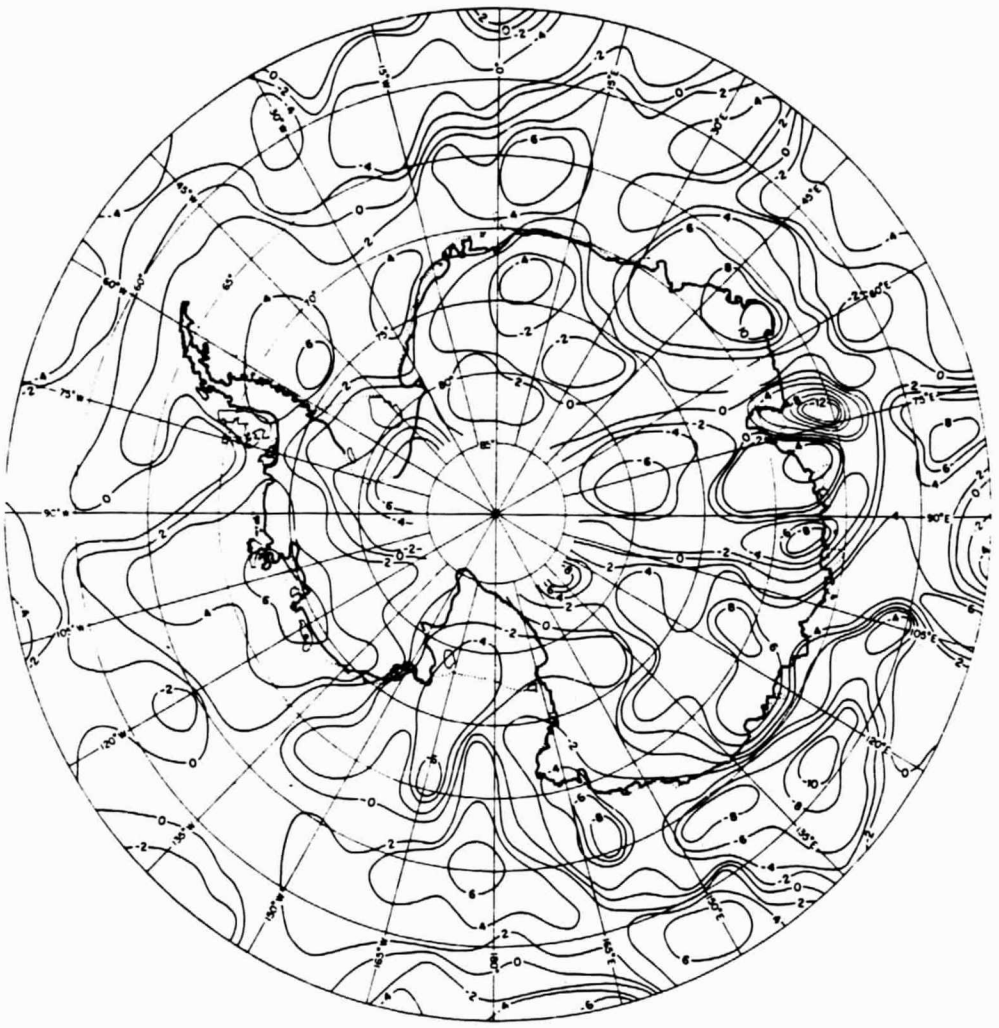

Figure 8: Vertical, ΔZ, anomaly map. Signs of anomalies reversed from the profile data so that positive is directed away from the earth's surface. Average elevation: 470 km. Average standard deviation: 2.0 nT. Contour interval: 2 nT.

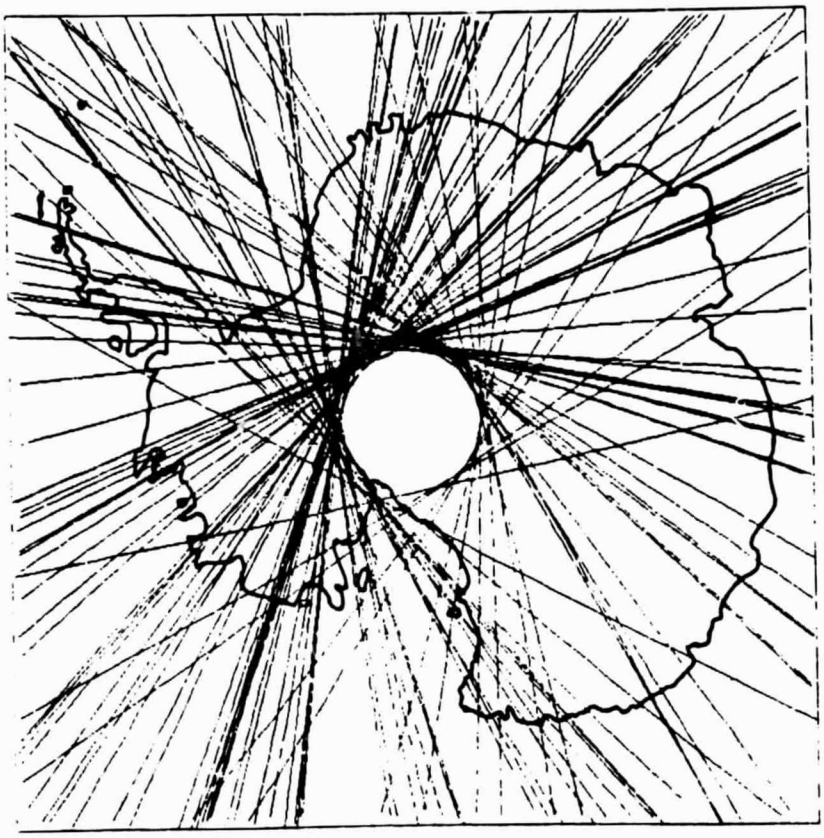

Figure 9: Approximate flight paths of the 88 passes over Antarctica used as data in this study.

data from two of NASA's passes. We have adopted the following convention in referring to pass numbers: our pass n contains data from NASA's south-going pass n and north-going pass n + 1. However, when referring to other characteristics of our pass n over Antarctica, such as dates, times, etc., we have chosen these values from NASA's pass n + 1 since these values were determined when the satellite was at its southern node.

In constructing Figures 5-8, if any ΔB, ΔX, ΔY, and ΔZ values within a bin departed, respectively, by more than 4, 10, 10, and 5 nT from the average for that bin, these data points were rejected and the averages and standard deviations recomputed. Between 10 and 15% of the data were rejected on this basis. The average ΔB, ΔX, ΔY, and ΔZ anomaly values for each bin in the 24 x 24 array can be seen in Tables III-VI, Appendix VI.

If data are nearly normally distributed within each bin, magnetic values will cluster around the bin-average which is hoped to be close to the magnitude of the crustal field. Field aligned currents will create data values well away from the bin-average, though to the degree these effects are random around the bin-mean, averaging will diminish their effect by cancellation. A map of the scalar-map bin-standard-deviations, calculated before discarding data based on the 4 nT discardal-criterion, shows that in 3 of the 4 quadrants the anomalies of Figure 5 are based on data with standard deviations less than 3 nT. However, in the grid-southeast quadrant, the quadrant nearest to the geomagnetic

South Pole, standard deviations are significantly higher, ranging up to 6 nT. Thus, the features in the grid-southeast quadrant of Figure 5 have to have larger "mental" error-bars assigned to them than the features in the remaining quadrants. As will be discussed in section III, possible perturbations due to the horizontal anomaly can be seen in Figure 13. The continental portion of the grid-southeast quadrant is relatively unaffected by the horizontal component of the magnetic anomalies. Thus, the large variances in this quadrant must be due to variations in ΔZ. However, discarding data more than 4 nT from the bin-average acts to delete "affected" data points so that the recalculated bin-average should be closer to the value of the crustal field. This reduces the size of errors in all quadrants appreciably. Non-normal distributions of data within a bin (e.g. bimodal distributions) will make this technique sub-optimal, however visual scrutiny of the data indicates that most values do lie around the mean with a smaller percentage of outliers on either side.

Finally, the bin-values were hand-contoured yielding the maps in Figures 5-8, in which the average bin elevations for each map is approximately 470 km and the average bin standard variations are 1.5, 4.1, 4.3, and 2.0 nT, respectively. The ΔZ map in Figure 8 contains a sign reversal so that the correlation with the scalar anomaly map will be clearer. The subtraction of the polynomial makes the map-average the zero-level on each map.

This zero-level is arbitrary but reasonable. Since the map is comprised of approximately half continental and half oceanic regions, the former on the average higher in magnetic amplitude than the latter, this choice of zero-level approximately bisects the interval between oceanic basin lows and thick continental highs. This is a desirable location for the zero-level. Notice that in Figure 5 the zero-contour approximately corresponds to the edge of the continental shelf between the Wilkes Land magnetic high and the Wilkes Abyssal Plain low, as we would desire.

The anomalies on these maps have not been reduced-to-the-pole nor have data been continued to a single elevation before processing. However, since all of Antarctica is above 60°S geomagnetic latitude, reduction-to-the-pole will have minimal effect. Furthermore, studies performed elsewhere (R. Sailor, personal communication, 1982) indicate that maps created in the way described above are "qualitatively and quantitatively similar" to those continued to the average-bin elevation from the same data set, using the equivalent source technique of Mayhew (1979). That is, effects due to data points that are higher than average approximately balance the effects due to points lower than average so that their net effect on the average is small. Since fewer passes meet the selection criteria at high latitudes the data set is less dense so that cancellation will be less perfect than in lower latitudes. A map consisting of average-bin eleva-

tions shows considerable variability, but the elevation variations appear to be unrelated to variations appearing on the scalar anomaly map in Figure 5. Furthermore, the data set has been partitioned into two subsets, one containing data from passes with an average elevation less than 475 km and the other containing data with average elevations greater than 475 km. Each subset contains 44 passes. The maps are highly correlated with each other and with Figure 5, though, as expected, the lower elevation map shows anomalies with somewhat larger amplitudes than the anomalies in Figure 5. These tests appear to indicate that elevation variations in the data have not generated an appreciable error in Figure 5.

III. ORIGIN OF THE ANOMALIES

A. Scalar Anomalies

The reduction of the data consisted of modeling magnetic fields generated in the core and magnetosphere and discarding passes which showed signs of severe field-aligned current effects registered in the vector anomalies. Any remaining field-aligned current effects random within the five month data window are hoped to be stacked out in creating the 3° square bins. How successful have we been at eliminating fields from each of these sources in the scalar anomaly map?

First, considering the accuracy of the core-field model, Carle and Harrison (1982) have argued that the field remaining after removal of the spherical harmonic core-model will have a significant long-wavelength component. The majority of the core field remaining after removal of the model field is of very long spatial-wavelengths and is removed by the polynomial fit to the data. It is unclear what percentage of the remaining anomalies is due to the core, though it is reasonable to believe that a fraction of very long-wavelength anomalies (> 3000 km) has its origin in the core. We believe that this fraction is insignificant.

Figure 10 shows the two-dimensional finite Fourier transform of the map in Figure 5. A significant amount of the power is in wavelengths greater than 3000 km. However, we will argue that

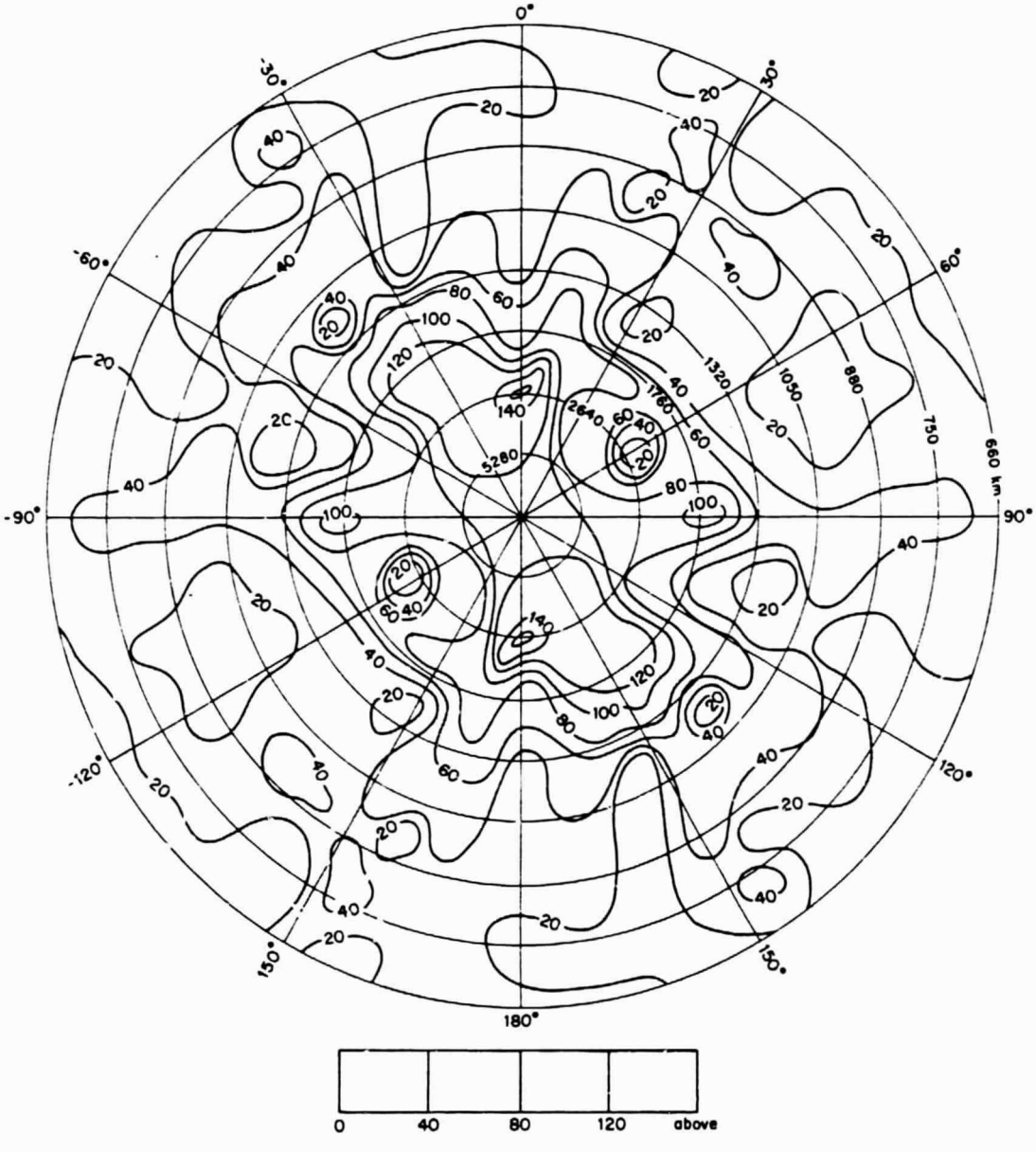

Figure 10: Two-dimensional finite Fourier transform of a 36° x 36° centered square subset of the bins of data used to construct Figure 1. Nyquist wavelength is 660 km and the D.C. component is at the center. Contour interval is 40 nT/cycle.

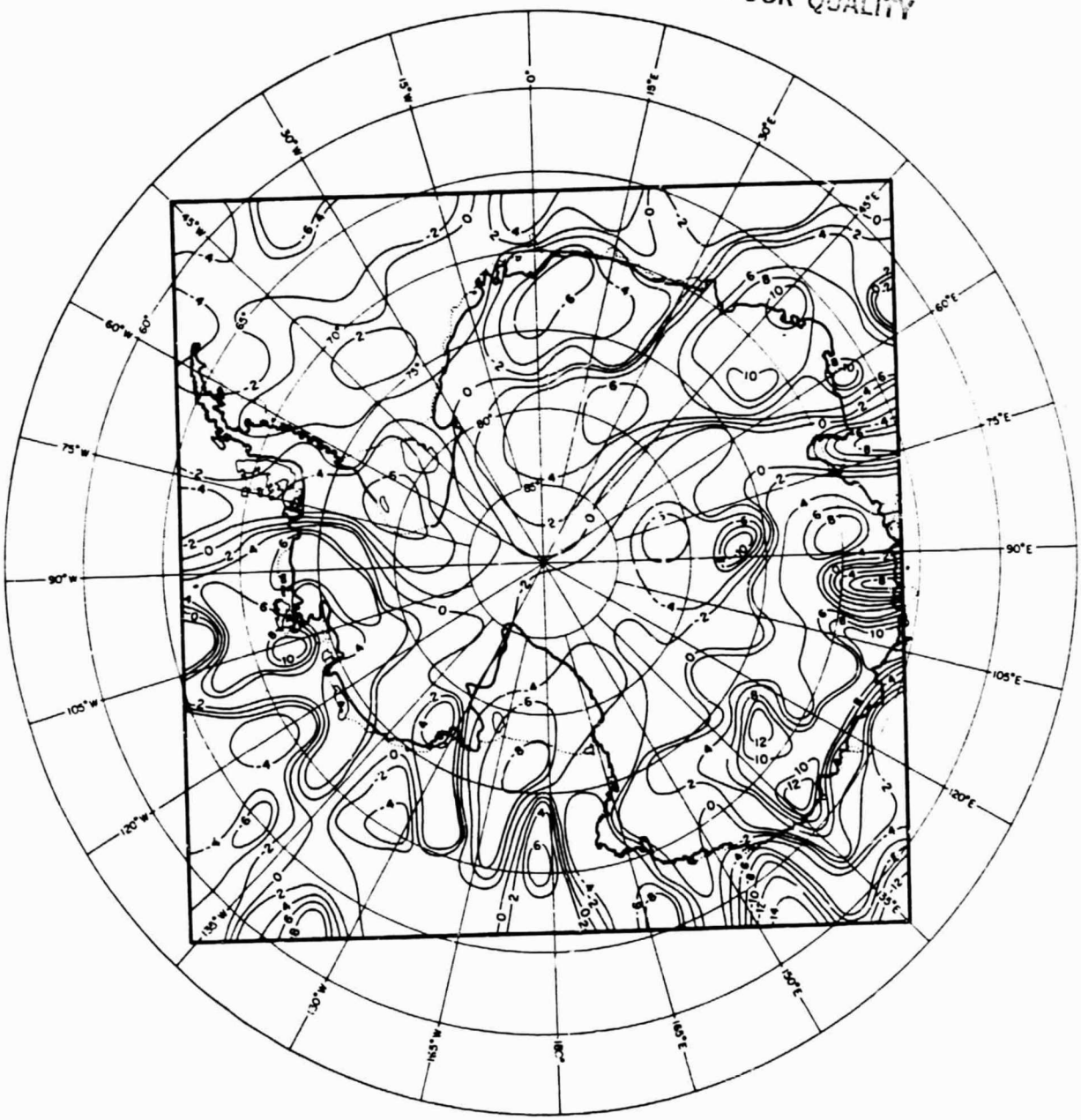

Figure 11: Scalar anomaly map constructed by use of the two-dimensional finite Fourier transform filter described in Appendix II.

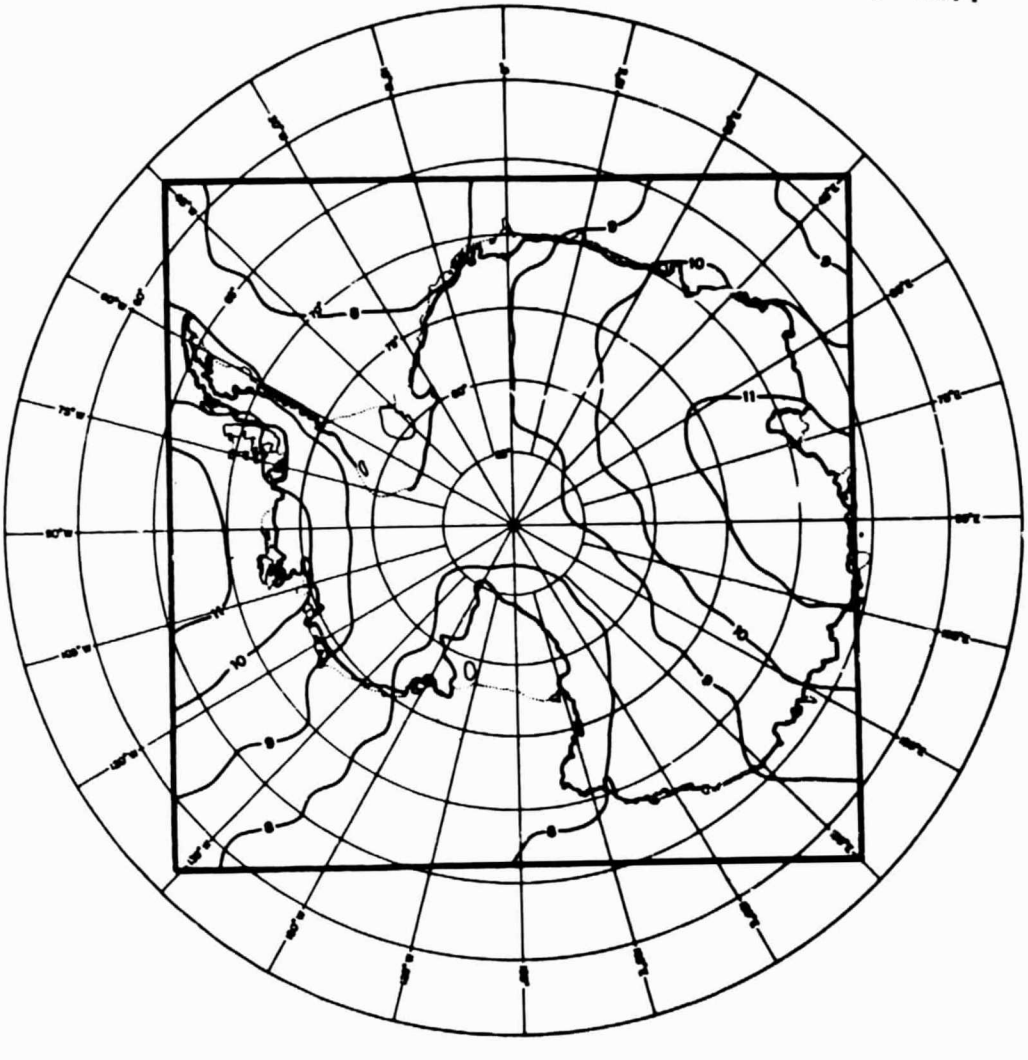

Figure 12: Static field model produced by the two-dimensional finite Fourier transform filter described in Appendix II.

the source of a large fraction of this power is believed to reside outside the core. In Appendix 2 we describe an alternate method for deriving a scalar magnetic anomaly map using two-dimensional Fourier filtering rather than one-dimensional polynomial fitting to each pass. Figure 11 is the scalar anomaly map derived by this procedure and Figure 12 is the model of fields derived in the core (which have not been filtered by MGST(4/81)) and in the magnetosphere. Figure 12 is just the difference between a map of B-BMOD and a high-passed version of this map, where $b = \sqrt{X^2 + Y^2 + Z^2}$. Since the core field is relatively static over the five-month data window, Figure 12 is believed to be a good model of the fields generated in the core greater than 4000 km in wavelength remaining after the removal of MGST(4/81). Since the qualitative correlation between Figures 5 and 11 is high and core field effects due to wavelengths greater than 4000 km are believed to be successfully filtered from Figure 11, the long-wavelength power in Figure 5 is probably not due to the fields arising in the core which have not been successfully filtered. This argument only holds for wavelengths greater than about 4000 km. However, Langel and Estes (1982) have shown that the maximum amplitude of the core field between about 3000 km (GSFC(9/80) degree 13) and about 4000 km (GSFC(9/80) degree 10) wavelengths is approximately 20 nT at the earth's surface. (The core field model in our study removed terms of these wavelengths.)

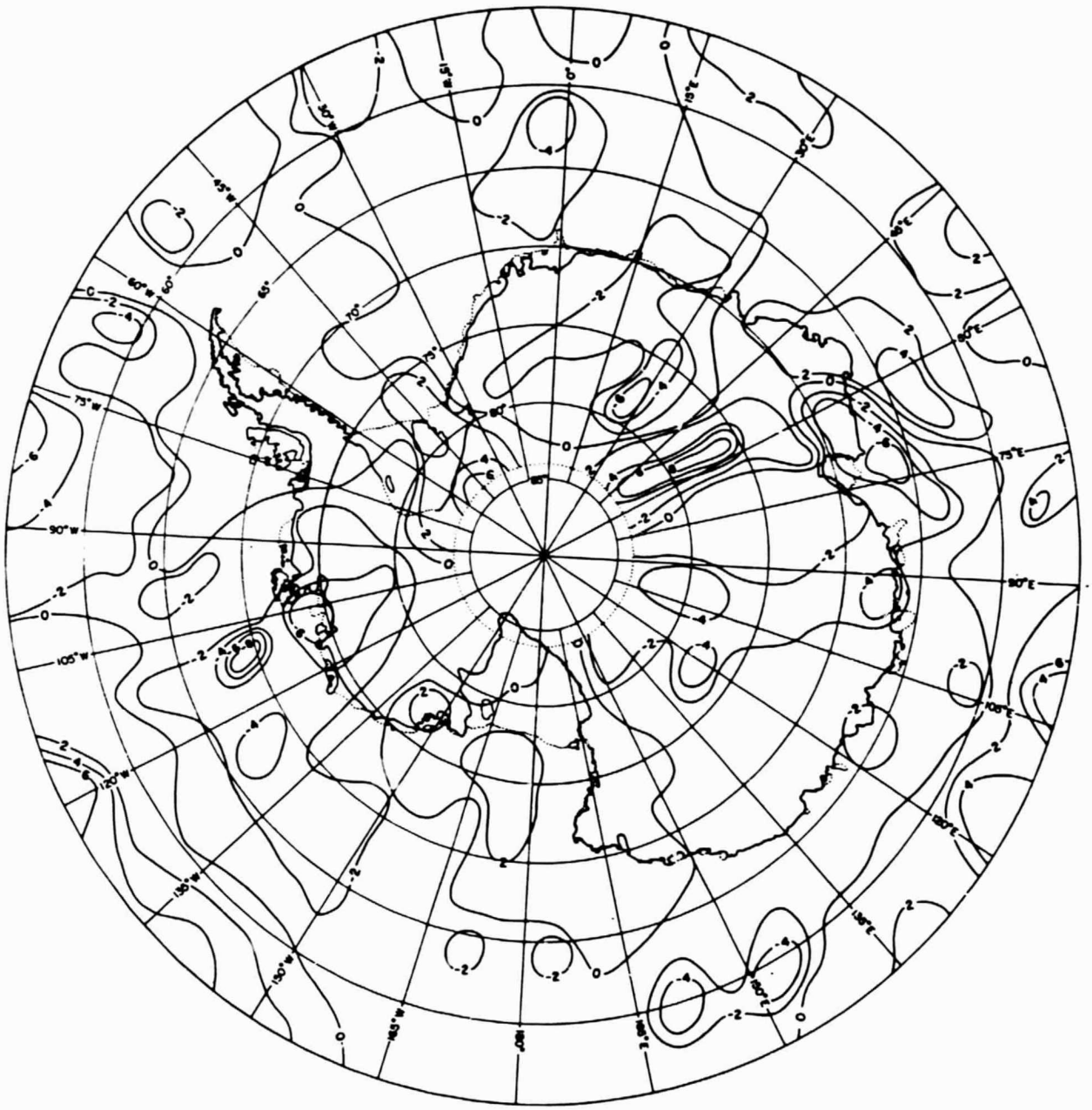

Figure 13: Map of perturbations in the scalar field due to the horizontal anomalies found in Figures 6 and 7, if these anomalies are stable over MAGSAT's lifetime.

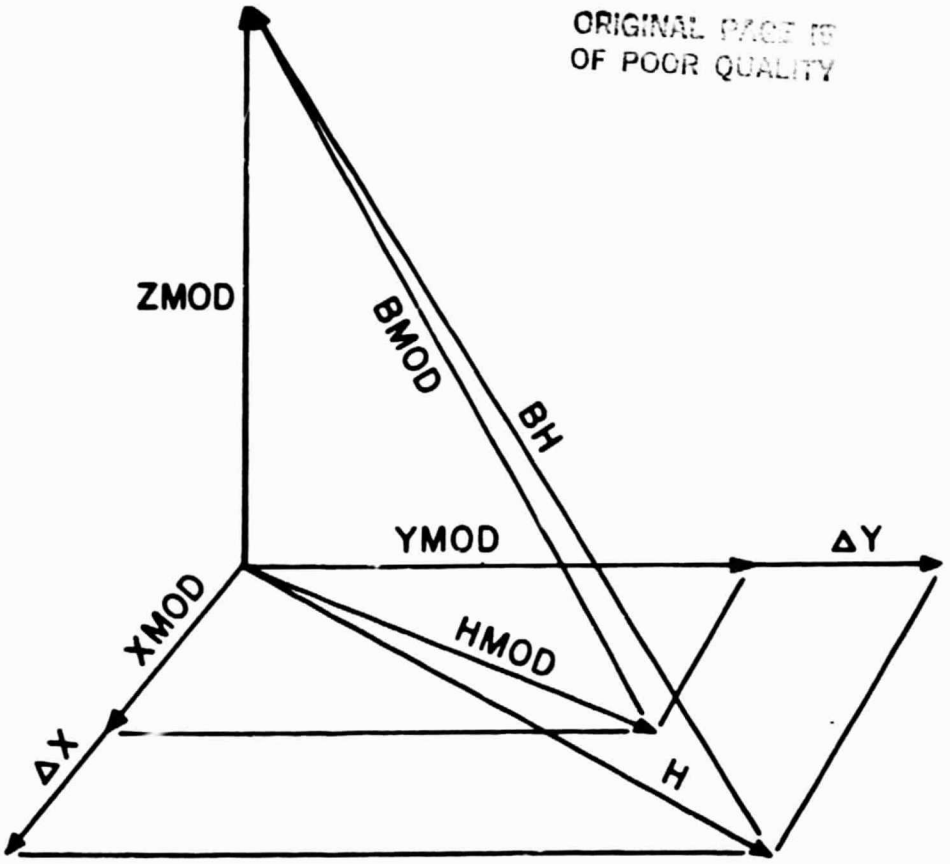

Figure 14: Schematic drawing showing how variations in the horizontal field can create perturbations in the measured scalar field. XMOD, YMOD, and ZMOD are the components of the core-field model; HMOD is the amplitude of the horizontal model field; BMOD is the amplitude of the scalar core-field model; ΔX and ΔY are anomalies in the x and y directions, respectively; H is the horizontal component of the measured field and BH is the measured scalar field resulting from the core field and horizontal anomalies. Then BH-BMOD is the perturbation in the scalar field caused by the horizontal anomalies.

Errors in the model between wavelengths of 3000 and 4000 km, a fraction of the field at these wavelengths, should be insignificant in relation to the fields generated in the crust. Therefore, it appears that the long-wavelength magnetic anomaly features in Figure 5 are on the average not due to fields generated in the core.

Second, since the major source of magnetospheric fields measured near the earth is due to equatorial ring currents found at an elevation exceeding three earth radii, the d.c. component of the ring current would generate a very long-wavelength magnetic field over Antarctica. Furthermore, since high power terms of the magnetospheric field change only very slowly in relation to the 25 minutes it takes the satellite to complete a pass between 55°S and 55°S over the pole (Report of the Kakioka Magnetic Observatory, 1981), magnetospheric fields generated by ring-currents should be well-modeled by a quadratic polynomial fit to the data over Antarctica. (Actually, in hindsight, two quadratics separately fit to half of each pass would have created a better magnetospheric model). Magnetospheric fields should not find their way into Figure 5 in any significant proportion.

This leaves us with the question: do fields generated by field-aligned currents seriously affect the scalar anomaly map? This is a difficult question.

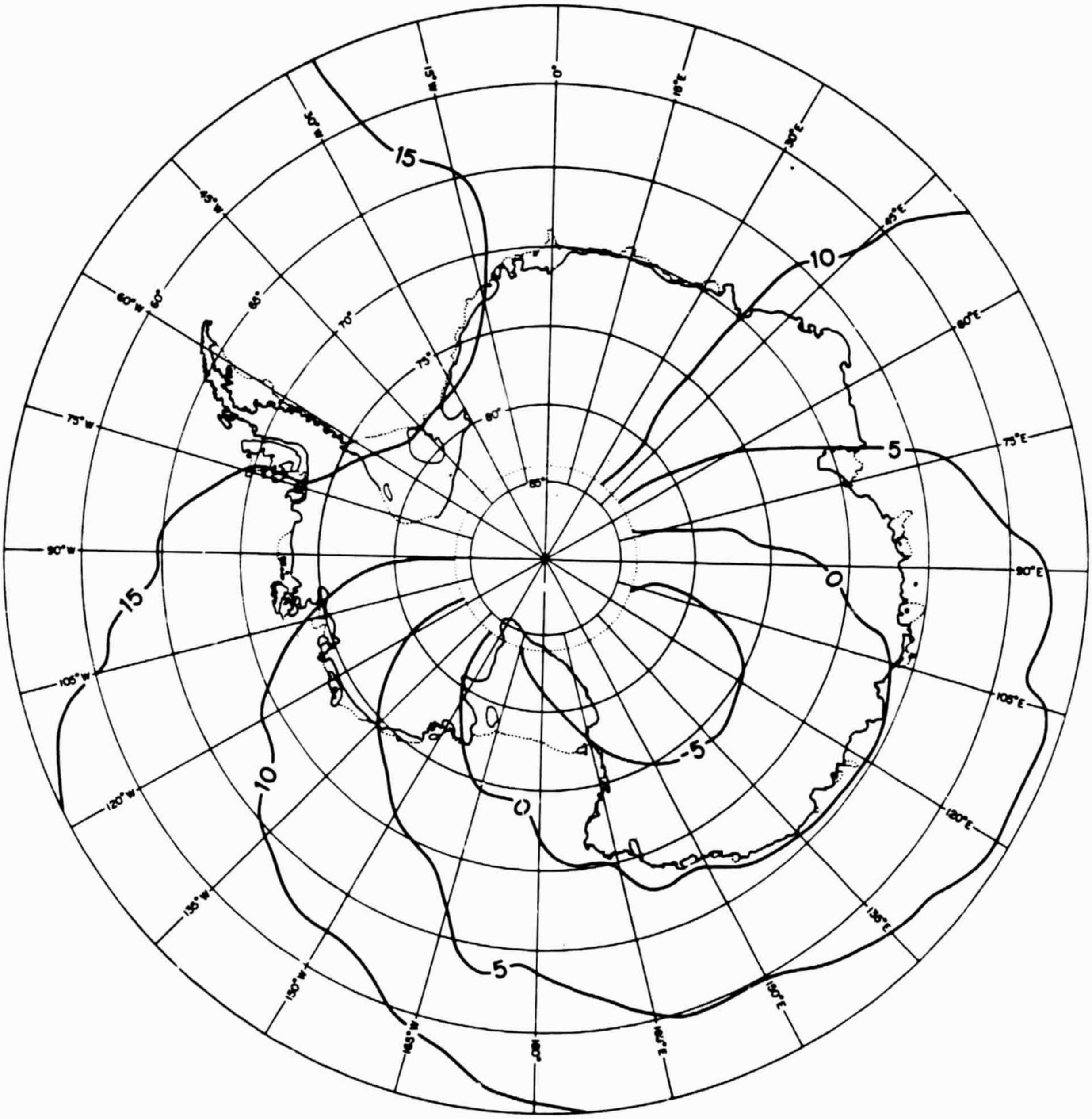

Figure 15: Average vector core-field model, XMOD, in the x-direction (radial). Positive away from South Pole. Contours in 10^3 nT.

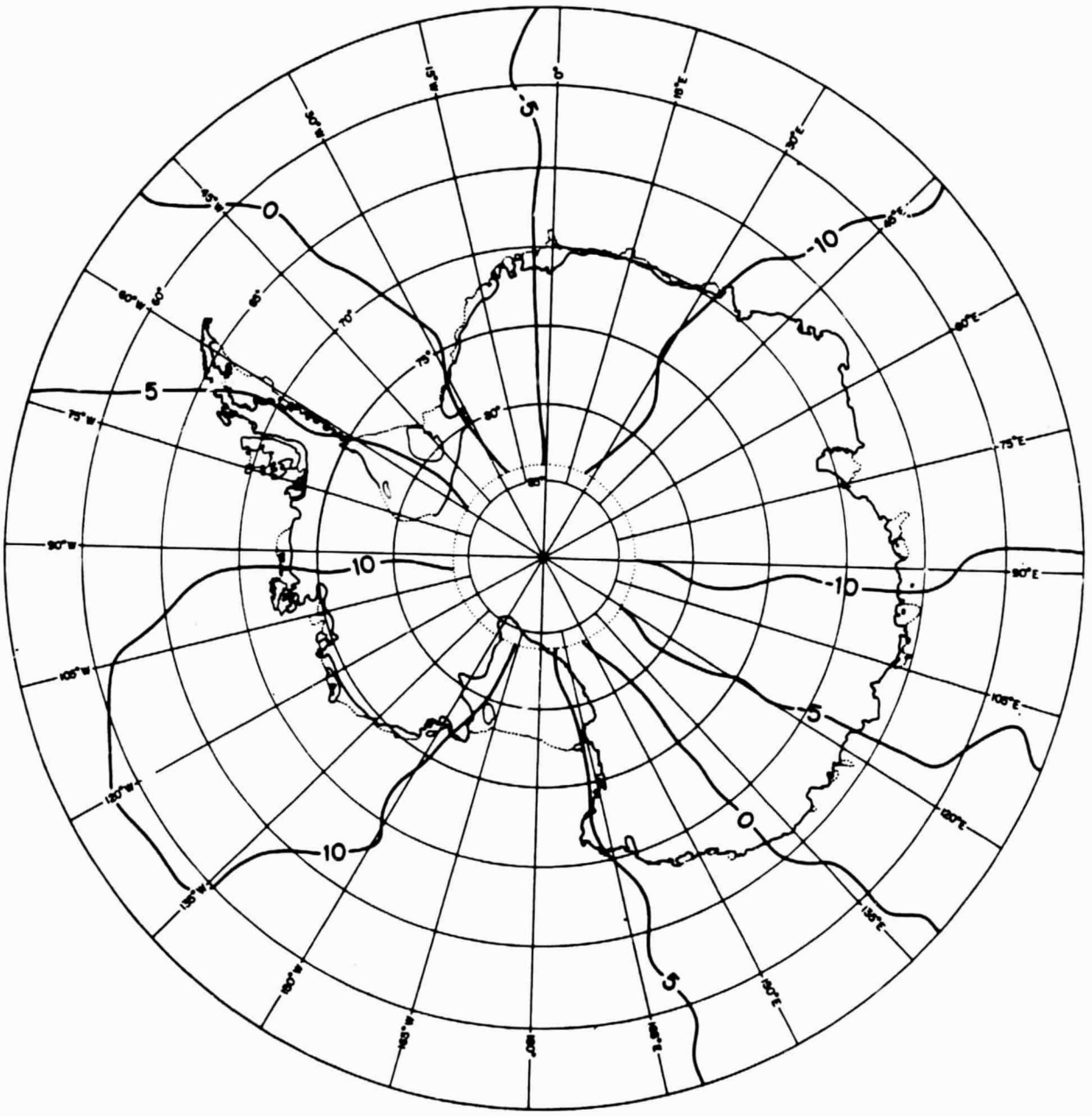

Figure 16: Average vector core-field model, YMOD, in the y-direction (tangential). Positive clockwise. Contours in 10^3 nT.

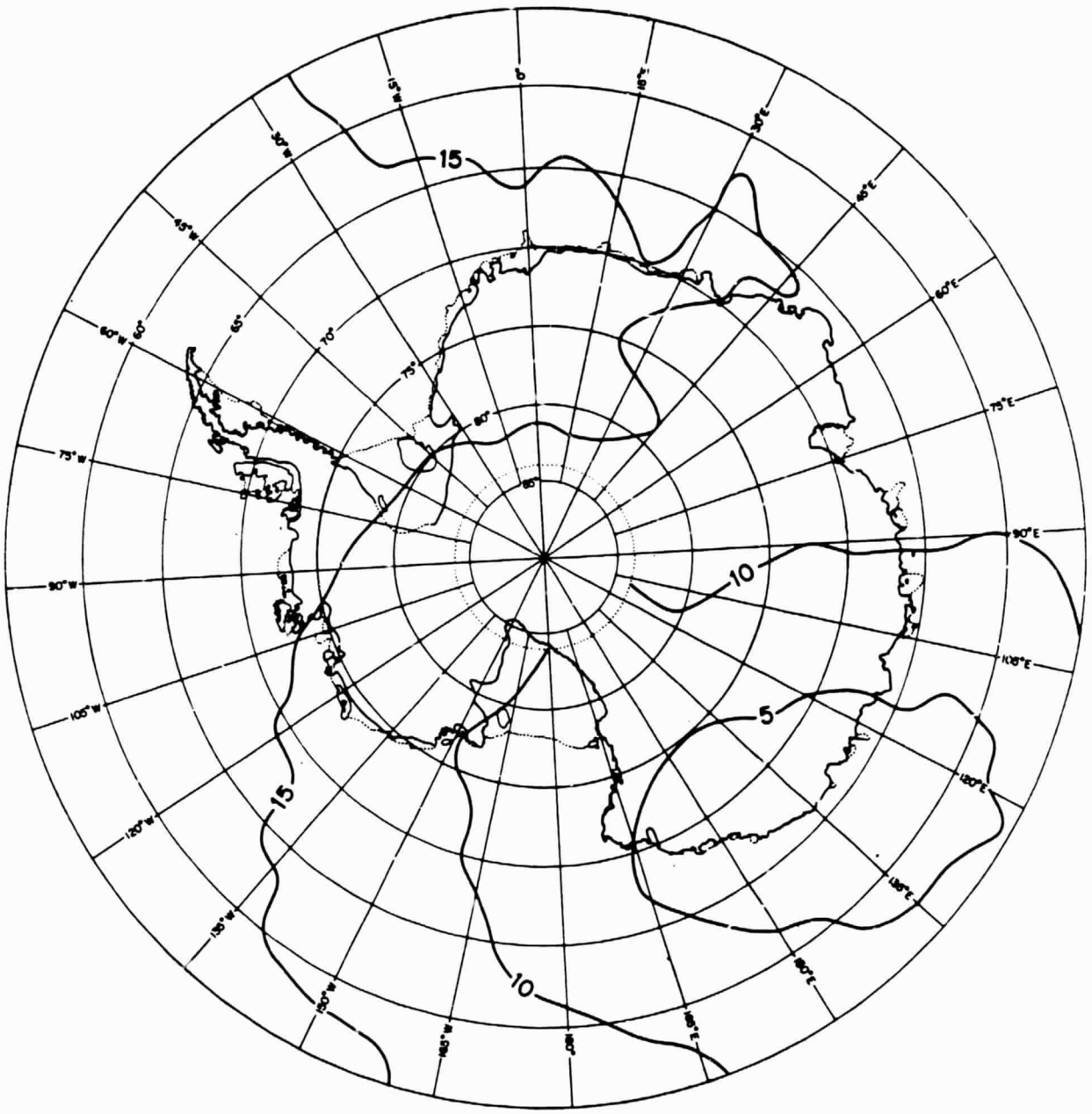

Figure 17: Average horizontal component of the core-field model, HMOD. Contours in -10^3 nT.

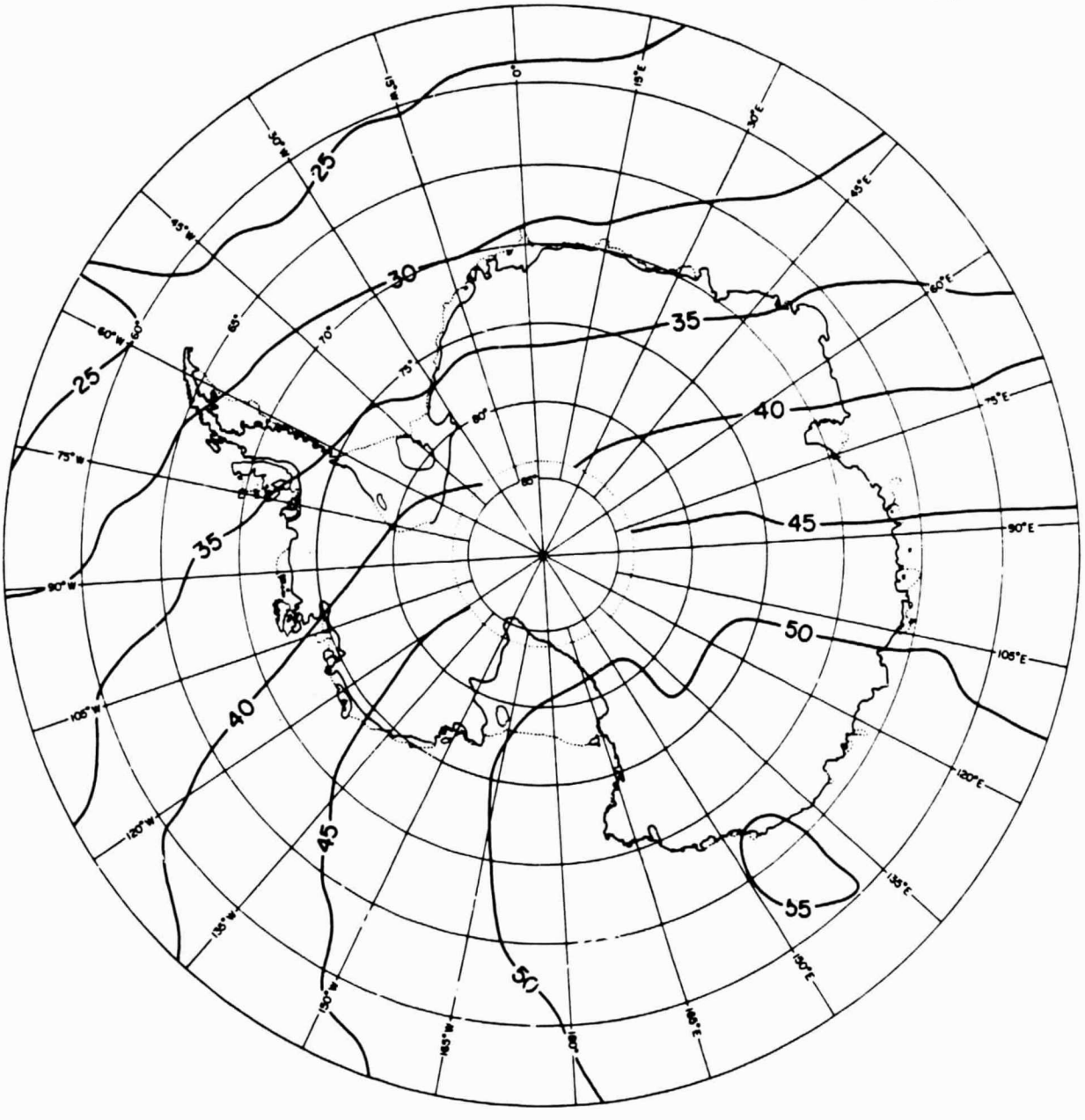

Figure 18: Averaged vertical component of the core-field model, ZMOD. Positive out of page. Contours in 10^3 nT.

The vector core field model (XMOD, YMOD, ZMOD) in Figures 15, 16, and 18 varies over Antarctica so that the relationship between the horizontal field and the vertical field changes during a flight pass. In areas away from the geomagnetic south pole the horizontal component of the core model field, HMOD in Figure 17, will be a large fraction of the vertical component, ZMOD, making variations in the horizontal anomaly $\sqrt{H = (\Delta X^2 + \Delta Y^2)}$, more likely to contribute to ΔB. However, auroral phenomena away from the geomagnetic pole are less intense so that it is rather unclear which areas are expected to be most affected by the field-aligned currents. Nevertheless, in all auroral regions, variations in ΔZ due to field-aligned currents should contribute to perturbations in ΔB. However, as shown in Section II, high-frequency field-aligned current effects do not find their way into ΔB, though longer-period variations in ΔZ and ΔH may still contaminate the scalar map. If long-period field-aligned current effects exist which perturb all three components of the vector magnetometer, then the scalar anomaly would show field-aligned current effects also. The horizontal anomalies are the places to look for the presence of field-aligned current effects.

If we assume that Figures 6 and 7 represent the magnetic fields in the North and East directions generated by the long-period components (> 5 months) of the time-varying field-aligned currents, then Figure 13 is the map showing the perturbation

these fields have on the scalar anomaly map. The values on the map were calculated in the way illustrated in Figure 14, in which BMOD is the value of the scalar core field model and BH is the scalar field containing perturbations due to ΔX and ΔY. The values of BH-BMOD for each bin is what is found in Figure 13. The poor correlation between Figures 13 and 5 probably implies that the ΔX and ΔY maps are not good representations of the long-period field-aligned current effects. However, if we retreat a little and only assume that Figures 6 and 7 indicate the general location of the long-period anomalies if, indeed, they exist, then Figure 13 would be interpreted as flagging areas of potential perturbation in the scalar anomaly map. The notable continental areas sensitive to perturbations in the scalar field then would be the Pensacola Mountains region, the region inland of Thurston Island in Marie Byrd Land, southern Enderby Land, and the Amery Ice Shelf region. These features all lie within the region between 10° and 25° of the geomagnetic south pole in the region of highest field-aligned current activity. However, too much should not be read into this since most of Antarctica lies between these latitudes. To the extent that we believe that long-period field aligned current effects exist and that Figures 6 and 7 capture the general location of these effects, we have to be concerned about the possibility of fields generated by field-aligned currents intruding the scalar anomalies in Figure 1.

Further tests concerning the existence of fields generated by long-period field-aligned currents are continuing to be run.

Even though sensitive areas exist in Figure 13, two factors contribute to the belief that the anomaly features in Figure 5 are mostly not the result of field aligned currents. First, a necessary characteristic of fields generated in the earth's crust is temporal stability over periods during which the inducing field and the thermal conditions of the studied area change little. Comparison of Figure 5 with the POGO map generated by Regan et al (1975), shows the good qualitative correlation between the MAGSAT and the POGO scalar anomaly fields. The differences are mainly in amplitude, due to the lower orbit of MAGSAT, and in short-spatial wavelength features, perhaps due to MAGSAT's greater resolution, data reduction differences between the method of Regan et al and ours, or some field-aligned current effects not detectable using POGO's scalar magnetometers. In general, the correlation is quite good, indicating that over the 10 year period spanning the POGO missions and MAGSAT's lifetime, the features represented in Figure 5 are stable. This lends credence to the proposition that the source of the anomalies in Figure 5 lies in the crust. However, it is still unclear if there exists a field-aligned current component stable over this time period, so this argument cannot be taken too far.

Second, however, the correlation between the magnetic anomalies in Figure 5 and known geologic features, especially in oceanic regions, is remarkable. This is interpreted to mean that the crustal field is significantly represented in Figure 5 even where the horizontal field is believed to perturb the scalar field. These correlations will be dealt with in detail in Section IV. Thus, the temporal stability of the anomaly features in Figure 5 together with the remarkable correlation between the anomalies and known geologic structures, lead us to believe that field-aligned currents probably do not severely contaminate the scalar anomaly map except in a few isolated regions.

In summary then, the sources of the anomaly features in Figure 5 appear to reside mainly in the earth's crust since sources below and above the crust appear to have significant effect only in exceptional regions.

B. Vertical Anomalies

The vertical anomaly map found in Figure 8 is in remarkable agreement with the scalar map. This is as we would expect in high latitude regions in which the earth's magnetic field is nearly normal to its surface. The rapid variations in ΔZ observed in Figures 1b and 4b appear mostly to be filtered in the averaging and data-discarding process. However, the amplitudes of the anomalies in Figure 8 generally are greater than those in Fig-

ure 5. It is unclear which map better represents the crustal field, but they are similar enough to make this matter relatively unimportant. Vertical anomalies in Antarctica are of approximately the same amplitude as those found elsewhere in the world.

As shown above, the horizontal anomaly maps in Figures 6 and 7 result mostly from fields generated external to the Earth. We suspect that the vast majority of the power has field-aligned currents as its source. Thus, the amplitude of the horizontal anomalies, found in Figures 6 and 7, can be generally considered to be a good approximation to the amplitude of the field-aligned current effect. Therefore, horizontal anomalies over Antarctica have much larger amplitudes than those over other regions. However, it is unclear if this is related to any real long-period field generated by field-aligned currents, which would perturb the ΔB map, or just to uncompensated random short period variations which are believed not to effect the scalar anomalies.

Crustally-generated magnetic fields over most of the studied region will have a small horizontal component due to the nearly vertical nature of the core field. However, in the low geomagnetic latitudes north of the Antarctic Peninsula, the earth's field has a strong enough horizontal component to register a horizontal anomaly of crustal origin. Unfortunately, however, the contour intervals in Figures 6 and 7 are insufficiently refined to detect a crustal signal in this region. Continental remanent

magnetization may affect the horizontal anomalies if the earth's field was nearly horizontal during the period of batholith solidification. The map resolution problem together with the latitudinal stability of Antarctica during the last 400 million years (implying a vertical geomagnetic field) imply that a remanent effect probably is not noticeable in Figures 6 and 7.

IV. GEOLOGICAL INTERPRETATION

The interpretation of MAGSAT data, though still in its infancy, should hold great interest to the Antarctic geoscientist, for here is the first coherent continent-wide data set with information about the Antarctic crust. Furthermore, MAGSAT magnetic anomalies appear to be highly correlated with known Antarctic geologic and tectonic features, especially in oceanic regions where the geology is simplest and best known.

Oceanic magnetic anomalies are almost invariably associated both with basins (negative)(cf. Frey, 1982a) and spreading ridges (positive). (All oceanic feature names will be taken from Heezen and Tharp, 1980.) Three of the four major oceanic basins surrounding Antarctica (the Weddell, Enderby, and Wilkes Abyssal Plains) have strongly negative anomalies associated with them, and even the fourth (the Bellingshausen Abyssal Plain) is relatively low. (Geographic names are indexed in Figure 5.) The most striking conjunction of a positive anomaly with a spreading ridge occurs where the Mid-Indian Ocean Ridge and the East Pacific Ridge meet grid south of the Ross Sea embayment ("grid" directions refer to a Cartesian coordinate system laid across the polar map, with grid north parallel to the 0° meridian, grid east parallel to 90°E, etc.). The set of positive anomalies running between 140°E and 120°W, north of 65°S, lies closely over the East Pacific Ridge on the grid west and he Mid-Indian Ocean Ridge on the grid

east. There are also highs associated with aseismic volcanic ridges and plateaus, such as the Kerguelen Plateau (about 80°E) and Maud Rise (65°S, 0°E)(cf. Frey, 1982a), and a relative high in an otherwise pronounced low is associated with the South Sandwich Islands and Trench (60°S, 25°W).

There are, however, some interesting anomalies that do not fit this norm. For example, a positive anomaly runs grid northeast from Maud Rise right into the Enderby Abyssal Plain, and another extends grid west of Thurston Island into the Bellingshausen Abyssal Plain. The cause of these anomalies is puzzling, and deserves further study.

The correlation between magnetic anomalies and continental structures is also striking. In East Antarctica, the mountains of Queen Maud Land (negative), the mountains of Enderby Land (positive), much of Wilkes Land (positive), the Gamburtsev Subglacial Mountains (negative), and the Amery Ice Shelf (negative) all have magnetic anomalies associated with them. Although it is not certain, of course, what these associations mean, some speculation may nevertheless be useful. We believe that the Enderby Land high may stem from a relatively high crustal magnetization -- aeromagnetic surveys in parts of the area (Wellman and Tingey, 1982) suggest to us that the mean susceptibility of the upper crustal rocks, at least, is higher than the continental norm. We suggest that the low over the Gamburtsev Subglacial Mountains

results from an elevated Curie isotherm; this idea finds some support in the low surface-wave group velocities along paths traversing these mountains (Dewart and Toksöz, 1965; see discussion in Bentley, in press), since a warming of the mantle causes seismic wave velocities to diminish. Perhaps these mountains are relatively young. The pronounced relative magnetic low overlying the Amery Ice Shelf/Lambert Glacier region supports the belief that this is a failed rift deeply filled by non-magnetic sedimentary rocks (Masolov et al, 1981); most continental rift features, unless characterized by extensive extrusive volcanism, show a negative anomaly (Frey, 1982a). The apparent extension of the anomaly into the ocean is probably just a failure to resolve closely adjacent continental and oceanic lows.

On a larger scale, the coincidence of depressed topography, satellite-measured free-air gravity lows, and other features extending from Wilkes Land across the ocean into Australia, led Veevers (1982) to suggest that the whole vast region is being held down dynamically by downward currents in the mantle. The positive magnetic anomaly in Wilkes Land (and the corresponding one in Australia -- see below) is consistent with this suggestion since a convection-convergence zone would be relatively cool.

A noteworthy feature of the anomaly map is the absence of magnetic anomalies over the Transantarctic Mountains. Instead of exhibiting a characteristic anomaly pattern of their own, they

mark a distinct boundary zone between largely separate East and West Antarctic anomalies. (It is likely that the negative anomaly that cross-cuts them from the Ross Ice Shelf is, in fact, another case of two separate lows that have not quite been resolved.)

Several anomalies appear in West Antarctica, but their tectonic association is not at all clear. The volcanic province or provinces comprising the Antarctic Peninsula, Thurston Island and Marie Byrd Land all show distinct highs as would be expected, but along the whole region the centers of the highs are inexplicably shifted oceanward. A pronounced low over the Ross Sea may support the concept of a failed rift zone here, but it is not centered over the postulated axis of the rift found from gravity measurements in the grid eastern part of the sea (Hayes and Davey, 1975; Bentley, in press, Figure 9). The anomaly does disappear under the Ross Ice Shelf -- that is in agreement with the gravity evidence (Davey, 1981).

What may be a mirroring negative anomaly appears in the Weddell Sea embayment between (and partly overlying) the Ellsworth and Pensacola Mountains. However, if this is a rift-zone negative, it is surprising that it does not extend farther grid northward under the Weddell Sea continental shelf.

Comparison of the Gondwana reconstruction of Norton and Sclater (1979) (Figure 19) with Figure 5 and the global anomaly

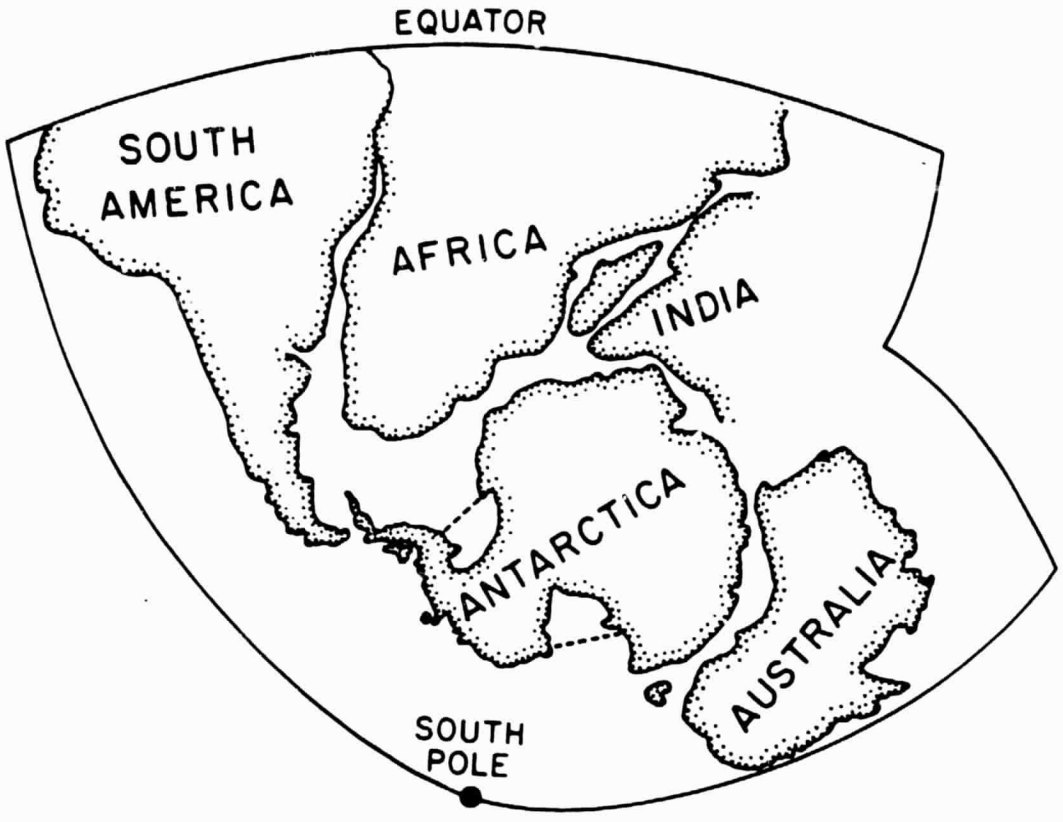

Figure 19: Gondwanaland reconstruction, modified from Norton and Sclater (1979).

map of Langel et al (1982a) shows that the pronounced high in Wilkes Land is mirrored by an even more pronounced high in the Australian shield; there is, in fact, a general similarity between the magnetic appearances of Wilkes Land and Australia. Moreover, the low in Queen Maud Land appears to correspond well to lows in southern and southeastern Africa. On the other hand, there is no clear correspondence between the West Antarctic positive anomalies and any g else. It appears, unfortunately, that the MAGSAT map is not yet going to solve the puzzle of where to put the West Antarctic microplates before the break-up of Gondwanaland! For East Antarctica, nevertheless, the Gondwana magnetic reconstruction is very good, implying that the anomaly features in Antarctica were formed prior to break-up. A more exact comparison requires that all data be reduced to the pole.

V. CONCLUSION

We have argued that of the four high-power sources of magnetic fields in high latitudes (the core, magnetospheric ring-currents, field-aligned currents, and the crust) the crust is the source of most of the anomalies observed in the scalar (Figure 5) and vertical (Figure 8) vector anomaly maps and that field-aligned currents generate the anomalies seen on the two horizontal anomaly maps (Figures 6 and 7).

Errors in the core-field model do not provide a significant fraction of the power observed in Figure 5. Errors in the model contained in degrees 1 and 2 are compensated by the quadratic polynomial fit to each pass, and errors contained in degrees between 10 and 13 are known to be too low in power to seriously contaminate Figure 5. Errors in terms between degrees 3 and 9 may appear on the scalar anomaly map, but the power between these wavelengths is not a large fraction of the total power of the map. Fields generated by magnetospheric ring-currents are known to vary slowly relative to the time it takes MAGSAT to traverse the observed region and are therefore well modeled by the quadratic fit to each pass. Finally, though the horizontal anomaly data indicate that field-aligned current activity is significant on every pass and that high-frequency variations in these currents cause the anomalies seen in the horizontal anomaly maps, we do not believe they are significantly contaminating the scalar anoma-

ly map. Short-period field-aligned current effects do not disturb the scalar anomalies, though longer-period currents can. However, very long-period field-aligned current effects have not been observed, not because they do not exist but because they must be much lower in power than the high-frequency variations. The good correlation between the scalar anomaly map and the POGO anomaly map over Antarctica implies that the source of most of the power of the map is stable over 15 years. Since field-aligned current terms longer than 15 years in period are not strong enough to cause the observed field, long-period field-aligned currents are believed not to significantly alter the scalar anomaly map. Furthermore, the remarkable correlation of magnetic anomalies with known oceanic geology implies a crustal origin of the oceanic anomalies even in very high geomagnetic latitudes.

The scalar anomaly map is consistent with the following hypotheses that we associate with the cited authors:

1. The Gamburtsev Mountains are tectonically unrelated to either the Highland Massifs (Drewry, 1975) of Wilkes Land or the mountains of Enderby Land;
2. Wilkes Land is the site of cool convergence in the mantle which accounts for the topographic depression and gravity low (Veevers, 1982);

3. West Antarctica comprises the set of tectonic microplates postulated by Dalziel and Elliot (1982); and
4. Both the Ross Embayment (Hayes and Davey, 1975) and the Amery Ice Shelf mark the site of ancient continental failed rifts.

Finally, a comparison of the anomalies observed over Antarctica with anomalies over the other Gondwanaland continents indicates that the source of the anomalies on the scalar map has been stable since before rifting of Gondwanaland occurred.

In the future, we will attempt a comparison between existing aeromagnetic surveys in Antarctica and the MAGSAT results. The only data available to us are from West Antarctica (extensive work has also been done east of the Weddell Sea by the Soviet Union, and in the Enderby Land region by Australia). It remains to be seen whether the lateral extent of the West Antarctic survey is great enough to yield a meaningful upward continuation to MAGSAT heights.

Modeling of MAGSAT anomalies is of questionable value at this stage, for two reasons. First, too little is known about the large-scale structure of the anomaly-associated features in Antarctica to provide any realistic geologic control on the models. Second, we believe further testing for auroral-zone current effects by comparing dusk-side passes with dawn-side passes is needed. If it can then be shown that the data are

sufficiently decontaminated, we would suggest looking first at the Queen Maud Land anomaly, together with the associated negative in Africa where the geology is better known. The anomalies in the Enderby Land/Amery Ice Shelf area and in Wilkes Land will presumably be attended to by MAGSAT principal investigators from Australia.

REFERENCES

Anderson, H.R. and R.R. Vondrak, 1975: Observations of Birkeland currents at auroral latitudes, Revs. Geophys. Space Phys., 13, 243-262

Bentley, C.R., in press: Crustal structure of Antarctica from geophysical evidence. Paper submitted to IV Symposium on Antarctic Earth Sciences, Adelaide, Australia, 1982.

Bevington, P.R., 1969: Data Reduction and Error Analysis for the Physical Sciences. McGraw-Hill, 336 p., New York, New York.

Cain, J.C., 1976: Introductory remarks (abstract), EOS, Trans. A.G.U., 57, 907.

Cain, J.C., D.R. Schmitz, and L. Muth, 1982: Small Scale Features observed by MAGSAT. Unpublished manuscript.

Carle, H.M. and C.G.A. Harrison, 1981: A problem in representing the core magnetic field model of the earth using spherical harmonics. Geophys. Res. Let., 9, 265-268.

Coles, R.L., G.V. Haines, G. Jansen van Beek, A. Nandi, and J.K. Walker, 1982: Magnetic anomaly maps from 40° N to 83° N derived from MAGSAT satellite data. Geophys. Res. Let., 9, 281-284.

Dalziel, I.W.D. and D.H. Elliot, 1982: West Antarctica: Problem Child of Gondwanaland. Tectonics, 1, 3-19.

Davey, F.J., 1981: Geophysical studies in the Ross Sea region. Journal of the Royal Society of New Zealand, 11, 465-479.

Dewart, G. and M.N. Töksöz, 1965: Crustal structure in East Antarctica from surface wave dispersion. J. Geophys , 10, 127-139.

Drewry, D.J., 1975: Terrain units in Eastern Antarctica, Nature, 256, 194-195.

Frey, H., 1982a: MAGSAT scalar anomaly distribution: the global perspective. Geophys. Res. Let., 9, 277-290.

Frey, H., 1982b: MAGSAT scalar anomalies and major tectonic boundaries in Asia. Geophys. Res. Let., 9, 299-302.

Galliher, S.C. and M.A. Mayhew, 1982: On the possibility of detecting large-scale crustal remanent magnetization with MAGSAT vector magnetic anomaly data. Geophys. Res. Let., 9, 325-328.

Hall, D.H., 1974: Long-wavelength aeromagnetic anomalies and deep crustal magnetization in Manitoba and northwestern Ontario, Canada. J. Geophys., 40, 403-430.

Hayes, D.E. and F.T. Davey, 1975: A geophysical study of the Ross Sea, Antarctica. Initial Reports of the Deep Sea Drilling Project, 28, 229-240.

Heezen, B.C. and M. Tharp, 1980: The Floor of the Oceans. Marie Tharp Oceanographic Cartographer, South Nyack, New York.

Hinze, W.J., R.R.B. Von Frese, M.B. Longacre, L.W. Braile, E.G. Lidiak, G.R. Keller, 1982: Regional magnetic and gravity anomalies of South America. Geophys. Res. Let., 9, 314-317.

Krutikhovskaya, Z.A. and I.K. Pashkevich, 1977: Magnetic model for the Earth's crust under the Ukrainian shield. Can. J. Earth Sci., 14, 2718-2728.

Langel, R.A. and R.H. Sweeney, 1971: Asymmetric ring current at twilight local time. J. Geophy. Res., 76, 4420-4427.

Langel, R.A. and R.H. Estes, 1982: A geomagnetic field spectrum. Geophys. Res. Let., 9, 250-253.

Langel, R.A., J.D. Phillips, and R.J. Horner, 1982a: Initial scalar magnetic anomaly map from MAGSAT. Geophys. Res. Let., 9, 269-272.

Langel, R.A., J.D. Phillips, and R.J. Horner, 1982b: Initial vector anomaly map from MAGSAT. Geophys. Res. Let., 9, 273-276.

Langel, R.A., R.H. Estes, C.D. Mead, E.B. Fabiano, and E.R. Lancaster, 1980: Initial geomagnetic field model from MAGSAT vector data. Geophy. Res. Let., 7, 793-796.

Masolov, V.N., R.G. Kurinin, and G.E. Grikurov, 1981: Crustal structures and tectonic significance of Antarctic rift zones (from geophysical evidence). IN: Cresswell, M.M., and P. Vella (eds.), Gondwana Five, A.A. Balkema, Rotterdam, 303-310.

Mayhew, M.A., 1979: Inversion of satellite magnetic anomaly data. J. Geophys., 45, 119-128.

Mayhew, M.A., 1982: Application of satellite magnetic anomaly data to Curie isotherm mapping. J. Geophys. Res., 87, 4846-4854.

Norton, I.O. and J.G. Sclater, 1979: A model for the evolution of the Indian Ocean and the breakup of Gondwanaland. J. Geophys. Res., 84, 6803-6830.

Pakiser, L.C. and I. Zietz, 1965: Transcontinental crustal and upper mantle structure. Review of Geophysics, 3, 505-520.

Potemra, T.A., 1979: Current systems in the earth's magnetosphere. Revs. Geophys. Space Physics, 17, 640-656.

Regan, R.D., J.C. Cain, and W.M. Davis, 1975: A global magnetic anomaly map. J. Geophys. Res., 86, 9567-9573.

Ritzwoller, M.H. and C.R. Bentley, 1982: MAGSAT magnetic anomalies over Antarctica and the surrounding oceans. Geophys. Res. Let., 9, 285-288.

Sailor, R.V., A.R. Lazarewicz, and R.F. Brammer, 1982: Spatial resolution and repeatability of MAGSAT crustal anomaly data over the Indian Ocean. Geophys. Res. Let., 9, 289-292.

Schunk, R.W. and A.F. Nagy, 1980: Ionospheres of the Terrestial Planets, Revs. Geophys. Space Physics, 18, 813-852.

Veevers, J.J., 1982: Australian-Antarctic depression from the mid-ocean ridge to adjacent continents. Nature, 295, 315-317.

Wasilewski, P. and E. Padovani, 1980: Magnitization in the lower crust (abstract). EOS, 61, 222.

Wasilewski, P. and D.M. Fountain, 1982: The Ivrea Zone as a model for the distribution of magnetization in the continental crust. Geophys. Res. Let., 9, 333-336.

Wasilewski, P. and M.A. Mayhew, 1982: Crustal xenolith magnetic properties and long-wavelength anomaly source parameters, Geophys. Res. Let., 9, 329-332.

Wasilewski, P.J., H.H. Thomas, and M.A. Mayhew, 1979: The Moho as a magnetic boundary. Geophys. Res. Let., 6, 541-544.

Wellman, P. and R.J. Tingey, 1982: A gravity survey of Enderby and Kemp Lands, Antarctica. IN: Craddock, C. (ed.), Antarctic Geoscience, University of Wisconsin Press, Madison, Wisconsin, 937-940.

Zietz, I., E.R. King, W. Geddes, and E.G. Lidiak, 1966: Crustal study of a continental strip from the Atlantic Ocean to the Rocky Mountains. Geol. Soc. of Am. Bull., 77, 1427-1448.

APPENDIX I

Ritzwoller and Bentley (1982)

GEOPHYSICAL RESEARCH LETTERS, VOL. 9, NO. 4, PAGES 285-288, APRIL 1982

MAGSAT MAGNETIC ANOMALIES OVER ANTARCTICA AND THE SURROUNDING OCEANS

[illegible] Ritzwoller and Charles R. Bentley

[illegible]sical and Polar Research Center
University of Wisconsin, Madison, WI 53706

Abstract. A procedure to select and reduce satellite magnetic anomaly data in high southern latitudes is described, and a map of Antarctica, constructed using this procedure, is shown. The map is qualitatively analyzed for error and geologic significance. Correlations are noted between magnetic anomalies and mountain ranges, subglacial basins, tectonic provinces, regional gravity anomalies, a hypothetical continental rift feature, oceanic basins, and oceanic rises. Overall, the correlation between the magnetic anomaly patterns and known geological features is good.

Introduction

The Earth's magnetic field is principally a superposition of fields generated in four regions: the core, the crust above the Curie isotherm, the ionosphere, and the magnetosphere. Isolating the crustal field at satellite elevations is difficult, especially at high latitudes, though attempts span more than a decade (e.g. Zeitz, et al., 1970; Langel, 1974; Regan, et al., 1975; Coles, et al., 1976; Coles, 1979; Coles, et al., 1979; Mayhew, et al., 1980; Langel, et al., 1980a). The difficulty arises due to the proximity to the satellite of the ionospheric and magnetospheric currents, which are amplified in auroral regions. In this paper we describe a method for extracting the crustal field from the total field measured by MAGSAT at high latitudes and give a brief interpretation of some features of the Antarctic crustal magnetic anomaly field.

Data Selection and Reduction

The crustal magnetic anomaly, ΔB, is calculated by subtracting a core field model and an external field model from the total scalar magnetic field measured by MAGSAT. The degree and order 13 spherical harmonic model MGST4/81 created by Langel, et al. (1980b) was used as the core field model. No such general external field model exists; therefore, we followed the procedure described below in filtering external field effects.

External fields primarily consist of two components: a long-wavelength, slow-varying field generated by ring currents in the magnetosphere and a shorter wavelength, faster-varying field generated by field-aligned currents in the ionosphere. The rapid variations in field-aligned currents make them difficult to model, so we deleted all passes showing signs of their effect. This was done in two ways. First, we selected data only from passes during which the planetary magnetic activity index, Kp, was less than or equal to 1$^-$ for at least 6 hours. The extended time period was chosen because auroral ionospheric activity abates more slowly than low-latitude activity. Second, data were selected only from passes showing no sign of anomaly amplitudes greater than those theoretically expected from the crust. This was done since field-aligned currents, because of their proximity to the satellite, can generate much larger measured magnetic effects than the crust. Specifically, we have required that ΔB be no larger than 15 gammas(nT). This amplitude criterion can be applied only after the long-wavelength external field is modeled and removed. Over the 8000 km flight path we have considered, the long-wavelength field is modeled as a quadratic polynomial (e.g. Mayhew, 1979) upon which the crustal and ionospheric fields are superimposed.

An example of this procedure is given in Figure 1, in which traces A result from the measured magnetic field after the core field has been removed, traces B are the models of the field generated by the ring currents, and traces C depict ΔB, which results by subtracting B from A. The tracks of the 87 passes (out of a total of approximately 2300) over Antarctica between November 1, 1979 and April 1, 1980, that satisfied the selection criteria are shown in Figure 2.

The ΔB data from the selected passes were averaged over areas measuring 3° of latitude by 3° of longitude, and were plotted and contoured, yielding the scalar anomaly map shown in Figure 3. Anomalies on this map have not been corrected for elevation variations in the satellite path, nor have they been reduced to the pole. Both corrections will eventually be applied, since the 200 km elevation variations that occur between MAGSAT orbits alter the amplitudes even of very long wavelength magnetic anomalies by as much as a factor of two (Regan, 1979; Bhattacharyya, 1977), and since the geomagnetic latitude varies by more than 45° across the map so that fields induced in the crust by the Earth's dipole field are latitudinally dependent. At present, however, we assume that elevation variations evenly smear most anomalies and note that for most of the map, reduction to the pole will have minimal effect. Other refinements of the data planned for the near future include rectangular gridding, the incorporation of a cross-correlation selection criterion for adjacent and crossing satellite paths, and data selection based on analyzing the vector-magnetic anomaly data for field-aligned current signatures.

Accuracy of Data

Disregarding magnetometer and tracking error, the accuracy of the magnetic anomaly map in

Paper number 2L0154.
0094-8276/82/2L-0154$03.00

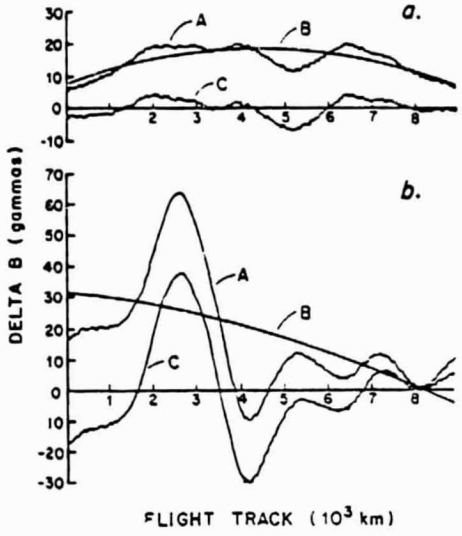

Fig. 1. Graphs of magnetic anomalies for: (a) a pass unaffected by field-aligned currents, and (b) an affected pass where A is the total-field minus the core field model, B is the quadratic polynomial model of the magnetospheric field, and C is A minus B, i.e. ΔB.

Figure 3 depends on the degree to which the core field model and the external field model are in error. We concerned ourselves chiefly with errors found in the external field models, since they are both more primitive and shorter in wavelength than the core field model. Two tests based on the time-varying nature of the external fields were performed. First, we partitioned the MAGSAT data into two successive 2½-month data sets and employed the data selection and reduction scheme described above to each. The correlation between the two maps was good, suggesting that most of the external field effects with periods less than five months were successfully filtered. Second, we compared the MAGSAT map with the POGO map of Regan, et al. (1975) covering Antarctica. The same general continental features exist on both maps, further suggesting that most external field effects with periods less than ten years were filtered out. The results of these tests are encouraging, but a more telling test, previously performed for high northern latitudes by Langel, et al. (1980a) and Coles (1979), would be to compare Figure 3 with lower altitude data continued up to satellite elevations. Until recently, data were not available from any magnetic survey over Antarctica that was large enough in area and dense enough in coverage to warrant comparison with MAGSAT. However, an aeromagnetic map soon to be published (referred to by Jankowski, et al., 1981), covering almost 10^6 km² in West Antarctica, will provide an excellent check of MAGSAT data.

Source of Anomalies

We expect that two major factors will contribute to continental crustal magnetic anomalies: the depth to Curie isotherm and the magnetic susceptibilities. It is still not certain to what degree continental remanent magnetization may affect long-wavelength magnetic anomalies. Some workers, at least, consider the effect negligible (M. Mayhew, personal communication, 1981); lacking better information we ignore it here. Thus we assume that the main sources of magnetic anomalies are located above the Curie isotherm and above Moho (Wasilewski, et al., 1979), and principally in the lower crustal layer where susceptibilities are greatest (Hall, 1974). Therefore, continental highs indicate either a thick crust with a deep Curie isotherm (low heat flow), or exceptionally high magnetic susceptibility in the lower crust, or both. On the other hand, continental lows imply some combination of a thin crust, a shallow Curie isotherm (high heat flow), and low susceptibilities in the lower crust.

The highest susceptibility region in the oceanic crust is in layers 2 and 3, nearer the surface than in the continental crust, and generally well above the Curie isotherm. Therefore, oceanic magnetic anomalies should reflect regional crustal thicknesses and susceptibility differences, but probably do not reflect heat flow except in extreme circumstances. Remanent magnetization in the rocks of oceanic rift zones can also yield magnetic anomalies at satellite elevations, as can be shown by model calculations.

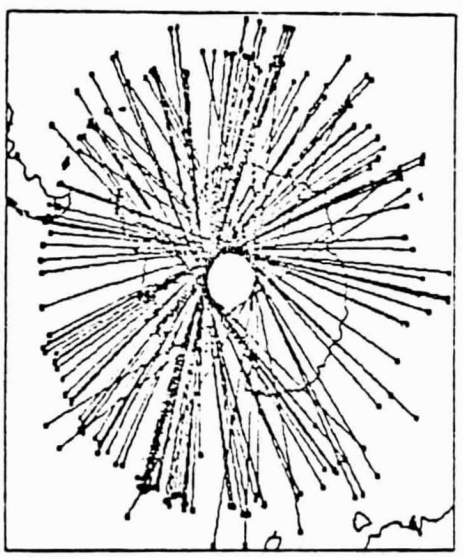

Fig. 2. Flight tracks of the 87 accepted passes over Antarctica and the surrounding oceans.

Geological Interpretation

The interpretation of satellite magnetic anomaly data is clearly ambiguous, especially over regions with little collateral data. However, the major associations between geologic features and magnetic anomalies are worth noting in both continental and oceanic regions.

Over the Antarctic continent there are magnetic anomalies associated with many topographic and geologic features. In East Antarctica, the mountains of western Queen Maud Land (magnetic low), the mountains of Enderby Land (high), the Prince Charles Mountains (low), the "Highland Massifs" beneath the ice in Wilkes Land (high)(Drewry, 1975), the Gamburtsev Subglacial Mountains (low), and the Pensacola Mountains (high) all have magnetic anomalies associated with them. Also, there is a magnetic low over a subglacial basin generally along 150°E in East Antarctica that is further characterized by a strongly negative regional isostatic gravity anomaly. This suggests that the process associated with the isostatic imbalance may be associated with high heat flow and does not support a model of cool convergence in the circulation of the upper mantle.

In West Antarctica, the Antarctic Peninsula, eastern Marie Byrd Land, and the Thurston Island region are associated with magnetic highs, whereas the Ronne Ice Shelf/Ellsworth Mountains region shows a pronounced magnetic low. Several of these anomalies seem to be closely associated with tectonic microplates suggested by D.H. Elliot (personal communication, 1981). Hayes and Davey (1975) have argued from the occurrence of a striking linear positive gravity anomaly that an actual ancient rift zone, which was probably active during the separation of Antarctica from Australia 65 m.y. ago, underlies the western Ross Sea. If so, the crust should be anomalously thin and the heat flow higher than could be normal there. A magnetic low covers much of this area, although the trends of the two features differ.

Fig. 3. MAGSAT total-field magnetic anomaly map over Antarctica. Units in gammas(nT). Capital letters indicate the approximate location of: A - Queen Maud Land, B - Enderby Land, C - Prince Charles Mountains, D - American Highlands, E - Gamburtsev Mountains, F - Wilkes Land, G - Transantarctic Mountains, H - Ross Embayment, I - Marie Byrd Land, J - Thurston Island, K - Ellsworth Mountains, L - Pensacola Mountains, M - Antarctic Peninsula.

Two continental regions that differ only in crustal thickness will tend to show different magnetic anomalies, with more positive values over the thicker crust. Bentley (1973) and Dewart and Toksöz (1954) have estimated crustal thickness to be 40 km in East Antarctica and 30 km in West Antarctica; the magnetic anomalies over East Antarctica are generally more positive.

Comparing the Gondwana reconstruction of Craddock, et al. (1970) with Figure 3 and the global magnetic anomaly map of Langel, et al. (this issue), shows that the low over the Ross Sea and the Transantarctic Mountains corresponds to the low along the Adelaide and Tasman orogens in eastern Australia, that the high in Wilkes Land is mirrored by a high in the Australian shield, and that, in fact, there is a general similarity between the magnetic appearances of Antarctica and Australia. Moreover, the Enderby Land high seems to be expressed in the Indian Shield, though this is unclear due to the latitude difference between the two regions. The Queen Maud Land low appears to correspond to a low in southern Madagascar and the Ellsworth low may be reflected in a low over the Cape orogen in South Africa. On the other hand, no feature similar to the Antarctic Peninsula high is apparent along the Andean orogen in South America. Thus, the Gondwana reconstruction seems largely consistent with the magnetic data shown in Figure 3 and Langel's map, but some discrepancies exist. A more exact comparison requires reduction of all data to the pole.

Oceanic magnetic anomalies are associated with both basins and rises. All four major ocean basins around Antarctica exhibit magnetic lows, and with the exception of the linear magnetic low along 170°W, all the oceanic negative anomalies are associated with these basins. Oceanic basin anomalies presumably are mainly negative because of the thin oceanic crust. Conversely, many of the oceanic rises in the region exhibit highs, and most oceanic magnetic highs lie above known rises. However, not all oceanic rises exhibit a magnetic high. We believe the primary cause for the magnetic highs is remanent magnetization over spreading ridges, although specific modeling has not yet been carried out.

Conclusions

Preliminary tests indicate that the primary source of the magnetic anomalies shown in Figure 3 lies within the Earth's crust. Though the

data used to construct the magnetic anomaly map were not corrected for the effects of elevation and latitude variations in the satellite flight path, both continental and oceanic anomaly features show a good agreement with known geologic structures. Further research will focus on improving the quality of the magnetic anomaly map and modeling the sources of the anomalies seen.

Acknowledgments. This study was supported by NASA grant number NAS5-25977. The author would like to thank D.D. Blankenship, L.L. Greischar, C.S. Lingle and R.P. Meyer for valuable discussions and criticism, and B. Karsh and J. Luetgert for computer assistance. R.A. Langel, NASA project scientist, has been extremely helpful throughout our research.

References

Bentley, C. R., Crustal structure of Antarctica, Tectonophysics, 20, 229-240, 1973.

Bhattacharyya, B. K., Reduction and treatment of magnetic anomalies of crustal origin, J. Geophys. Res., 82, 2279-2290, 1977.

Coles, R. L., Some comparisons among geomagnetic models, observatory and airborne magnetometer data: Implications for broad-scale anomaly studies over Canada, J. Geomag. Geoel., 31, 459-478, 1979.

Coles, R. L., and G. V. Haines, Long-wavelength magnetic anomalies over Canada, using polynomial and upward continuation techniques, J. Geomag. Geoel., 31, 545-566, 1979.

Coles, R. L., G. V. Haines, and W. Hannaford, Large-scale magnetic anomalies over Western Canada and the Arctic: a discussion, Can. J. Earth Sci., 13, 790-802, 1976.

Craddock, C. C., et al., Geologic maps of Antarctica, Antarctic Map Portfolio Series, American Geographical Society, 1970.

Dewart, G., and M. N. Toksöz, Crustal structure in East Antarctica from surface wave dispersion: J. Geophys., 10, 127-139, 1965.

Drewry, D. J., Terrain units in eastern Antarctica, Nature, 256 194-195, 1975.

Hall, D.H., Long-wavelength aeromagnetic anomalies and deep crustal magnetization in Manitoba and Northwestern Ontario, Canada, J. Geophys., 40, 403, 1974.

Hayes, D. E., and F. J. Davey, A geophysical study of the Ross Sea, Antarctica, Initial Reports of the Deep Sea Drilling Project, 28, 229-240, 1973.

Jankowski, E. J., and D. J. Drewry, The structure of West Antarctica from geophysical studies, Nature, 291, 17-21, 1981.

Langel, R. A., Near-earth magnetic disturbance in total field at high latitudes; 1. Summary of data from Ogo 2, 4 and 6, J. Geophys. Res., 79, 2363-2371, 1974.

Langel, R. A., J. D. Phillips, and R. J. Horner, Initial scalar magnetic anomaly map from MAGSAT, Geophys. Res. Letters, this issue.

Langel, R. A., R. L. Coles, and M. A. Mayhew, Comparisons of magnetic anomalies of lithospheric origin measured by satellite and airborne magnetometers over Western Canada, Can. J. Earth Sci., 17, 876-887, 1980a.

Langel, R. A., R. H. Estes, G. D. Mead, E. F. Fabiano, and E. R. Lancaster, Initial geomagnetic field model from MAGSAT vector data, Geophys. Res. Letters, 7, 793-796, 1980b.

Mayhew, M. A., Inversion of satellite magnetic anomaly data, J. Geophys., 45, 119-128, 1979.

Mayhew, M. A., B. D. Johnson, and R. A. Langel, Magnetic anomalies at satellite elevations over Australia, NASA Tech. Mem., 80664, 1980.

Regan, R. D., The reduction and analysis of satellite magnetometer data, Geophys. Surveys, 3, 331-349, 1979.

Regan, R. D., J. C. Cain, and W. M. Davis, A global anomaly map, J. Geophys. Res., 80, 794-802, 1975.

Wasilewski, P. J., H. H. Thomas, and M. A. Mayhew, The Moho as a magnetic boundary, NASA Tech. Mem., 80245, 20 pp., 1979.

Zietz, I., and G. E. Andreasen, Magnetic anomalies from satellite magnetometer, J. Geophys. Res., 75, 4007-4015, 1970.

Geophysical and Polar Research Center, University of Wisconsin-Madison, Contribution No. 398.

(Received November 4, 1981;
accepted January 19, 1982.)

APPENDIX II

Alternate Data Reduction Procedure: Two-Dimensional Finite Fourier Transform Method

Filtering polynomials from MAGSAT passes in non-polar regions where passes do not cross is the source of the latitudinal striping apparent in Langel et al (1982). Removal of the polynomials amounts to removal of most long-wavelength North-South power so that only long-wavelength East-West power remains; thus, the East-West striping. In polar regions, flight paths cross so that this problem is not generated. Therefore, Antarctica is the perfect proving ground for testing alternate data reduction procedures to the standard procedure employing polynomial fitting. Cain et al (1982) have tested a whole-earth two-dimensional spherical harmonic method with what they feel to be surprisingly good results. We have tested another method on a continental scale with somewhat ambiguous, though heartening, results.

Instead of subtracting a polynomial from each pass we have merely taken the unreduced data (observed values minus core-field model for each pass) and averaged them in 3° square bins. The resulting map was then high pass filtered using a two-dimensional finite Fourier transform (2DFFT) filter so that spectral peaks between 4200 km and 5280 km were diminished by 1/3, peaks corresponding to wavelengths greater than or equal to 5280 km were

diminished by 1/2, and the d.c. component was set equal to zero. The surface subtracted in this way is shown in Figure 12. This surface differs from the polynomials used in the standard method in that it is static over the 5 month data window whereas the polynomials in the standard reduction procedure can be viewed as two-dimensional slices of a three-dimensional surface varying during the same 5 months. The map produced can be seen in Figure 11. The question is, how well does the static model correspond to the dynamic model?

The difficulty in comparing the effects of the two models is exacerbated by the fact that the no-data region due to the tilt in the satellite's orbit had to be filled in by linear interpolation to perform the Fourier transform. The spectrum will be affected, probably by adding long-wavelength power, since the linear interpolation acts to create a long-wavelength feature. Furthermore, the zero-levels of the two maps are not the same -- they are the averages of each map, separately, and since Figure 11 does not possess as much oceanic region as Figure 5 its average will be somewhat higher -- approximately .4 nT. Thus, features on Figure 11 are d.c. shifted by about .4 nT below features on Figure 5. Comparing the maps indicates that there is a pretty good qualitative correlation -- highs in Figure 5 are matched with highs in Figure 11, and lows with lows. There are two major exceptions, the Antarctic Peninsula high in Figure 5 is matched to a low in Figure 11, though this region is still a high rela-

tive to Ellsworth Land and the surrounding oceans. Also, the radial feature found at approximately 75°S and 150°W is not found in Figure 5. In general, however, the qualitative agreement between the two maps is good. The radial striping in Figure 11 is reminiscent of that found in Ritzwoller and Bentley (1982), which was believed largely to result from field-aligned current effects disturbing individual passes.

The quantitative agreement is not so good, however. Amplitudes can be a factor of two greater in Figure 11 than in Figure 5. This is the result of the fact that the static model cannot accomodate daily and seasonal changes taking place in the magnetosphere or long-spatial wavelength changes due to field-aligned currents. The latter is a problem specific to high latitudes.

Keeping the problems specific to polar regions in mind, i.e., anomalies in Figure 11 can be generated by field-aligned currents and the data gap, the correlation between the two maps should be considered heartening to the low-latitude investigator who mourns for North-South magnetic features.

In conclusion, experimentation with modifications of the static field model by low-latitude investigators is believed to be warranted. Two-dimensional filtering should be carried out after the removal of a magnetospheric field model (e.g. the model of Langel et al (1982a)). If the magnetospheric field model contains fields generated solely in the magnetosphere, subtraction of this model will not create a striping problem. Perhaps

then magnetic anomalies associated with such North-South features as the Mid-Atlantic Ridge, the East Pacific Ridge, and the Andes may appear more clearly.

APPENDIX III

Core Field Model

Langel et al (1980) describe the procedure by which a geomagnetic core field model (MGST(6/80)) is constructed from the MAGSAT vector data. A similar procedure is followed in the construction of the reference field used in this study. The geomagnetic field is expanded in terms of spherical harmonics such that the potential, V, from which the geomagnetic field is derivable is given by:

$$V = a \sum_{n=1}^{N} (a/r)^{n+1} \sum_{m=0}^{n} (g_n^m \cos m\phi + h_n^m \sin m\phi) P_n^m(\Theta)$$

where a denotes the radius of a reference sphere, r the geocentric radial distance, Θ the geocentric colatitude and ϕ the longitude of the point at which the potential is to be found, and $P_n^m(\Theta)$ denotes the associated Legendre function of degree n and order m.

A complete description of the earth's geomagnetic field should extend to $n = m = \infty$. However, Cain (1976) has argued that a thirteenth degree and order representation is sufficient to represent the main field of the earth, and MGST(4/81) contains just these terms which are similar to those listed by Langel et al (1980). The average vector core model field (XMOD, YMOD, ZMOD) is shown in Figures 15, 16, and 18. The figures were separ-

ately constructed by taking the vector model values at each data location and elevation and averaging in the same 3° square bins used for the construction of the anomaly maps. Thus, these figures represent the average vector core field model employed over the 5-month period of data acquisition.

APPENDIX IV

External Magnetic Fields

This discussion is largely based on the excellent review of the current patterns external to the earth written by Schunk and Nagy (1980). The regions of magnetic field generation relevant to MAGSAT research lie in the magnetosphere and the ionosphere. The magnetosphere is that region where forces generated by the earth's magnetic field dominate and extends to approximately 9 earth radii. The ionosphere is the layered region of near-earth plasma lying between about 90 and 500 km elevation formed in the sunlit hemisphere by ionization of the earth's tenuous upper atmosphere. A schematic illustration of the earth's bow shock and magnetosphere is shown in Figure 20.

Sunward, shocked solar wind plasma in the magnetosheath can flow directly into the ionosphere via the polar cusp. At MAGSAT elevations the cusp occupies a narrow latitudinal band centered near noon with considerable longitudinal extent. Within this band, energetic particle precipitation can provide measurable magnetic disturbances, but the disturbances are less appreciable than field-aligned current effects.

The magnetospheric mantle is an intermediate region through which magnetosheath plasma travels on its way to the plasma sheet. The ring current represented in Figure 21 is the earthward extension of the plasma sheet. Trapped energetic protons and elec-

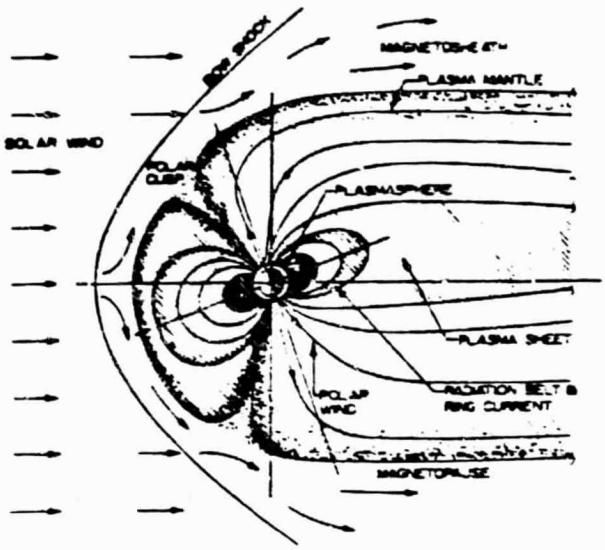

Figure 20: Schematic illustration of the earth's bow shock and magnetosphere. Taken from Schunk and Nagy (1980).

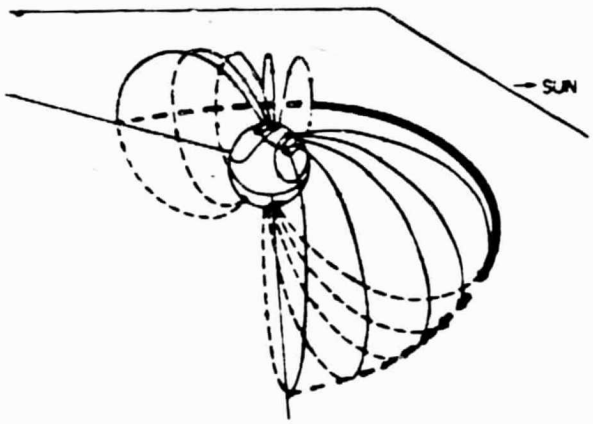

Figure 21: Schematic representation of a partial ring current (bold arrows) and field-aligned currents (thin arrows). Taken from Anderson and Vondrak (1975).

trons grad-B drift in opposite directions causing ring currents to flow around the earth. The current flow is large enough to effect magnetic measurements greatly and is believed to be the major source of level bias variations between MAGSAT passes over Antarctica.

The electric potential difference across the tail of the magnetosphere pointing from dawn to dusk, generated by the interaction of the shocked solar wind with the geomagnetic field, is mapped into the high-latitude ionosphere as an electric field normal to the geomagnetic field. This electric field generates the auroral electrojets, flows of ions parallel to the earth. Only the high-latitude ionosphere is influenced directly by the magnetospheric field since the ring-current effectively shields plasma from leaving the plasmasphere at low latitudes.

The horizontal ionospheric field is further coupled to the magnetosphere through field-aligned (Birkeland) currents. The field-aligned current pattern during a quiet and a disturbed period is shown in Figure 22. The current patterns are concentrated in two areas encircling the geomagnetic poles, one poleward and one equatorward. The current flow is into the ionosphere in the morning sector and away from the ionosphere on the evening- side in the poleward current region, whereas flow is opposite to this at a given local time in the equatorward regions. The net flow appears to be inward in the morning sector and outward on the evening side in the northern hemisphere. It is the field-

Figure 22: Summary of the distribution of flow directions of large-scale field-aligned currents for (a) weakly disturbed conditions and (b) active periods. Taken from Potemra (1979).

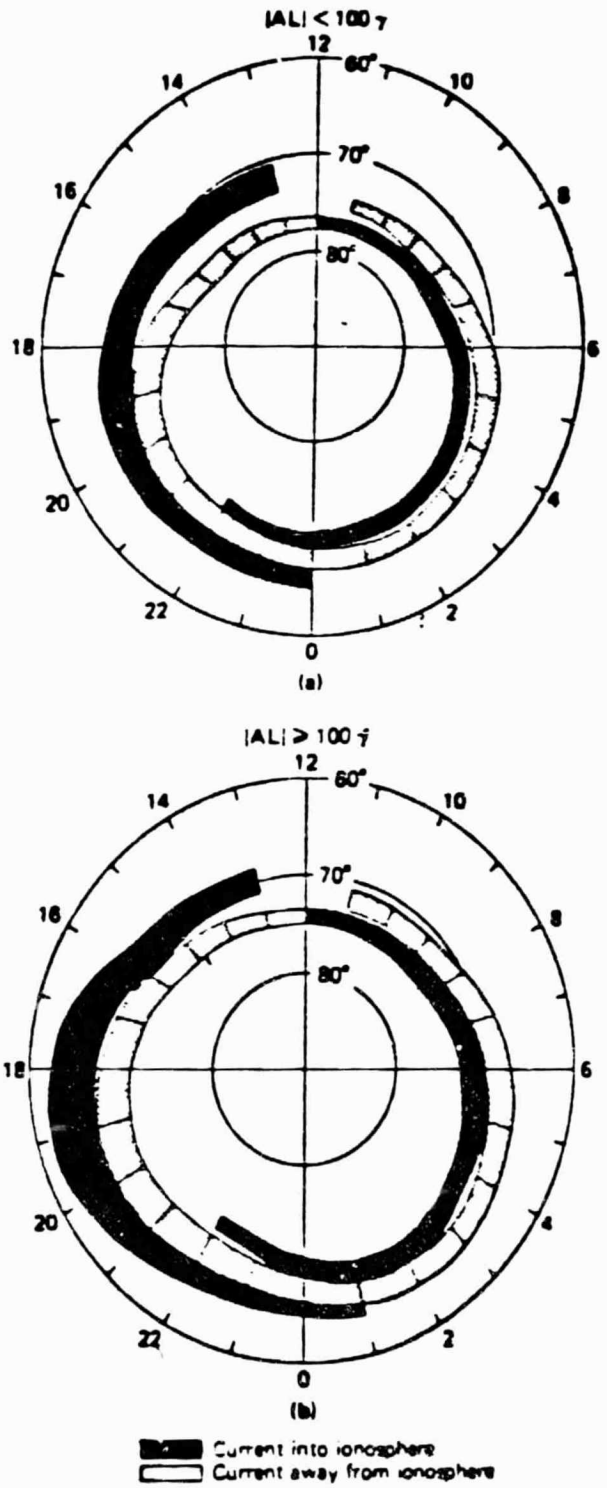

aligned currents that are believed to be the principal cause of magnetic disturbances observed in the MAGSAT data.

APPENDIX V

Computer Programs

List of Programs:

1. IBMTR
2. REFMT
3. ANTAP
4. MRGRD
5. BIN
6. RDBIN
7. FFT2D

```
C*************************************************************
C       $IBMTR TRANSLATES THE IBM-FORMATTED NASA TAPE
C     TO HARRIS-FORMATTED CODE.  THE KEY TO THE PRO-
C     GRAM LIES IN THE SUBROUTINES S.RTRNSL AND S.ITRNSL
C     WHICH TRANSLATE THE REAL AND THE INTEGER WORDS
C     RESPECTIVELY.  THE OUTPUT IS FORMATED NEARLY
C     IDENTICALLY TO THE FORMAT OF THE NASA TAPE.
C     EACH PASS BEGINS AT 90S WITH A HEADER RECORD,
C     FOLLOWED BY A STRING OF DATA RECORDS CONTAINING
C     INFORMATION ABOUT 30 MAGNETIC VALUES.  THE
C     HEADER RECORD IS FORMATED AS FOLLOWS:
C
C       WORD #          NASA VARIABLE
C       1               ITYPEX
C       2               NTYPEX
C       3               MJDX
C       4               IPASSX
C       5-6             ASCX(2)
C       7-8             DSCX(2)
C       9-10            MSECX(2)
C       11-12           ALTMX(2)
C       13-14           ALONX(2)
C       15-16           IKP(2)
C       17-22           GSM(2,3)
C       23-34           DST(2,6)
C       35              NMAX
C       36              NMAXT
C       37              MODEXT
C       38              TZERO
C       39              ABAR
C       40-328          GH(17,17)
C       329-524         GHT(14,14)25
C       525-527         E(3)
C
C     THE DATA RECORDS ARE FORMATED AS FOLLOWS:
C
C       WORD #             NASA VARIABLE
C       1                ITYPER
C       2                NTYPER
C       3                MJDR
C       4                MSECR
C       5                IPASSR
C       6                TINTR
C       7-36             LAT
C       37-66            LON
C       67-96            RAD
C       97-126           MLT
C       127-156          INVLAT
C       157-186          DIPLAT
```

```
C          187-216          BS
C          217-246          BV
C          247-276          X
C          277-306          Y
C          307-336          Z
C          337-366          BVA
C          367-396          XA
C          397-426          YA
C          427-456          ZA
C          457-486          BVSD
C          487-516          XSD
C          517-546          YSD
C          547-576          ZSD
C          577-606          BMD
C          606-636          XMD
C          637-666          YMD
C          667-696          ZMD
C          697              QUAL.
C          698              SPARE
C
C
C       FOR A DESCRIPTION OF THE NASA VARIABLES
C       SEE "MAGSAT INVESTIGATOR-B TAPE GENER-
C       ATION PROGRAM REQUIREMENTS".   NASA PUB-
C       LICATION, CONTRACT NAS5-24391, JULY, 1980.
C
C
C*************************************************************
      INTEGER*6 NEWVAR(40)
      DOUBLE PRECISION NEWORD(760),DX(40),HARRIS(760)
      INTEGER BUF(1010),B(3030),ICOUNT,IWORD,RCOUNT
      CALL LINK
      WRITE(1,1)
1     FORMAT(' FOR INPUT TAPE')
      CALL ASSTAP('12)
      WRITE(1,2)
2     FORMAT(' FOR OUTPUT TAPE')
      CALL ASSTAP('13)
C******THIS LOOP CREATES AN ARRAY CALLED B WHICH IS
C       COMPRIZED OF WORDS EACH POSSESSING ONE BYTE OF THE CORRES-
C       PONDING WORD FROM THE ARRAY NAMED BUF(I).   THE BUFFER IN
C       BEFORE IT FILLS BUF.
      LOOP
      BUFFER IN('12,BUF,B,1010,ISTAT,IWORD)
      CALL STATUS('12)
      EXIT LOOP IF(ISTAT.EQ.3)
      FOR J=1,IWORD
      I=3*J-2
      B(I)=BUF(J).AND.'77600000
      B(I)=B(I).SHIFT.-16
      B(I+1)=BUF(J).AND.'177400
      B(I+1)=B(I+1).SHIFT.-8
```

```
      H(J+2)=BUF(J).AND.'377
      ENDFOR
C
C******TRNSLATION OF IBM REALS INTO HARRIS REALS
C
      ICOUNT=1
      RCOUNT=1
      IF(IWORD.EQ.1008) GOTO 6
C
C*******TRANSLATION OF HEADER RECORD
      CALL ITRNSL(ICOUNT,1,16,B,NEWVAR)
      CALL RTRNSL(RCOUNT,17,32,B,NEWORD)
      CALL ITRNSL(ICOUNT,33,40,B,NEWVAR)
      CALL RTRNSL(RCOUNT,41,56,B,NEWORD)
      CALL ITRNSL(ICOUNT,57,64,B,NEWVAR)
      CALL RTRNSL(RCOUNT,65,136,B,NEWORD)
      CALL ITRNSL(ICOUNT,257,268,B,NEWVAR)
      CALL RTRNSL(RCOUNT,269,2228,B,NEWORD)
      GOTO 300
C
C*******TRANSLATION OF DATA RECORD
6     CALL ITRNSL(ICOUNT,1,20,B,NEWVAR)
      CALL RTRNSL(RCOUNT,21,2784,B,NEWORD)
      CALL ITRNSL(ICOUNT,2785,2904,B,NEWVAR)
      CALL RTRNSL(RCOUNT,2905,3024,B,NEWORD)
C
C******CREATE A NEW DBL PRECISION REAL ARAY HARRIS FOR BUFFEROUT
C
C******FIRST, IFLOAT NEWVAR
300   FOR I=1,40
      DX(I)=NEWVAR(I)
      ENDFOR
      IF(IWORD.EQ.1008) THEN
      FOR I=1,5
      HARRIS(I)=DX(I)
      ENDFOR
      FOR I=6,696
      HARRIS(I)=NEWORD(I-5)
      ENDFOR
      FOR I=697,726
      HARRIS(I)=DX(I-691)
      ENDFOR
      FOR I=727,756
      HARRIS(I)=NEWORD(I-35)
      ENDFOR
      ELSE
      FOR I=1,4
      HARRIS(I)=DX(I)
      ENDFOR
      FOR I=5,8
      HARRIS(I)=NEWORD(I-4)
      ENDFOR
```

```
      FOR I=9,10
      HARRIS(I)=DX(I-4)
      ENDFOR
      FOR I=11,14
      HARRIS(I)=NEWORD(I-6)
      ENDFOR
      FOR I=15,16
      HARRIS(I)=DX(I-8)
      ENDFOR
      FOR I=17,34
      HARRIS(I)=NEWORD(I-8)
      ENDFOR
      FOR I=35,37
      HARRIS(I)=DX(I-26)
      ENDFOR
      FOR I=38,527
      HARRIS(I)=NEWORD(I-11)
      ENDFOR
      ENDIF
      IF(B(4).EQ.1) THEN
      IW=1054
      ELSE
      IW=1512
      ENDIF
      BUFFEROUT('13,HARRIS,B,IW,JSTAT,JWORD)
      CALL STATUS('13)
      ENDLOOP
      FOR I=1,3
      CALL XXYY('13,'06)
      ENDFOR
      STOP
      END
C
C
      SUBROUTINE RTRNSL(RCOUNT,INIT,FIN,B,NEWORD)
C
      INTEGER*6 MANT1,B2,B3,B4,BB1,BB2,BB3,BB4,BB5
      DOUBLE PRECISION SIGN,EXP,MANT,NEWORD(760)
      INTEGER B(3030),SIGN1,EXP1,INIT,FIN,NUMWRD,RCOUNT
      NUMWRD=((FIN-INIT)+1)/4
      FOR I=1,NUMWRD
      J=INIT+4*(I-1)
      SIGN1=B(J).AND.'200
      SIGN1=SIGN1.SHIFT.-7
      IF(SIGN1.EQ.1) THEN
      SIGN1=-1
      ELSE
      SIGN1=1
      ENDIF
      SIGN=SIGN1
      BB1=B(J+1)
      BB2=BB1.AND.'200
```

```
      BB3=BB2. SHIFT. 17
      BB4=BB1. AND. '177
      BB5=BB4. SHIFT. 16
      B2=BB5. OR. BB3
      B3=B( J+2 ). SHIFT. 8
      B4=B( J+3 )
      MANT1=B2. OR. B3. OR. B4
      MANT=MANT1
      IF( MANT1. EQ. 0 ) THEN
      NEWORD( RCOUNT )=0.
      ELSE
      EXP1=B( J ). AND. '177
      EXP1=EXP1-70
      EXP=16. **EXP1
      NEWORD( RCOUNT )=SIGN*EXP*MANT
      ENDIF
      RCOUNT=RCOUNT+1
      ENDFOR
      RETURN
34    END
C
C
      SUBROUTINE  ITRNSL( ICOUNT, INIT, FIN, B, NEWVAR )
C
      INTEGER*6  MANT1, B2, B3, B4, NEWVAR( 40 ), SIGN2, B1, BB1, BB2, BB3, BB4, BI
      INTEGER  B( 3030 ), SIGN1, INIT, FIN, NUMWRD, ICOUNT
      NUMWRD=( ( FIN-INIT )+1 )/4
      FOR  I=1, NUMWRD
      J=INIT+4*( I-1 )
      SIGN1=B( J ). AND. '200
      SIGN1=SIGN1. SHIFT. -7
      IF( SIGN1. EQ. 1 ) THEN
      SIGN1=-1
      ELSE
      SIGN1=1
      ENDIF
9     SIGN2=SIGN1
      BB1=B( J )
      B1=BB1. SHIFT. 25
      BB2=B( J+1 ). AND. '177
      BB3=B( J+1 ). AND. '200
      BB4=BB2. SHIFT. 16
      BB5=BB3. SHIFT. 17
      B2=BB4. OR. BB5
      B3=B( J+2 ). SHIFT. 8
      B4=B( J+3 )
      MANT1=B1. OR. B2. OR. B3. OR. B4
      NEWVAR( ICOUNT )=SIGN2*MANT1
      ICOUNT=ICOUNT+1
      ENDFOR
      RETURN
32    END
```

```
C*****************************************************************
C       $REFMT TAKES A TAPE CREATED BY $FORMTR
C       AND REFORMATS IT, CREATING RECORDS
C       CONTAINING DATA FROM ONE FLIGHT TRACK
C       OVER ANTARCTICA AND INTERPOLATING OVER
C       REGIONS WHERE THE MAGNETOMETER MISFIRED.
C       DATA FROM 2 NASA PASSES ARE CONTAINED IN
C       IN EACH RECORD. THEREFORE HEADER VARIABLES
C       ARE LISTED TWICE, E.G., KP1 AND KP2.
C       THE FORMAT OF THE DATA OUTPUT IS:
C
C           WORD #              DESCRIPTION
C           1                   MJDX1
C           2                   IPASS1
C           3                   MSECX1(ANT)
C           4                   MSECX1(ARC)
C           5                   KP1(ANT)
C           6                   KP1(ARC)
C           7                   MJDX2
C           8                   IPASS2
C           9                   MSECX2(ANT)
C           10                  MSECX2(ARC)
C           11                  KP2(ANT)
C           12                  KP2(ARC)
C           13                  # OF DATA POINTS
C           14-283              LAT
C           284-553             LON
C           554-823             ELEV
C           824-1093            DELR
C           1094-1363           DELX
C           1364-1633           DELY
C           1634-1903           DELZ
C
C
C*****************************************************************
      DOUBLE PRECISION RUE(757)
      DIMENSION XLAT(270),XLON(270),ELEV(270),DELX(270),DELY(270),
     +XMSQR(30),RR(270),DELZ(270),DELS(270),RSQ(30),
     +XX(6),X(6),WORD(1905),LOC(30)
      INTEGER SMILOC
      CALL LINK
      WRITE(1,1)
1     FORMAT(' FOR INPUT TAPE')
      CALL ASSIGN(12)
      WRITE(1,2)
2     FORMAT(' FOR OUTPUT TAPE')
```

C-2

```
      CALL ASSTAP('13')
C
C         CHECKING FOR FIRST DOWNGOING DATA RECORD
C
300   BUFFERIN('12,BUF,B,1513,ISTAT,IWORD)
      CALL STATUS('12')
      IF(BUF(1).EQ.1)  THEN
325   .   FORMAT(1X,F14.2)
      .   X(1)=BUF(3)

      .   X(2)=BUF(4)
      .   X(3)=BUF(9)
      .   X(4)=BUF(10)
      .   X(5)=BUF(15)
      .   X(6)=BUF(16)
      .   FOR I=1,6
      .   .   WRITE(4,325) X(I)
      .   ENDFOR
      .   CALL REWIND(4)
      .   GOTO 300
      ELSEIF(BUF(36).GT.BUF(35))
      .   GOTO 300
      ENDIF
      LL=1
      K=0
      KK=0
      GOTO 302
      LOOP
     LOOP   NO PATH TO HERE
      .   LL=1
      .   K=0
      .   KK=0
301   .   BUFFERIN('12,BUF,B,1513,ISTAT,IWORD)
      .   CALL STATUS('12')
      .   EXITLOOP IF(ISTAT.EQ.3)
C
C         CHECK TO SEE IF DOWNGOING OR UPGOING RECORD
C
      .   IF(BUF(1).EQ.1) THEN
      .   .   LL=2
      .   .   X(1)=BUF(3)
      .   .   X(2)=BUF(4)
      .   .   X(3)=BUF(9)
      .   .   X(4)=BUF(10)
      .   .   X(5)=BUF(15)
      .   .   X(6)=BUF(16)
      .   .   GOTO 301
      .   ENDIF
      .   IF(LL.EQ.2)  THEN
      .   .   IF(BUF(36).LT.BUF(35))  GOTO 309
```

```
      .   ENDIF
C
C         CREATE ARRAYS OF APPROPRIATE DATA
C
302   .   FOR I=1,30
      .      XLAT(I+KK)=BUF(I+6)
      .      XLON(I+KK)=BUF(I+36)
      .      ELEV(I+KK)=BUF(I+66)-6357.
      .      DELX(I+KK)=BUF(I+246)-BUF(I+606)
      .      DELY(I+KK)=BUF(I+276)-BUF(I+636)
      .      DELZ(I+KK)=BUF(I+306)-BUF(I+666)
      .      RSQ(I)=BUF(I+246)**2+BUF(I+276)**2+BUF(I+306)**2
      .      XMSQ(I)=BUF(I+606)**2+BUF(I+636)**2+BUF(I+666)**2
      .      DELS(I+KK)=SQRT(RSQ(I))-SQRT(XMSQ(I))
      .   ENDDO
      .   K=K+1

      .   KK=30*K
      .   GOTO 301
305   .   FORMAT(8(1X,F9.2))
C
C         FIND 9999. LOCATIONS IN LAT() & DELETE THEM FROM ALL VARS.
C
309   .   NUM9=0
      .   IEXIST=1
      .   FOR I=1,KK
      .      IF(XLAT(I).EQ.99999.) THEN
      .         NUM9=NUM9+1
      .         WRITE(3,310) I
310   .         FORMAT(1X,I3)
      .         IEXIST=2
      .      ENDIF
      .   ENDFOR
      .   KKK=KK-NUM9
      .   IF(IEXIST.EQ.1) GOTO 500
      .   CALL REWIND(3)
      .   FOR I=1,NUM9
      .      READ(3,*) LOC9(I)
      .   ENDFOR
      .   CALL REWIND(3)
      .   SMLLOC=LOC9(1)
      .   LRGLOC=LOC9(1)
      .   FOR I=2,NUM9
      .      IF(LOC9(I).GT.LRGLOC) LRGLOC=LOC9(I)
      .      IF(LOC9(I).LT.SMLLOC) SMLLOC=LOC9(I)
      .   ENDDO
      .   KK=ELOC1(KKK)
      .   FOR I=1,KK
      .      IF(I.LT.SMLLOC) THEN
      .         BB(I)=XLAT(I)
```

```
.    .   ELSEIF( ).GT.LARGLOC ) THEN
.    .    .   BB( )=NUMY )=XLAT( ) )
.    .   ENDIF
.   ENDFOR
.   FOR )=1,KK
.    .   XLAT( ) )=BB( ) )
.   ENDFOR
.   FOR )=1,KK
.    .   IF( ).LT.SMALLOC ) THEN
.    .    .   BB( ) )=XLON( ) )
.    .   ELSEIF( ).GT.LARGLOC ) THEN
.    .    .   BB( )=NUMY )=XLON( ) )
.    .   ENDIF
.   ENDFOR
.   FOR )=1,KK
.    .   XLON( ) )=BB( ) )
.   ENDFOR
.   FOR )=1,KK
.    .   IF( ).LT.SMALLOC ) THEN
.    .    .   BB( ) )=ELEV( ) )
.    .   ELSEIF( ).GT.LARGLOC ) THEN
.    .    .   BB( )=NUMY )=ELEV( ) )
.    .   ENDIF

.   ENDFOR
.   FOR )=1,KK
.    .   ELEV( ) )=BB( ) )
.   ENDFOR
.   FOR )=1,KK
.    .   IF( ).LT.SMALLOC ) THEN
.    .    .   BB( ) )=DELS( ) )
.    .   ELSEIF( ).GT.LARGLOC ) THEN
.    .    .   BB( )=NUMY )=DELS( ) )
.    .   ENDIF
.   ENDFOR
.   FOR )=1,KK
.    .   DELS( ) )=BB( ) )
.   ENDFOR
.   FOR )=1,KK
.    .   IF( ).LT.SMALLOC ) THEN
.    .    .   BB( ) )=DELX( ) )
.    .   ELSEIF( ).GT.LARGLOC ) THEN
.    .    .   BB( )=NUMY )=DELX( ) )
.    .   ENDIF
.   ENDFOR
.   FOR )=1,KK
.    .   DELX( ) )=BB( ) )
.   ENDFOR
.   FOR )=1,KK
.    .   IF( ).LT.SMALLOC ) THEN
```

```
      .    .    RR( ) )=DELY( ) )
      .    ELSEIF( ). GT. LARGLOC) THEN
      .    .    RR( )-NUMY )=DELY( ) )
      .    ENDIF
      .  ENDDO
      .  FOR )=1, KK
      .    DELY( ) )=RR( ) )
      .  ENDDO
      .  FOR )=1, KK
      .    IF( ). LT. SMLLOC) THEN
      .    .    RR( ) )=DELZ( ) )
      .    ELSEIF( ). GT. LARGLOC) THEN
      .    .    RR( )-NUMY )=DELZ( ) )
      .    ENDIF
      .  ENDDO
      .  FOR )=1, KK
      .    DELZ( ) )=RR( ) )
      .  ENDDO
      .  FOR )=1, KK
      .    RR( ) )=0.
      .  ENDDO
C
C
C        AUTOMATIC CLIPPING
C
C
C              CHECKING FIRST TWO VARS. FOR CLIPPING & THEN FLAGGING
C
      .  FOR )=1, 2
      .    IF( ABS( XLAT( ) ). GT. 500. ) THEN

      .    .    XLAT( ) )=9.
      .    ORIF( ABS( XLON( ) ). GT. 500. ) THEN
      .    .    XLON( ) )=9.
      .    ORIF( ABS( ELEV( ) ). GT. 800. ) THEN
      .    .    ELEV( ) )=9.
      .    ORIF( ABS( DELS( ) ). GT. 500. ) THEN
      .    .    DELS( ) )=9.
      .    ORIF( ABS( DELX( ) ). GT. 500. ) THEN
      .    .    DELX( ) )=9.
      .    ORIF( ABS( DELY( ) ). GT. 500. ) THEN
      .    .    DELY( ) )=9.
      .    ORIF( ABS( DELZ( ) ). GT. 500. ) THEN
      .    .    DELZ( ) )=9.
      .    ENDIF
      .  ENDDO
500   .  FOR )=1, KK
      .    IF( ABS( XLAT( ) ). GT. 500. ) THEN
      .    .    IF( ABS( XLAT( )+1 ) ). GT. 500. ) THEN
      .    .         XLAT( ) )=( XLAT( )-1 ):XLAT( )-2 ) )/2.
```

```
      ELSE
        XLAT(I)=(XLAT(I-1)+XLAT(I+1))/2.
      ENDIF
    ENDIF
  ENDDO
  DO I=1,KK
    IF(ABS(XLON(I)).GT.500.) THEN
      IF(ABS(XLON(I+1)).GT.500.) THEN
        XLON(I)=(XLON(I-1)+XLON(I-2))/2.
      ELSE
        XLON(I)=(XLON(I-1)+XLAT(I+1))/2.
      ENDIF
    ENDIF
  ENDDO
  DO I=1,KK
    IF(ABS(ELEV(I)).GT.800.) THEN
      IF(ABS(ELEV(I+1)).GT.800.) THEN
        ELEV(I)=(ELEV(I-1)+ELEV(I-2))/2.
      ELSE
        ELEV(I)=(ELEV(I-1)+ELEV(I+1))/2.
      ENDIF
    ENDIF
  ENDDO
  DO I=1,KK
    IF(ABS(DELS(I)).GT.500.) THEN
      IF(ABS(DELS(I+1)).GT.500.) THEN
        DELS(I)=(DELS(I-1)+DELS(I-2))/2.
      ELSE
        DELS(I)=(DELS(I-1)+DELS(I+1))/2.
      ENDIF
    ENDIF
  ENDDO
  DO I=1,KK
    IF(ABS(DELX(I)).GT.500.) THEN
      IF(ABS(DELX(I+1)).GT.500.) THEN
        DELX(I)=(DELX(I-1)+DELX(I-2))/2.
      ELSE

        DELX(I)=(DELX(I-1)+DELX(I+1))/2.
      ENDIF
    ENDIF
  ENDDO
  DO I=1,KK
    IF(ABS(DELY(I)).GT.500.) THEN
      IF(ABS(DELY(I+1)).GT.500.) THEN
        DELY(I)=(DELY(I-1)+DELY(I-2))/2
      ELSE
        DELY(I)=(DELY(I-1)+DELY(I+1))/2.
      ENDIF
    ENDIF
```

```
      .   ENDFOR
      .   FOR I=1,KK
      .   .   IF(ABS(DELZ(I)).GT.500.) THEN
      .   .   .   IF(ABS(DELZ(I+1)).GT.500.) THEN
      .   .   .   ..  DELZ(I)=(DELZ(I-1)+DELZ(I-2))/2.
      .   .   .   ELSE
      .   .   .   ..  DELZ(I)=(DELZ(I-1)+DELZ(I+1))/2.
      .   .   .   ENDIF
      .   .   ENDIF
      .   ENDFOR
C
C             FINDING FLAGGED VARS (OF FIRST TWO) AND CLIPPING THEM.
C             CLIPPING MEANS MAKING THE AVERAGE OF THE ARRAY.  THIS
C             SPELLS TROUBLE FOR LAT AND LON WHICH MUST BE EXACT SO
C             RECORDS THAT DON'T BEGIN WITH APPROPRIATELY SMALL LATS
C             AND LONS MUST BE SCRUTINIZED TO DETERMINE REAL LAT & LO
C             VALUES.
C
      .   FOR J=1,2
      .   .   IF(XLAT(J).EQ.9.) THEN
      .   .   .   TOT=0.
      .   .   .   FOR I=1,KK
      .   .   .   .   TOT=XLAT(I)+TOT
      .   .   .   ENDFOR
      .   .   .   XLAT(J)=TOT/FLOAT(KKK)
      .   .   ORIF(XLON(J).EQ.9.) THEN
      .   .   .   TOT=0.
      .   .   .   FOR I=1,KK
      .   .   .   .   TOT=XLON(I)+TOT
      .   .   .   ENDFOR
      .   .   .   XLON(J)=TOT/FLOAT(KKK)
      .   .   ORIF(ELEV(J).EQ.9.) THEN
      .   .   .   TOT=0.
      .   .   .   FOR I=1,KK
      .   .   .   .   TOT=ELEV(I)+TOT
      .   .   .   ENDFOR
      .   .   .   ELEV(J)=TOT/FLOAT(KKK)
      .   .   ORIF(DELS(J).EQ.9.) THEN
      .   .   .   TOT=0.
      .   .   .   FOR I=1,KK
      .   .   .   .   TOT=DELS(I)+TOT
      .   .   .   ENDFOR
      .   .   .   DELS(J)=TOT/FLOAT(KKK)
      .   .   ORIF(DELX(J).EQ.9.) THEN
```

```
      .  .  .  TOT=0.
      .  .  .  FOR I=1,KK
      .  .  .  .  TOT=DELX(I)+TOT
      .  .  .  ENDFOR
      .  .  .  DELX(J)=TOT/FLOAT(KKK)



      .  .  ORIF(DELY(J).EQ.9.) THEN
      .  .  .  TOT=0.
      .  .  .  FOR I=1,KK
      .  .  .  .  TOT=DELY(I)+TOT
      .  .  .  ENDFOR
      .  .  .  DELY(J)=TOT/FLOAT(KKK)
      .  .  ORIF(DELZ(J).EQ.9.) THEN
      .  .  .  TOT=0.
      .  .  .  FOR I=1,KK
      .  .  .  .  TOT=DELZ(I)+TOT
      .  .  .  ENDFOR
      .  .  .  DELZ(J)=TOT/FLOAT(KKK)
      .  .  ENDIF
      .  ENDFOR
C
C
C
      .  FOR I=1,6
      .  .  READ(4,-) XX(I)
      .  ENDFOR
      .  CALL REWIND(4)
      .  FOR I=1,6
      .  .  WORD(I)=XX(I)
      .  .  WORD(I+6)=X(I)
      .  ENDFOR
      .  WORD(13)=FLOAT(KKK)
      .  FOR I=1,270
      .  .  WORD(I+13)=XLAT(I)
      .  .  WORD(I+283)=XLON(I)
      .  .  WORD(I+553)=ELEV(I)
      .  .  WORD(I+823)=DELS(I)
      .  .  WORD(I+1093)=DELX(I)
      .  .  WORD(I+1363)=DELY(I)
      .  .  WORD(I+1633)=DELZ(I)
      .  ENDFOR
      .  BUFFEROUT( 13,WORD,B,3806,JSTAT,JWORD)
         CALL STATUS( 13)
         FOR I=1,6
            WRITE(4,325) X(I)
         ENDFOR
```

```
      CALL  REWIND( 4 )
      CALL  BUFFER( 12, $100 )
      DO( )=1,270
         XLAT( ) =0.
         XLON( ) =0.
         ELEV( ) =0.
         DEL.S( ) =0.
         DEL.X( ) =0.
         DEL.Y( ) =0.
         DEL.Z( ) =0.
      END-DO

      END.LOOP
      DO( )=1,3
         CALL  XXYY( 13, 06 )
      END DO
100   STOP
      END
```

```
      DIMENSION BUF(1905),XR(270,2),XQUAD(270,2),ANOM(270,2),
     +WORK(1400),XKP(1500)
C*************************************************************
C       %ANTAP CREATES A TAPE OF ANOMALY DATA BY SUB-
C       TRACTING A POLYNOMIAL FIT TO EACH PASS.  IT
C       ALSO SELECTS PASSES THAT SATISFY THE KP-CRIT-
C       ERION REQUIRING KP.LE.1- FOR 3 CONSEQUTIVE
C       PASSES.  OUTPUT IS FORMATTED AS FOLLOWS:
C
C         WORD #                DESCRIPTION
C         1-13                  SAME AS %REFMT
C         14                    TYPICAL ELEVATION
C         15-17                 POLYNOMIAL COEFFS.
C         18-287                LAT
C         288-557               LON
C         558-827               DELR
C         828-1097              DELR-POLYNOMIAL
C         1093-1367              ELEV
C
C
C*************************************************************
      CALL LINK
      WRITE(1,9)
9     FORMAT(' FOR INPUT TAPE:')
      CALL ASSTAP('13')
      WRITE(1,1)
1     FORMAT(' WHICH ANOMALY VALUES ARE DESIRED?'/'   1-DELS'/
     +'   2-DELX'/'   3-DELY'/'   4-DELZ')
      READ(1,2) J
2     FORMAT(I1)
      WRITE(1,3)
3     FORMAT(' WHERE IS DATA GOING?'/'   1-TERMINAL'/
     +'   2-MBUAT1'/'   3-TAPE'/'   6-LINEPRINTER')
      READ(1,4) JJ
4     FORMAT(I1)
      IF(JJ.EQ.3) THEN
      .   WRITE(1,10)
10    .   FORMAT(' FOR OUTPUT TAPE:')
      .   CALL ASSTAP('12')
      ENDIF
      N=0
      LOOP
      .   BUFFERIN('13,BUF,R,3806,ISTAT,IWORD)
      .   CALL STATUS('13)
      .   EXITLOOP IF(ISTAT.EQ.3)
C
```

```
      KKK=IFIX(RUF(13))
      IF(J.EQ.1) THEN
.   .   FOR I=1,KKK
.   .   .   XR(I,2)=RUF(823+I)
.   .   ENDFOR
.   .   ORIF(J.EQ.2) THEN
.   .   .   FOR I=1,KKK
.   .   .   .   XR(I,2)=RUF(1093+I)
.   .   .   ENDFOR
.   .   ORIF(J.EQ.3) THEN
.   .   .   FOR I=1,KKK
.   .   .   .   XR(I,2)=RUF(1363+I)
.   .   .   ENDFOR
.   .   ELSE
.   .   .   FOR I=1,KKK
.   .   .   .   XR(I,2)=RUF(1633+I)
.   .   .   ENDFOR
.   .   ENDIF
.   .   FOR I=1,KKK
.   .   .   XR(I,1)=FLOAT(I)
.   .   ENDFOR
C
C
C         QUADRATIC FIT ROUTINE
C
C
.   .   YSUM=0.
.   .   XSUM=0.
.   .   XYSUM=0.
.   .   X2SUM=0.
.   .   X3SUM=0.
.   .   X4SUM=0.
.   .   X2YSUM=0.
.   .   FOR I=1,KKK
.   .   .   YSUM=YSUM+XR(I,2)
.   .   .   XSUM=XSUM+XR(I,1)
.   .   .   XYSUM=XYSUM+XR(I,1)*XR(I,2)
.   .   .   X2SUM=X2SUM+XR(I,1)**2
.   .   .   X3SUM=X3SUM+XR(I,1)**3
.   .   .   X4SUM=X4SUM+XR(I,1)**4


C         CHOOSING APPROPRIATE VALUES
C
C           CHOOSING ONLY GOOD PASSES
C
      II=IFIX(RUF(8))
      N=N+1
      XKP(N)=RUF(1)
      IF(N.GE.4.AND.XKP(N).LE.  .AND.XKP(N-1).LE.7 .AND.XKP(N-2)
     * .LE.7 .AND.XKP(N-3).LE.   ) THEN
```

```
      .      X2YSUM= X2YSUM+XB( I, 1 )*XB( I, 1 )*XB( I, 2 )
      .   ENDFOR
      .   A1=YSUM*( X2SUM*X4SUM-X3SUM**2 )
      .   A2=XSUM*( X3SUM*X2YSUM-XYSUM*X4SUM )
      .   A3=X2SUM*( XYSUM*X3SUM-X2SUM*X2YSUM )
      .   B1=REAL( I3 )*( XYSUM*X4SUM-X3SUM*X2YSUM )
      .   B2=YSUM*( X3SUM*X2SUM-XSUM*X4SUM )
      .   B3=X2SUM*( XSUM*X2YSUM  XYSUM*X2SUM )
      .   C1=REAL( I3 )*( X2SUM*X2YSUM-XYSUM*X3SUM )
      .   C2=XSUM*( XYSUM*X2SUM-XSUM*X2YSUM )
      .   C3=YSUM*( XSUM*X3SUM-X2SUM**2 )
      .   D1=REAL( I3 )*( X2SUM*X4SUM-X3SUM**2 )
      .   D2=XSUM*( X3SUM*X2SUM-XSUM*X4SUM )
      .   D3=X2SUM*( XSUM*X3SUM-X2SUM**2 )
      .   DELTA=D1+D2+D3
      .   A=( A1+A2+A3 )/DELTA


      .   BBB=( B1+B2+B3 )/DELTA
      .   C=( C1+C2+C3 )/DELTA
C
C
C
C     CALCULATE EXTERNAL FIELD VALUES FROM QUADRATIC PARAMS A, BBB, C
C
      .   FOR( )=1, KKK
      .   .   XQUAD( ), 2 )=C*( FLOAT( I )**2 )+BBB*FLOAT( I )+A
      .   .   XQUAD( ), 1 )=FLOAT( I )
      .   ENDFOR
C
C     CALCULATE ANOMALY VALUES
C
      .   FOR I )=1, KKK
      .   .   ANOM( ), 2 )=XB( ), 2 )-XQUAD( ), 2 )
      .   .   ANOM( ), 1 )=FLOAT( I )
      .   ENDFOR
C
C     CREATE OUTPUT FILE
C
      .   FOR K )=1, I3
      .   .   WORK( K )=REAL( I )
      .   ENDFOR
      .   WORK( 14 )=REAL( A00 )
      .   WORK( 15 )= A
      .   WORK( 16 )=BBB
      .   WORK( 17 )=C
          FOR I )=1, 270
      .       WORK( I+17 )=REAL( I+15 )
              WORK( I+288 )=REAL( I+288 )
              WORK( I+559 )=XB( I, 1 )
              WORK( I+829 )=YSUM( I, 1 )
```

```
                WORD(I+1092)-BUF(I+553)
             .  ENDFOR
C
C        OUTPUT DATA
C
      .  .   IF(XKP(N).EQ.1 .OR.XKP(N).EQ.2..OR.XKP(N-1).EQ.1 .OR.
     +.  .   XKP(N-1).EQ.2 .OR.XKP(N-2).EQ.1 .OR.XKP(N-2).EQ.2..OR
     +.  .   XKP(N-3).EQ.1 .OR.XKP(N-3).EQ.2.)  GOTO 100
      .  .   IF(JJ.EQ.1) GOTO 50
      .  .   IF(JJ.EQ.2) GOTO 50
      .  .   IF(JJ.EQ.6) GOTO 50
      .  .   IF(JJ.EQ.3) THEN
      .  .  .   BUFFEROUT('12,WORD,8,2734,JSTAT,JWORD)
      .  .  .   CALL STATUS('12)
      .  .   ENDIF
      .  .   GOTO 100
50    .  .   FOR I=1,1367,5
      .  .  .   WRITE(JJ,11) WORD(I),WORD(I+1),WORD(I+2),WORD(I+3),WORD(
11    .  .  .   FORMAT(5(1X,F12.2))
      .  .   ENDFOR
100   .  ENDIF
      ENDLOOP
      FOR I=1,3

      .  CALL XXYY('12,'06)
      ENDFOR
      STOP
      END
```

```
      DIMENSION WORD(1915),XLAT(275),XLON(275),Y(275),X(275)
C*************************************************************
C
C         $MRGRD GRIDS DATA INTO THE (X',Y',Z') MAP COOR-
C         DINATE SYSTEM FROM SPHERICAL COORDINATES. OUTPUT
C         IS FORMATTED AS FOLLOWS:
C
C            WORD #                  DISCRIPTION
C            1-1367                  LIKE $ANTAP
C            1368-1637               X'
C            1638-1907               Y'
C
C*************************************************************
      CALL LINK
      WRITE(1,1)
1     FORMAT(' INPUT TAPE')
      CALL ASSTAP('13)
      WRITE(1,2)
2     FORMAT(' OUTPUT TAPE')
      CALL ASSTAP('12)
      RDPRDG=.017453293
      LOOP
      .  BUFFERIN('13,WORD,B,2734,ISTAT,IWORD)
      .  CALL STATUS('13)
      .  EXITLOOP IF(ISTAT.EQ.3)
      .  IF(WORD(2).LT.0.) GOTO 100
      .  NUM=IFIX(WORD(13))
      .  FOR I=1,NUM
      .  .  XLAT(I)=WORD(17+I)
      .  .  XLON(I)=WORD(287+I)
      .  ENDFOR
      .  FOR I=1,NUM
      .  .  IF(XLON(I).GE.0..AND.XLON(I).LE.90.) THEN
      .  .  .  XLON1=XLON(I)*RDPRDG
      .  .  .  X(I)=(90.+XLAT(I))*SIN(XLON1)
      .  .  .  Y(I)=(90.+XLAT(I))*COS(XLON1)
      .  .  ELSEIF(XLON(I).GE.-90..AND.XLON(I).LT.0.) THEN
      .  .  .  XLON1=-1.*XLON(I)*RDPRDG
      .  .  .  X(I)=-1.*(90.+XLAT(I))*SIN(XLON1)
      .  .  .  Y(I)=(90.+XLAT(I))*COS(XLON1)
      .  .  ELSEIF(XLON(I).LT.-90..AND.XLON(I).GE.-180.) THEN
      .  .  .  XLON1=-1.*(XLON(I)+90.)*RDPRDG
      .  .  .  X(I)=-1.*(XLAT(I)+90.)*COS(XLON1)
      .  .  .  Y(I)=-1.*(XLAT(I)+90.)*SIN(XLON1)
      .  .  ELSE
      .  .  .  XLON1=(XLON(I)-90.)*RDPRDG
```

```
.           X( ) = ( XLAT( ) )+90. )*COS( XLONI )
.           Y( ) =-1. *( XLAT( ) )+90. )*SIN( XLONI )
.       ENDIF
.     ENDIF
.     K=NUM+1367
.     FOR )=1368, K
.       WORD( ) = X( )-1367 )
.     ENDIFOR
.     KJ=K+1
.     FOR )=K1, 1637
.       WORD( ) =0.
.     ENDIFOR
.     KK=1637+NUM
.     FOR )=1638, KK
.       WORD( ) =Y( )-1637 )
.     ENDIFOR
.     KKJ=KK+1
.     FOR )=KK1, 1907
.       WORD( ) = 0.
.     ENDIFOR
.     BUFFEROUT( 12, WORD, B, 3814, ISTAT, JWORD )
      CALL  STATUS( 12 )
100   ENDLOOP
      FOR )=1, 3
.     CALL  XXYY( 12, 06 )
      ENDIFOR
      STOP
      END
```

```
      DIMENSION WORK(1915),ANUM(275),ELEV(275),X(275),Y(275)
     +,ARRAY(675),IBOX(275)
C*************************************************************
C
C         $BIN TAKES GRIDDED DATA CREATED BY $MRGRD
C         AND PLACES DATA WITHIN EACH 3 DEG DATA
C         BIN (OVER ANTARCTICA (16 DEG BY 16 DEG
C         SQUARE) INTO AN UNBLOCKED DISC-FILE.
C         ELEVATIONS ARE ALSO INCLUDED.  THE
C         DISC-FILE IS DEVOTED INTO 1024 12-SECTOR
C         SLICES, EACH SLICE CONTAINING DATA FROM
C         ONE BIN.  WITHIN EACH SECTOR:
C
C             REAL WORD              DESCRIPTION
C             1                      BIN NUMBER, KEY
C                                    ON ATTACHED MAP
C             2                      # DATA POINTS
C             3-337                  MAGNETIC DATA
C             338-672                ELEVATIONS
C
C*************************************************************
      CALL LINK
      OPEN 3
      CALL ASSTAP(713)
C
C             INITIALIZE BOX NUMBERS ON DISC
C
      N=0
      LOOP
     .  ARRAY(1)=FLOAT(N/12)
     .  FOR J=2,672
     .  .  ARRAY(J)=0.
     .  ENDFOR
     .  CALL SETCRA(3,N)
     .  BUFFEROUT(3,ARRAY,R,1344,ISTAT1,IWORD1)
     .  CALL STATUS(3)
     .  N=N+12
     .  EXITLOOP IF(N.GT.12300)
      ENDLOOP
C
C
C             MAIN LOOP
C
      LOOP
     .  BUFFERIN(13,WORD,R,3814,ISTAT,IWORD)
     .  CALL STATUS(713)
```

```
        .   EXITLOOP IF(ISTAT.EQ.3)
        .   JJJJ=IFIX(WORD(2))
        .   IF(JJJJ.EQ.1553) GOTO 100
        .   NUM=IFIX(WORD(13))
        .   FOR I=1,NUM
        .   .   ANOM(I)=WORD(827+I)
        .   .   X(I)=WORD(1367+I)
        .   .   Y(I)=WORD(1637+I)
        .   .   ELEV(I)=WORD(1097+I)

        .   ENDFOR
C
C           SET BOX NUMBERS FOR LATER USE
C
        .   FOR I=1,NUM
        .   .   IF(X(I).GE.0..AND.Y(I).GE.0.) THEN
        .   .   .   IBOX(I)=IFIX((X(I)+3.)/3.)+16*(IFIX(Y(I)/3.))
        .   .   ELSEIF(X(I).LT.0..AND.Y(I).GE.0.) THEN
        .   .   .   IBOX(I)=IFIX((-1.*X(I)+3.)/3.)+16*IFIX(Y(I)/3.)+256
        .   .   ELSEIF(X(I).LT.0..AND.Y(I).LT.0.) THEN
        .   .   .   IBOX(I)=IFIX((-1.*X(I)+3.)/3.)+16*IFIX(-1.*Y(I)/3.)+51
        .   .   ELSE
        .   .   .   IBOX(I)=IFIX((X(I)+3.)/3.)+16*IFIX(-1.*Y(I)/3.)+768
        .   .   ENDIF
        .   ENDFOR
C
C           WRITE DATA TO DISC FILE MRDISC (LUN 3)
C
        .   FOR I=1,NUM
        .   .   ISCTOR=12*IBOX(I)
        .   .   CALL SETCRA(3,ISCTOR)
        .   .   BUFFERIN(3,ARRAY,8,1344,ISTAT2,IWORD2)
        .   .   CALL STATUS(3)
        .   .   M=IFIX(ARRAY(2))
        .   .   IF(M.LT.335) THEN
        .   .   .   ARRAY(2)=ARRAY(2)+1.
        .   .   .   ARRAY(M+3)=ANOM(I)
        .   .   .   ARRAY(338+M)=ELEV(I)
        .   .   ELSE
        .   .   .   WRITE(2,-) IBOX(I)
        .   .   ENDIF
        .   .   CALL SETCRA(3,ISCTOR)
        .   .   BUFFEROUT(3,ARRAY,8,1344,ISTAT3,IWORD3)
        .   .   CALL STATUS(3)
        .   ENDFOR
            WRITE(4,-) WORD([illegible])
100     ENDLOOP
        CALL SETCRA(3,[illegible])
        FOR I=1,3
            CALL XXYY(3,0A)
```

```
      ENDIF(IR
      STOP
      END

      SUBROUTINE SETCRA(LFN,IPOS)
C     SUBROUTINE TO SET THE CURRENT RECORD ADDRESS FOR A DISK FILE.
C
C     LFN   THE FILE NUMBER.
C     IPOS  THE CRA VALUE TO SET.
C
:ASSE
        TMA*  IPOS
        TAM   CRA
        TMA*  LFN
        LLA   6
        OOR   =17
        TAM   SET
        TLO   SET
        RLU   $1/0
:END
      RETURN
:ASSE
SET     BLOK  1
CRA     BLOK  1
:END
      END
```

```
      DIMENSION ARRAY(675),ARR(350),ELEV(350)
      REAL MTOTAV, MAGTOT, MAGAVG,NMAGAV,NETAV,NVAR,NVRTOT,NETTOT
     +,NMGTOT,NMTTAV,NETTAV,NVRAV
C*****************************************************************
C
C        $RDBIN READS THE MAGNETIC VALUES AND ELEV-
C        ATIONS FROM THE UNBLOCKED DISC-FILE CREATED
C        BY $BIN AND AVERAGES THEM AND COMPUTES STAN-
C        DARD DEVIATIONS IN THE MAGNETIC VALUES.  IT
C        APPLIES THE DATA-DISCARDING WINDOW OF A USER-
C        SPECIFIED SIZE, AND THEN RECALCULATES THE
C        AVERAGE MAGNETIC VALUE, AVERAGE ELEVATION,
C        AND MAGNETIC VARIANCE.  ALL THIS IS PRINTED
C        OUT TO A USER-SPECIFIED LOCATION.
C
C*****************************************************************
      CALL LINK
      OPEN 3
      N=0
      WRITE(1,7)
7     FORMAT(' SIZE OF ANOM. DIFF. ALLOWED IN EACH BIN?')
      READ(1,-) XL
      WRITE(1,6)
6     FORMAT(' WHERE IS DATA TO  GO?  1-TERMINAL  6-PRINTER')
      READ(1,-) LOC
      WRITE(LOC,1)
1     FORMAT('       BIN',',      OPTS',',      OELEV',',       OMAG',
     +',       OVAR',',       NPTS',',      NELEV',',       NMAG',
     +',       NVAR')
      NDATA=0
      MAGTOT=0.
      ELVTOT=0.
      VARTOT=0.
      NVRTOT=0.
      NETTOT=0.
      NMGTOT=0.
C
C           MAIN LOOP
C
      LOOP
C
C           ORIGINAL VALUES
        VAR=0.
        MAGAVG=0.
        ELEVAV=0.
        CALL SETBOX(3,N)
```

```
      .   BUFFER IN(3,ARRAY,8,1344,ISTAT,IWORD)
      .   CALL STATUS(3)
      .   EXIT IF(IOR(IFC(ISTAT.EQ.3)
      .   M1=IFIX(ARRAY(2))
      .   MM=M1+337
      .   M=M1+2
      .   SUM=0.
      .   IF(M1.NE.0) THEN
      .      FOR I=3,M
      .         SUM=SUM+ARRAY(I)
      .      ENDFOR
      .      MAGAVG=SUM/ARRAY(2)
      .      FOR I=3,M
      .         DIFFSQ=((ARRAY(I)-MAGAVG)**2)/ARRAY(2)
      .         VAR=VAR+DIFFSQ
      .      ENDFOR
      .      ESUM=0.
      .      FOR I=338,MM
      .         ESUM=ESUM+ARRAY(I)
      .      ENDFOR
      .      EIFVAV=ESUM/ARRAY(2)
      .      NDATA=NDATA+1
      .      MAGTOT=MAGTOT+MAGAVG
      .      EIVTOT=EIVTOT+EIFVAV
      .      VARTOT=VARTOT+VAR
      .   ENDIF
C
C        NEW VALUES
      .   NMAGAV=0.
      .   NEIAV=0.
      .   M2=1
      .   M3=0
      .   IF(M1.GT.0) THEN
      .      FOR J=1,M1
      .         DIFF=ABS(ARRAY(2+I))-MAGAVG)
      .         IF(DIFF.LE.X1) THEN
      .            ARR(M2)=ARRAY(2+I)
      .            EIFV(M2)=ARRAY(337+I)
      .            M2=M2+1
      .         ENDIF
      .      ENDFOR
      .      NVAR=0
4     .      SUM1=0.
      .      SUM2=0.
      .      M3=M2-1
      .      IF(M3.EQ.0) GOTO 100
      .      FOR I=1,M3
               SUM1=SUM1+ARR(I)
               SUM2=SUM2+EIFV(I)
```

```
      .  .   ENDFOR
      .      NMAGAV=SUM1/FLOAT(M3)
      .      NELAV=SUM2/FLOAT(M3)
      .  .   FOR J=1,M3
      .  .  .   DIFESQ=((ARR(J)-NMAGAV)**2)/FLOAT(M3)
      .  .  .   NVAR=NVAR+DIFESQ
      .  .   ENDFOR
      .  .   NMGTOT=NMGTOT+NMAGAV
      .  .   NELTOT=NELTOT+NELAV
      .  .   NVRTOT=NVRTOT+NVAR
100       ENDIF
C
C            WRITE OUT
C
      .   XM2=FLOAT(M3)
      .   WRITE(LOC,2) ARRAY(1),ARRAY(2),ELEVAV,MAGAVG,VAR

      .   1,XM2,NELAV,NMAGAV,NVAR
       1,     INVALID  STATEMENT
2     .   FORMAT(9(2X,F8.1))
      .   N=N+12
      ENDLOOP
      MTOTAV=MAGTOT/FLOAT(NDATA)
      ETOTAV=ELVTOT/FLOAT(NDATA)
      VARAVG=VARTOT/FLOAT(NDATA)
      NMTTAV=NMGTOT/FLOAT(NDATA)
      NETTAV=NELTOT/FLOAT(NDATA)
      NVRAV=NVRTOT/FLOAT(NDATA)
      WRITE(LOC,3) NDATA, MTOTAV,ETOTAV,VARAVG,NETTAV,
     +NMTTAV,NVRAV
3     FORMAT(' NDATA:',2X,I4,/,' MAGAV:',2X,F8.2,/,
     +' ELEVAV:',2X,F8.2,/,' VARAV:',2X,F8.2,/' NELEVAV:',2X,
     +F8.2,/,' NMAGAV:',2X,F8.2,/,' NVARAV:',2X,F8.2)
      STOP
      END
      SUBROUTINE SETCRA(LEN,IPOS)
C     SUBROUTINE TO SET THE CURRENT RECORD ADDRESS FOR A DISK FILE.
C
C     LEN   THE FILE NUMBER
C     IPOS  THE CRA VALUE TO SET
C
 ASSE
        LMA*  IPOS
        LAM   CRA
        LMA*  LEN
```

```
            LDA     6
            COM     #17
            TAM     SET
            TFO     SET
            BLU     $1/0
:END
            RETURN
:ASSE
SET         MOK     1
CKA         MOK     1
:END
            END
```

```
      COMMON X_Y(16),X(16),CDATA(16,16),RCOEFF(16,16),
     +FFT2D(16,16),RMFFT(16,16),RWIFFT(16,16),IFFT2D(16,16)
      REAL MOD(16,16),MOD2(16,16),RF(16,16),IM(16,16),RPMOD(16,16)
      DIMENSION SURF(16,16),DATA(16,16),XHAM(3),WNDDAT(16,16)
C*****************************************************************
C
C         *FFT2D CALCULATES THE 2DFFT OF DATA IN A DISC-FILE.
C         THE DATA IN THE DISC-FILE ARE IN A SINGLE COLUMN
C         SUCH THAT ROWS OF THE MAP ARE LISTED IN SEQUENCE FROM
C         TOP TO BOTTOM.  THE PROGRAM IS SPECIFICALLY ASSIGNED
C         TO DEAL WITH AN ARRAY OF 16 BY 16.  A HAMMING WINDOW OF
C         WIDTH 3 IS A USER OPTION.  THE HIGH-PASS FILTER IS ALSO
C         AN OPTION AND IS DESCRIBED IN APPENDIX II.  THE 2DFFT
C         PRINTED OUT HAS TO BE UNRAVELLED.
C
C*****************************************************************
      CALL LINK
C           READ IN DATA
      FOR I=1,16
      .   FOR J=1,16
      .   .   READ(2,-) DATA(I,J)
      .   ENDFOR
      ENDFOR
      WRITE(1,7)
7     FORMAT(' HAMMING WINDOW APPLIED? 1=YES 2=NO')
      READ(1,-) HAM
      IF(HAM.EQ.1) THEN
C           HAMMING WINDOW ARRAY XHAM(I)
      .   XHAM(1)=.08
      .   XHAM(2)=.31
      .   XHAM(3)=.77
      ELSE
      .   FOR I=1,3
      .   .   XHAM(I)=1.
      .   ENDFOR
      ENDIF
C           APPLY HAMMING WINDOW TO DATA TO GET WNDDAT(I,J)
      FOR I=1,16
      .   FOR J=1,16
      .   .   IF(I.EQ.1.OR.I.EQ.16.OR.J.EQ.1.OR.J.EQ.16) THEN
      .   .   .   WNDDAT(I,J)=XHAM(1)*DATA(I,J)
      .   .   ELSEIF(I.EQ.2.OR.I.EQ.15.OR.J.EQ.2.OR.J.EQ.15) THEN
      .   .   .   WNDDAT(I,J)=XHAM(2)*DATA(I,J)
      .   .   ELSEIF(I.EQ.3.OR.I.EQ.14.OR.J.EQ.3.OR.J.EQ.14) THEN
      .   .   .   WNDDAT(I,J)=XHAM(3)*DATA(I,J)
      .   .   ELSE
```

```
            WINDOW(I,J)=DATA(I,J)
         ENDIF
      ENDFOR
   ENDFOR
C
C           FFT
C
   SIGN=-1.
   N=4
C           FILL COMPLEX ARRAY CDATA WITH WINDOWED DATA FROM WINDOW
   FOR I=1,16
      FOR J=1,16
         CDATA(I,J)=CMPLX(WINDOW(I,J),0.)
      ENDFOR
   ENDFOR
C           TAKE FFT OF ROWS FIRST
   FOR I=1,16
      FOR J=1,16
         X(J)=CDATA(I,J)
      ENDFOR
      CALL  NLOGN(N,X,SIGN)
      FOR K=1,16
         ROWFFT(I,K)=X(K)
      ENDFOR
   ENDFOR
C           TAKE FFT OF COLUMNS NOW
   FOR J=1,16
      FOR I=1,16
         Y(I)=ROWFFT(I,J)
      ENDFOR
      CALL NLOGN(N,Y,SIGN)
      FOR K=1,16
         FFT2D(K,J)=Y(K)
      ENDFOR
   ENDFOR
C           SELECT IFFT
   WRITE(1,5)
5  FORMAT(' WANT IFFT? 1=YES 2=NO')
   READ(1,*) INV
   IF(INV.EQ.2) GOTO 6
C           APPLY HIGH PASS FILTER
   FOR I=1,16
      FOR J=1,16
         HPFFT(I,J)=FFT2D(I,J)
      ENDFOR
   ENDFOR
   HPFFT(1,1)=0.*HPFFT(1,1)
   HPFFT(1,2)=.5*HPFFT(1,2)
   HPFFT(1,16)=.5*HPFFT(1,16)
```

```
      HPFFT(2,1)=.5*HPFFT(2,1)
      HPFFT(2,2)=.67*HPFFT(2,2)
      HPFFT(2,16)=.67*HPFFT(2,16)
      HPFFT(16,1)=.5*HPFFT(16,1)
      HPFFT(16,2)=.67*HPFFT(16,2)
      HPFFT(16,16)=.67*HPFFT(16,16)
C           INFT
      S1GN=1.
C           TAKE INFT OF HPFFT(),J); ROWS INTO
      DO I=1,16
        DO J=1,16
          X(J)=HPFFT(I,J)
        ENDDO
        CALL NLOGN(N,X,S1GN)
        DO K=1,16
          RWINFT(I,K)=X(K)
        ENDDO
      ENDDO
C           TAKE INFT OF COLUMNS NOW
      DO J=1,16
        DO I=1,16
          Y(I)=RWINFT(I,J)
        ENDDO
        CALL NLOGN(N,Y,S1GN)
        DO K=1,16
          INFT2D(K,J)=Y(K)
        ENDDO
      ENDDO
      WRITE(6,20)
20    FORMAT(25X,'DIGITAL IMAGE')
      WRITE(6,4)
C           WRITE OUT DIGITAL ARRAY DATA(),J)
6     DO I=1,16
        WRITE(6,2) DATA(I,1),DATA(I,2),DATA(I,3),DATA(I,4),DATA(I,5),
     +  DATA(I,6),DATA(I,7),DATA(I,8),DATA(I,9),DATA(I,10),DATA(I,11),
     +  DATA(I,12),DATA(I,13),DATA(I,14),DATA(I,15),DATA(I,16)
2       FORMAT(16(1X,F6.2))
      ENDDO
      WRITE(6,4)
      WRITE(6,21)
21    FORMAT(25X,'WINDOWED DATA')
      WRITE(6,4)
C           WRITE OUT WINDOWED DATA
      DO I=1,16
        WRITE(6,2) WNDDAT(I,1),WNDDAT(I,2),WNDDAT(I,3),WNDDAT(I,4),
     +  WNDDAT(I,5),WNDDAT(I,6),WNDDAT(I,7),WNDDAT(I,8),WNDDAT(I,9),
     +  WNDDAT(I,10),WNDDAT(I,11),WNDDAT(I,12),WNDDAT(I,13),WNDDAT(I,14
     +  WNDDAT(I,15),WNDDAT(I,16)
      ENDDO
```

```
      WRITE(6,4)
      WRITE(6,22)
22    FORMAT(25X,'2DFFT')
      WRITE(6,4)
C           WRITE OUT 2DFFT
      DO I=1,16
        DO J=1,16
          MOD(I,J)=CABS(FFT2D(I,J))
        END DO
      END DO
      WRITE(1,-) MOD(I,1)
      DO I=1,16
        WRITE(6,2) MOD(I,1),MOD(I,2),MOD(I,3),MOD(I,4),MOD(I,5),
     +  MOD(I,6),MOD(I,7),MOD(I,8),MOD(I,9),MOD(I,10),MOD(I,11),
     +  MOD(I,12),MOD(I,13),MOD(I,14),MOD(I,15),MOD(I,16)
      END DO
      IF(INV.EQ.2) GOTO 4
      WRITE(6,4)
      WRITE(6,10)
10    FORMAT(25X,'HIGH-PASSED 2DFFT')
      WRITE(6,4)
C           WRITE OUT HIGH-PASSED DFFT
      DO I=1,16

        DO J=1,16
          HPMOD(I,J)=CABS(HPFFT(I,J))
        END DO
      END DO
      DO I=1,16
        WRITE(6,2) HPMOD(I,1),HPMOD(I,2),HPMOD(I,3),HPMOD(I,4),
     +  HPMOD(I,5),HPMOD(I,6),HPMOD(I,7),HPMOD(I,8),HPMOD(I,9),
     +  HPMOD(I,10),HPMOD(I,11),HPMOD(I,12),HPMOD(I,13),HPMOD(I,14),
     +  HPMOD(I,15),HPMOD(I,16)
      END DO
      WRITE(6,4)
      WRITE(6,11)
11    FORMAT(25X,'DFFT2D MODULUS')
      WRITE(6,4)
C           WRITE OUT DFFT2D MODULUS
      DO I=1,16
        DO J=1,16
          MOD2(I,J)=CABS(DFFT2D(I,J))
        END DO
      END DO
      DO I=1,16
        WRITE(6,2) MOD2(I,1),MOD2(I,2),MOD2(I,3),MOD2(I,4)
     +  ,MOD2(I,5),MOD2(I,6),MOD2(I,7),MOD2(I,8),MOD2(I,9)
     +  ,MOD2(I,10),MOD2(I,11),MOD2(I,12),MOD2(I,13),MOD2(I,14)
     +  ,MOD2(I,15),MOD2(I,16)
      END DO
```

```
      WRITE(6,4)
      WRITE(6,12)
12    FORMAT(25X,'FFT2D REAL')
      WRITE(6,4)
C           WRITE (OUT )FFT2D REAL
      FOR I=1,16
     .   FOR J=1,16
     .     RE(I,J)=REAL(FFT2D(I,J))
     .   ENDFOR
      ENDFOR
      FOR I=1,16
     .   WRITE(6,2) RE(I,1),RE(I,2),RE(I,3),RE(I,4),RE(I,5)
     +.    ,RE(I,6),RE(I,7),RE(I,8),RE(I,9),RE(I,10),RE(I,11)
     +.    ,RE(I,12),RE(I,13),RE(I,14),RE(I,15),RE(I,16)
      ENDFOR
      WRITE(6,4)
      WRITE(6,13)
13    FORMAT(25X,'FFT2D IMAGINARY')
      WRITE(6,4)
C           WRITE (OUT )FFT2D IMAGINARY
      FOR I=1,16
     .   FOR J=1,16
     .     IM(I,J)=AIMAG(FFT2D(I,J))
     .   ENDFOR
      ENDFOR
      FOR I=1,16
     .   WRITE(6,2) IM(I,1),IM(I,2),IM(I,3),IM(I,4),IM(I,5)
     +.    ,IM(I,6),IM(I,7),IM(I,8),IM(I,9),IM(I,10),IM(I,11)
     +.    ,IM(I,12),IM(I,13),IM(I,14),IM(I,15),IM(I,16)
      ENDFOR

C           WRITE (OUT SUBTRACTED SURFACE
      WRITE(6,4)
      WRITE(6,14)
14    FORMAT(25X,'SUBTRACTED SURFACE')
      FOR I=1,16
     .   FOR J=1,16
     .     SURF(I,J)=DATA(I,J)-RE(I,J)
     .   ENDFOR
      ENDFOR
      FOR I=1,16
     .   WRITE(6,2) SURF(I,1),SURF(I,2),SURF(I,3),SURF(I,4),SURF(I,5),
     +.    SURF(I,6),SURF(I,7),SURF(I,8),SURF(I,9),SURF(I,10),SURF(I,11),
     +.    SURF(I,12),SURF(I,13),SURF(I,14),SURF(I,15),SURF(I,16)
      ENDFOR
4     FORMAT(///)
      STOP
      END
```

APPENDIX VI

Tables

TABLE I

24 x 24 Array $D_{i,j}$ of Data Density

$D_{i,1}$	$D_{i,2}$	$D_{i,3}$	$D_{i,4}$	$D_{i,5}$	$D_{i,6}$	$D_{i,7}$	$D_{i,8}$
-	-	5	7	20	1	12	19
-	-	4	3	11	20	9	45
-	-	11	21	18	20	10	41
8	-	21	35	41	45	1	39
-	-	5	10	20	48	38	19
-	6	17	19	54	44	55	39
7	20	15	13	24	47	53	35
16	19	23	30	35	61	44	36
27	30	40	46	54	54	87	86
17	20	21	32	23	39	68	109
1	-	5	10	19	18	20	67
10	10	4	3	10	12	51	88
1	10	10	8	34	59	59	54
9	-	31	53	45	38	31	66
24	48	34	34	24	25	45	56
35	37	38	29	30	42	57	43
29	17	15	19	23	40	36	41
2	13	18	10	41	45	36	78
-	k4	6	56	35	33	29	71
10	10	43	22	42	22	12	80
-	6	27	32	14	20	26	69
4	4	-	11	14	10	71	38
-	-	-	5	14	69	40	28
-	-	-	-	10	3	45	21

$D_{i,9}$	$D_{i,10}$	$D_{i,11}$	$D_{i,12}$	$D_{i,13}$	$D_{i,14}$	$D_{i,15}$	$D_{i,16}$
27	6	10	44	26	47	65	18
31	9	6	58	24	68	46	22
55	10	-	60	44	91	10	29
38	35	1	69	62	69	20	35
41	47	39	47	100	35	31	53
47	33	78	53	80	44	64	14
83	36	77	124	40	74	67	32
64	72	104	130	77	77	61	57
68	66	183	146	129	104	107	66
92	135	311	307	275	147	73	24
113	256	306	-	-	145	155	95
171	335	-	-	-	-	152	66
115	335	-	-	-	-	109	68
77	199	159	-	-	54	76	48
108	88	136	102	53	37	37	16
99	66	88	94	20	34	37	10
106	62	53	59	71	58	38	28
51	46	51	42	49	63	51	32
44	51	35	47	19	54	64	41
42	49	14	35	40	34	38	62
46	34	1	48	40	12	39	35
43	28	-	40	40	20	23	35
28	28	5	26	32	42	2	32
27	28	10	25	23	48	2	14

$D_{1,17}$	$D_{1,18}$	$D_{1,19}$	$D_{1,20}$	$D_{1,21}$	$D_{1,22}$	$D_{1,23}$	$D_{1,24}$
18	1	9	4	9	10	-	-
20	14	15	21	27	-	-	-
29	26	31	39	4	-	-	-
35	42	21	15	23	4	-	-
46	11	29	25	15	17	3	-
24	28	37	31	25	19	24	16
26	46	46	38	49	45	44	8
64	68	50	24	8	14	16	17
36	21	10	15	19	17	8	-
30	9	18	20	21	10	9	8
72	61	54	29	17	10	10	9
41	51	38	48	40	49	37	22
55	21	23	29	38	21	30	32
32	48	22	7	6	20	21	17
28	17	35	23	12	1	3	16
33	12	18	26	23	13	6	-
21	27	6	20	21	23	10	2
-	38	25	3	22	17	21	4
16	19	18	17	11	33	11	10
21	14	38	11	3	2	12	4
50	17	18	20	15	-	-	-
31	37	19	26	13	7	-	-
28	18	27	16	11	10	-	-
34	9	5	-	19	-	-	-

TABLE II

Summary of Characteristics of the "Unaffected" Passes

PASS	DATE	TIME	KP	AVG ELEV
49	11/ 5/79	5:45	0	573
50	11/ 5/79	7:19	3	577
51	11/ 5/79	8:53	3	578
52	11/ 5/79	10:27	7	578
75	11/ 6/79	22:24	3	577
76	11/ 6/79	23:58	3	576
200	11/15/79	1:42	0	573
260	11/18/79	23:21	3	562
262	11/19/79	2:29	3	562
263	11/19/79	4:02	7	560
308	11/22/79	2:15	0	551
309	11/22/79	3:49	0	550
323	11/23/79	1:39	3	547
325	11/23/79	4:46	0	546
400	11/28/79	1:44	3	522
401	11/28/79	3:18	0	522
402	11/28/79	4:51	0	521
411	11/28/79	18:53	7	518
413	11/28/79	22:00	3	517
414	11/28/79	23:34	3	517
415	11/29/79	1:07	3	517
416	11/29/79	2:41	3	516
417	11/29/79	4:41	0	516
418	11/29/79	5:48	0	515
419	11/29/79	7:21	7	515
420	11/29/79	8:55	7	515
757	12/21/79	5:40	0	396
821	12/25/79	9:10	0	387
1019	1/ 7/80	4:48	0	385
1168	1/16/80	20:02	3	415
1169	1/16/80	21:35	3	415
1251	1/22/80	4:45	0	438
1282	1/24/80	4:48	0	448
1298	1/25/80	5:36	0	452
1299	1/25/80	7:09	7	453
1300	1/25/80	8:42	7	453
1461	2/ 4/80	18:08	3	494
1463	2/ 4/80	21:14	3	492
1464	2/ 4/80	22:47	- 3	495
1465	2/ 4/80	0:20	0	495
1466	2/ 5/80	1:53	0	495
1467	2/ 5/80	3:26	0	495
1468	2/ 5/80	4:59	0	496

1469	2/ 5/80	6:32	7	496
1556	2/10/80	21:12	7	507
1557	2/10/80	22:45	7	507
1559	2/11/80	1:50	3	508
1575	2/12/80	2:36	7	509
1576	2/12/80	4:08	0	509
1592	2/13/80	4:54	0	510
1593	2/13/80	6:26	0	510
1594	2/13/80	7:59	0	510
1695	2/19/80	20:10	3	506
1775	2/24/80	23:48	3	496
1868	3/ 1/80	23:24	3	475
1880	3/ 2/80	17:56	7	472
1889	3/ 3/80	7:49	3	470
1903	3/ 4/80	5:25	3	466
1928	3/ 5/80	19:59	7	459
1929	3/ 5/80	21:32	7	458
1930	3/ 5/80	23:04	7	456
2008	3/10/80	23:20	7	434
2014	3/11/80	8:35	3	432
2025	3/12/80	1:32	0	429
2026	3/12/80	3:05	0	428
2027	3/12/80	4:37	0	428
2028	3/12/80	7:42	0	427
2030	3/12/80	9:14	0	427
2033	3/12/80	13:52	0	426
2034	3/12/80	15:24	7	426
2035	3/12/80	16:57	7	425
2073	3/15/80	3:29	0	414
2074	3/15/80	5:02	0	413
2075	3/15/80	6:34	3	413
2076	3/15/80	8:06	3	413
2079	3/15/80	12:44	3	412
2080	3/15/80	14:16	3	412
2081	3/15/80	15:48	3	411
2082	3/15/80	17:21	3	411
2083	3/15/80	18:53	0	411
2084	3/15/80	20:26	0	411
2134	3/19/80	1:25	3	396
2135	3/19/80	2:57	3	396
2213	3/24/80	2:59	3	376
2214	3/24/80	4:31	7	375
2230	3/25/80	5:07	0	372
2231	3/25/80	6:40	3	372
2232	3/25/80	8:12	3	371

TABLE III

24 x 24 Array $\Delta B_{i,j}$ of Scalar Anomolies

$\Delta B_{i,1}$	$\Delta B_{i,2}$	$\Delta B_{i,3}$	$\Delta B_{i,4}$	$\Delta B_{i,5}$	$\Delta B_{i,6}$	$\Delta B_{i,7}$	$\Delta B_{i,8}$
-	-	-6	-5	2	14	7	6
-	-2	-2	-1	0	2	4	1
-	-	-2	-1	-1	-5	-3	-1
-5	-3	-2	-2	-2	-1	-3	-3
-4	-3	1	-2	1	1	-1	-1
-	-3	0	1	1	1	-1	0
-4	-3	-1	3	2	1	2	0
-2	-2	0	4	3	2	4	5
-2	-2	-1	2	4	3	3	4
1	1	1	2	1	2	2	1
0	-	0	0	1	-1	2	1
-1	0	1	1	1	4	3	-1
-2	-1	2	2	2	4	3	-1
-2	-	1	3	2	2	3	3
-2	-1	1	2	2	0	3	4
-2	1	0	0	0	1	1	2
1	0	-1	-1	-2	-1	-1	-1
-1	0	1	-1	-2	-2	-2	-2
-	2	2	1	0	0	-2	0
1	2	1	1	1	0	1	1
-	1	1	0	-1	0	0	1
-1	1	-	-1	-1	1	1	1
-	-	-	-	0	2	0	1
-	-	-	-	1	2	-2	-1

$\Delta B_{i,9}$	$\Delta B_{i,10}$	$\Delta B_{i,11}$	$\Delta B_{i,12}$	$\Delta B_{i,13}$	$\Delta B_{i,14}$	$\Delta B_{i,15}$	$\Delta B_{i,16}$
-1	1	-3	2	-2	-3	0	1
-3	-2	-7	-3	-4	-2	-1	-1
-4	-4	-	-3	1	1	1	1
-4	-3	0	2	5	4	2	2
0	1	1	3	2	1	-1	-2
2	3	0	-1	-5	-3	1	1
1	3	0	-5	-6	-3	1	3
1	2	-2	-2	-2	-1	2	3
-1	1	0	3	3	1	1	0
-2	-2	1	1	1	0	-1	-1
-2	-5	-3	-	-	-3	-3	-2
-4	-5	-	-	-	-	-4	-3
-1	0	-	-	-	-	-1	-1
3	3	2	-	-	5	2	3
1	2	0	0	0	1	1	5
3	2	-3	-2	-2	-3	-3	2
1	0	-3	-4	-1	0	-1	2
-1	0	-4	-1	-2	-1	2	1
-1	0	-2	2	0	-3	-2	-1
0	2	0	3	2	-1	-6	-2
1	3	4	4	4	4	-4	-1
1	2	-	3	3	3	2	0
0	-1	-1	2	-1	0	0	2
-2	-4	-1	-1	-5	-3	-7	-6

$\Delta B_{i,17}$	$\Delta B_{i,18}$	$\Delta B_{i,19}$	$\Delta B_{i,20}$	$\Delta B_{i,21}$	$\Delta B_{i.22}$	$\Delta B_{i,23}$	$\Delta B_{i,24}$
0	4	-2	-4	-4	-3	-	-
0	2	1	-1	-3	-	-	-
4	3	3	3	-7	-	-	-
2	1	2	-4	-5	-2	-	-
-2	-1	-1	-2	-3	-2	-4	-5
2	1	1	-3	-5	-4	-1	-1
3	6	4	-2	-2	0	1	0
4	6	4	-3	-3	-1	-1	1
4	5	5	-2	-5	-3	-2	-
3	0	-3	-4	-3	2	2	3
-1	3	5	3	1	2	0	-2
-2	4	5	3	-1	2	-1	-2
1	2	-3	-1	3	-2	-4	-5
3	5	4	4	2	1	-2	-5
4	7	5	7	1	-3	-1	0
8	7	8	1	-3	-3	-3	-
4	8	0	-4	-4	-3	-2	-
-	5	-5	-12	-6	-4	-3	-2
-2	-6	-6	-8	-3	-3	-1	4
-7	-6	-5	-7	-7	-	1	6
-2	0	-3	-2	-3	-	-	-
4	3	6	0	2	2	-	-
4	4	5	2	0	5	-	-
4	5	2	-	1	-	-	-

TABLE IV

24 x 24 Array $\Delta X_{i,j}$ of Radial Anomolies

$\Delta X_{i,1}$	$\Delta X_{i,2}$	$\Delta X_{i,3}$	$\Delta X_{i,4}$	$\Delta X_{i,5}$	$\Delta X_{i,6}$	$\Delta X_{i,7}$	$\Delta X_{i,8}$
-	-	-4	9	6	-1	-12	3
-	4	1	1	5	1	-8	-4
4	-	3	-3	0	1	-5	-5
4	-	-12	-14	-1	0	2	-2
4	3	-3	-2	-3	2	-1	-1
-	6	1	-3	-1	3	4	0
-8	-6	2	3	2	1	0	2
-10	-7	-8	-3	1	2	0	-3
-5	-3	-1	-2	2	3	2	1
-10	-7	-4	3	2	8	5	1
-11	-	-3	-4	2	0	3	-1
-6	-6	-5	-4	-5	-5	-5	1
-5	-6	-7	-5	-4	-2	2	-4
-2	-	-2	-3	-1	-1	-18	-8
4	2	0	-1	-7	-22	-9	-11
4	-1	-2	-5	-5	-7	-11	-12
5	-2	1	-3	-5	-15	-15	-10
-	15	12	3	-2	-7	-12	1
9	24	8	2	-1	-5	-6	6
-	7	8	7	3	-3	-4	0
-	1	5	16	10	4	-3	-3
2	6	-	8	18	8	0	-1
-	-	-	-	27	3	3	1
-	-	-	-	-1	1	3	4

$\Delta X_{i,9}$	$\Delta X_{i,10}$	$\Delta X_{i,11}$	$\Delta X_{i,12}$	$\Delta X_{i,13}$	$\Delta X_{i,14}$	$\Delta X_{i,15}$	$\Delta X_{i,16}$
2	4	-5	-2	3	-2	6	2
2	4	-2	-1	-1	-1	2	3
0	3	-	-4	-4	-3	-1	-1
0	0	-7	-6	-4	-3	-4	-1
-1	-1	-4	-8	-3	-3	-8	-6
1	-1	-3	-4	-3	-7	-8	-8
1	-1	-3	-2	-9	-5	-4	-2
1	-2	0	-4	1	11	0	15
9	1	-5	5	6	-18	0	1
0	8	9	2	-6	-1	-4	-8
-4	11	20	-	-	6	2	-4
5	17	-	-	-	-	1	-5
2	12	-	-	-	-	-18	-13
-8	-8	-6	-	-	12	-5	-7
-11	-8	-9	-10	-6	10	1	25
-9	-8	-6	-1	-7	-2	9	-6
-6	-2	6	-6	-1	-3	-36	14
4	9	6	-13	8	7	7	-5
2	7	12	-13	5	16	-1	18
4	3	-22	-16	6	21	6	4
1	-3	12	-3	14	30	1	-5
0	-3	-	-2	6	3	-3	-30
-4	-3	1	-1	2	8	8	-3
-4	-1	1	0	-1	8	10	-1

$\Delta X_{i,17}$	$\Delta X_{i,18}$	$\Delta X_{i,19}$	$\Delta X_{i,20}$	$\Delta X_{i,21}$	$\Delta X_{i,22}$	$\Delta X_{i,23}$	$\Delta X_{i,24}$
6	27	2	2	6	-1	-	-
7	2	8	1	1	-	-	-
0	5	0	-2	-10	-	-	-
-2	-2	-1	-1	2	17	-	-
-6	-6	-8	1	-2	-12	-28	-
-13	-14	2	0	-8	-8	-2	-3
8	24	7	6	2	-5	-14	-24
10	6	21	16	3	1	-6	-7
0	-13	-2	13	26	3	-5	-
-14	-13	-9	-34	-3	29	22	23
-13	-14	-7	4	0	-5	34	9
5	-8	-14	-10	-7	1	11	7
-15	-12	-5	-20	-8	23	28	17
-3	7	-29	-40	9	17	23	-2
-10	4	3	-27	31	-19	51	8
6	-13	6	-12	1	18	12	-
-1	-10	-8	4	-17	27	10	4
-	-9	4	-4	5	44	3	-7
7	-8	14	-2	-21	-4	-5	-5
-3	-26	11	40	17	4	1	-11
5	-39	11	-5	-2	2	-	-
-11	-10	4	3	-6	-8	-	-
-4	3	17	-6	4	-8	-	-
-1	3	1	-	-4	-	-	-

TABLE V

24 x 24 Array $\Delta Y_{i,j}$ of Tangential Anomalies

$\Delta Y_{i,1}$	$\Delta Y_{i,2}$	$\Delta Y_{i,3}$	$\Delta Y_{i,4}$	$\Delta Y_{i,5}$	$\Delta Y_{i,6}$	$\Delta Y_{i,7}$	$\Delta Y_{i,8}$
-	-	14	12	6	14	17	11
-	8	10	8	2	3	7	6
-	-	5	4	0	-2	3	4
13	-	3	0	2	0	4	3
10	3	-4	3	2	-1	2	3
-	2	1	1	-1	-3	0	0
-6	-4	3	6	-2	0	0	-1
6	8	4	2	1	-1	0	4
3	3	0	3	-1	-1	-2	-3
-4	-4	-2	-1	3	-1	-1	-3
-	-	-2	-3	3	8	0	0
-7	-3	-2	7	11	9	-2	-11
-2	-2	5	11	-4	-3	-3	-8
-6	-	0	-2	-4	-2	-6	-12
6	3	2	1	6	-8	-3	-10
3	4	1	0	-2	-2	-5	-3
6	1	2	9	1	-2	-2	-1
-4	0	9	0	0	-6	-5	-10
-	24	8	2	-2	-1	-8	-17
9	5	5	5	5	3	2	-9
-	3	8	11	5	3	3	2
9	-	7	10	10	3	7	-1
-	-	-	-	2	4	5	5
-	-	-	-	5	10	6	4

$\Delta Y_{i,9}$	$\Delta Y_{i,10}$	$\Delta Y_{i,11}$	$\Delta Y_{i,12}$	$\Delta Y_{i,13}$	$\Delta Y_{i,14}$	$\Delta Y_{i,15}$	$\Delta Y_{i,16}$
-1	5	-3	0	-3	2	1	1
-2	-4	-4	-1	0	2	-2	-4
0	-2	-	3	4	1	-4	-3
0	3	-8	1	-1	-1	-2	-4
4	2	-1	0	-9	-3	-5	-4
2	4	-2	-7	-6	-3	-2	-3
-2	-1	-3	-5	7	-1	-4	-3
-2	-4	1	2	13	14	20	12
-5	2	7	13	15	8	1	2
-	-1	7	3	-12	-8	-9	-35
-8	-5	4	-	-	-24	-9	1
-11	-10	-	-	-	-	0	5
-18	-12	-	-	-	-	38	27
-7	2	-16	-	-	19	26	25
-2	-2	0	-10	7	11	11	13
3	9	1	9	-1	0	15	8
1	5	13	8	6	7	29	12
-10	1	-5	14	8	12	5	6
-3	-4	-1	15	1	6	5	7
-2	-4	16	18	5	3	1	-3
-3	-4	-17	-2	-11	-3	-5	-16
-2	-	-	-2	-9	-13	-3	0
2	0	7	-1	-1	-9	-2	-9
-1	0	1	-2	-5	-8	-13	14

$\Delta Y_{i,17}$	$\Delta Y_{i,18}$	$\Delta Y_{i,19}$	$\Delta Y_{i,20}$	$\Delta Y_{i,21}$	$\Delta Y_{i,22}$	$\Delta Y_{i,23}$	$\Delta Y_{i,24}$
-3	-5	2	-2	-1	-1	-	-
0	2	1	-1	-	-	-	-
-2	-3	-1	1	-4	-	-	-
-7	-6	2	-3	-11	-13	-	-
-8	-6	-11	-8	-5	-9	-13	-
-18	-18	4	-1	-12	-13	1	1
7	12	7	-1	-4	-7	-5	-6
5	-4	7	-4	-2	-3	-4	-5
-	5	12	-	-2	-10	-7	-
-12	-18	15	7	2	17	10	5
3	1	3	7	15	1	1	-1
-3	-2	9	5	-3	-2	6	2
19	11	17	9	3	8	11	-2
13	9	1	6	8	8	1	-19
9	7	5	3	15	14	-7	-23
-6	13	5	22	13	3	-7	-
0	3	20	-11	5	-14	-15	-17
-	16	26	15	-2	-11	-16	-31
26	37	-6	-1	-5	-13	5	-7
10	-14	-13	-21	-13	-	-3	-9
-13	-12	-15	-12	-	-	-	-
-7	-17	1	-6	-12	-8	-	-
-7	-6	-1	-8	4	-4	-	-
-9	-18	-4	-	-	-	-	-

TABLE VI

24 x 24 Array of $\Delta Z_{i,j}$ of Vertical Anomalies

$\Delta Z_{i,1}$	$\Delta Z_{i,2}$	$\Delta Z_{i,3}$	$\Delta Z_{i,4}$	$\Delta Z_{i,5}$	$\Delta Z_{i,6}$	$\Delta Z_{i,7}$	$\Delta Z_{i,8}$
-	-	9	11	2	12	-3	-3
-	5	5	3	-1	-3	-5	-1
-	2	1	-	0	3	4	-1
8	-	4	5	2	2	4	3
5	2	0	5	0	-1	2	2
-	2	2	1	-1	-3	-2	0
4	4	4	0	-3	-3	-3	-2
4	5	2	-1	-2	-3	-4	-5
4	5	1	-1	-5	-3	-4	-6
1	0	0	-2	-1	-3	-4	-3
1	-	0	-3	0	1	-2	0
1	1	-1	0	1	-3	-5	-2
3	0	0	1	-4	-5	-5	-2
2	-	-2	-5	-4	-5	-6	-5
5	2	-1	-3	-4	-3	-5	-6
4	0	-1	0	-2	-3	-4	-5
1	1	1	1	2	-2	-3	-1
4	1	-1	0	1	-1	0	2
-	4	-1	-1	-1	-1	-1	0
0	-2	1	1	0	-1	-1	-2
-	-3	0	3	3	0	-1	-2
0	0	0	3	5	2	-1	-2
-	-	-	-	3	-1	0	-1
-	-	-	-	-2	0	1	2

$\Delta Z_{i,9}$	$\Delta Z_{i,10}$	$\Delta Z_{i,11}$	$\Delta Z_{i,12}$	$\Delta Z_{i,13}$	$\Delta Z_{i,14}$	$\Delta Z_{i,15}$	$\Delta Z_{i,16}$
0	-1	2	-2	0	4	3	2
2	2	5	3	5	4	1	3
4	5	-	4	1	-1	-2	-1
4	5	-4	-2	-7	-6	-3	-2
1	1	-3	-4	-7	-4	-2	0
-1	-2	-2	-3	0	0	-2	-2
-2	-5	-1	1	4	2	-3	-7
-2	-4	1	1	2	1	-1	-7
-2	-2	0	-2	0	2	2	1
1	0	-1	-2	-3	0	-1	-1
0	6	7	-	-	10	4	5
3	7	-	-	-	-	6	7
1	3	-	-	-	-	1	3
-3	-3	-1	-	-	-8	-2	-4
-3	-1	0	1	0	-1	-1	-5
-4	-3	3	4	2	2	5	-1
-1	2	5	4	1	0	1	-5
2	1	5	-2	2	2	1	0
1	1	6	-3	1	5	3	3
-1	-1	-1	-5	0	2	8	3
-2	-4	-4	-6	-5	-2	3	1
-2	-2	-	-4	-2	-4	-2	-4
0	1	2	-1	1	0	1	-2
1	5	1	2	4	4	8	5

$\Delta Z_{i,17}$	$\Delta Z_{i,18}$	$\Delta Z_{i,19}$	$\Delta Z_{i,20}$	$\Delta Z_{i,21}$	$\Delta Z_{i,22}$	$\Delta Z_{i,23}$	$\Delta Z_{i,24}$
3	3	4	5	6	5	-	-
2	-1	3	2	4	-	-	-
-2	-3	-4	[illegible]	10	-	-	-
-4	-4	-3	5	7	6	-	-
-1	0	3	3	4	8	2	-
-6	-4	-2	2	5	3	2	2
-6	-9	-5	0	1	1	2	7
-7	-9	-10	-4	2	0	2	2
-3	3	-2	1	-2	0	2	-
0	0	5	16	4	-7	-6	-7
4	2	-2	-4	1	-2	-8	-2
2	-3	-2	-2	2	-3	-3	1
1	3	5	8	0	-4	-2	2
2	-5	0	0	-5	-5	-2	6
-2	-9	-5	-4	-5	5	-7	-6
-4	-5	-7	0	3	0	0	-
-2	-6	-7	1	8	-1	-1	-1
-	-4	-5	11	6	-2	1	-2
3	8	7	9	6	1	2	-4
8	6	5	6	6	-3	-3	-7
2	-3	2	0	3	-	-	-
-6	-6	-5	-2	-3	-4	-	-
-5	-5	-3	-2	-1	-7	-	-
-5	-7	-3	-	-	-1	-	-